JAERI-M
88-146

ION-IMPACT DESORPTION

August 1988

Takashi OSHIYAMA*, Siro NAGAI and Kunio OZAWA**

日本原子力研究所
Japan Atomic Energy Research Institute

JAERI-Mレポートは，日本原子力研究所が不定期に公刊している研究報告書です。
入手の問合わせは，日本原子力研究所技術情報部情報資料課（〒319-11茨城県那珂郡東海村）あて，お申しこしください。なお，このほかに財団法人原子力弘済会資料センター（〒319-11茨城県那珂郡東海村日本原子力研究所内）で複写による実費頒布をおこなっております。

JAERI-M reports are issued irregularly.
Inquiries about availability of the reports should be addressed to Information Division Department of Technical Information, Japan Atomic Energy Research Institute, Tokai-mura, Naka-gun, Ibaraki-ken 319-11, Japan.

編集兼発行　日本原子力研究所
印　　刷　㈱高野高速印刷

JAERI-M 88-146

Ion-Impact Desorption

Takashi OSHIYAMA*, Siro NAGAI+ and Kunio OZAWA**

Research Committee on A & M Data
Tokai Research Establishment
Japan Atomic Energy Research Institute
Tokai-mura, Naka-gun, Ibaraki-ken

(Received July 13, 1988)

The ion-impact desorption is one of the elementary and important processes in plasma-surface interactions. We have compiled the data on desorption cross sections since 1984. At the same time, we have calculated the desorption cross section from a model based on the elastic collisional processes. Comparisons of the compiled data with the calculated results are presented and then the differences between them are discussed. Processes of ion-impact desorption are also discussed.

Keywords: Ion-Impact Desorption, Desorption Cross Section, Elastic Collision, Binding Energy, Reflection Coefficient, Sputtering Yield

---

+ Department of Research, Takasaki Radiation Chemistry Research Establishment

* Kyoto Sangyo University

** Energy Research Laboratory, Hitachi Ltd., Hitachi

イオン衝撃による脱着

日本原子力研究所東海研究所
原子分子データ委員会
押山　孝*・永井　士郎+・小沢国夫**

（１９８８年７月１３日受理）

イオン衝撃による脱着はプラズマ壁相互作用に於ける重要な素過程のひとつである。本報告書では，この脱着現象に関する収集データのなかから特に重要な脱着断面積を選び出し，既存のモデルによる計算値と比較検討した結果を報告する。既存のモデルの限界を明らかにすると共に，イオン衝撃による脱着のメカニズムについて議論する。

東海研究所：〒319-11 茨城県那珂郡東海村白方字白根２－４
＋高崎研究所研究部
＊京都産業大学
＊＊日立エネルギー研究所

Contents

目　　次

1. Introduction

The walls of fusion devices are known to suffer the effects of both particles-beams and electromagnetic radiation emitted from plasma region. In particular, the walls are bombarded by ions and neutral atoms of hydrogen, deuterium, tritium and helium. The adsorbates sticking to the walls are released due to these particle-impact. This process is called desorption. The released particles, i.e., ions, neutral atoms and molecules, enter into the plasma region as impurities, which reduce the temperature of plasma. A substantial fraction of the released particles may be hydrogen, which can be reused as fuel. Therefore, studies of the desorption processes are needed in the estimation of both hydrogen recycling and impurity influx in controlled thermonuclear fusion reactor. In other words, correct assessment of the desorption processes in fusion reactor is an inevitable problem to put it to practical use. The impurity or hydrogen influx caused by desorption processes can be roughly estimated from the known desorption cross section and the expected particle flux to the wall. A rough estimate[1] of the impurity influxes due to ion-impact desorption from stainless steel wall shows that the impurity influxes are about two orders of magnitude larger than those expected from electron- or photon-induced desorption, indicating that ion-impact desorption (IID) is the most important phenomenon in particle-impact induced desorption relevant to plasma-surface interactions.

We have calculated the cross section for ion-impact desorption according to the model proposed by Winters and Sigmund[2] based on binary elastic collisions. This model includes a few physical quantities such as reflection coefficient, sputtering yield and binding energy. These quantities should be correctly assessed because the calculated results have strong dependence on these quantities. For the reflection coefficient, certain analytical expression[3] is used, which has been derived by fitting to many experimental data. For the sputtering yield, we have an analytical presentation[4] of the experimental data, which shows good agreement with the experimental data especially at ion energies below 5 keV. In most of IID experiments, adsorption states of atoms and molecules have not been assigned definitely. When an atom or a molecule adsorbs chemically on a surface, it generally finds one location with respect to the surface atoms, i.e. bridge site, on-top site etc. The heat of chemisorption depends strongly on its location and binding energy of the adsorbed atom can be related to the heat of chemisorption. For the calculation of binding

energy, a semiempirical method[5] is used in this report, which relates the heat of chemisorption to the binding energy. The desorption cross section calculated from Winters and Sigmund's model are compared with the compiled experimental data[6]. It is found that the calculated results show good agreement with the experimental data for a few cases. For most of the cases, however, it is difficult to say that the experimental data can be quantitatively explained by the model.

In this report, we first review Winters and Sigmund's model and the physical quantities necessary to calculate the desorption cross section based on the model are briefly reviewed in chapter 2. Comparison of the experimental data with the model is presented in chapter 3. In chapter 4, we try to explain the data analytically on the basis of an elastic collisional model and consider other mechanisms responsible for desorption than Winters and Sigmund's model.

2. Theoretical considerations based on elastic collision

Studies of ion-impact desorption have been carried out on the surface covered with atoms and molecules which are different from the substrate atoms. The amount of adsorbed atoms is less than one monolayer in most of the IID experiments. It is expected that the process of ejection of adsorbed atoms differs from that of substrate atoms in a few points. For example, the emitted particle definitely comes only from the upper surface layer and changes in the kinematics of collision processes occurring at the surface due to the large mass difference betweeen adsorbate and substrate-atoms. The mass of substrate-atom is mostly heavier than that of adsorbed atom. The process of ejection was first investigated by Winters and Sigmund[2] for the specific case of a chemisorbed monolayer of nitrogen on tungsten. In section 2.1, the cross section for elastic collision is described. In section 2.2, Winters and Sigmund's model is outlined. In sections 2.3, 2.4 and 2.5, physical quantities involved in their model are presented from a standpoint of calculations of desorption cross sections, because the desorption cross section has very strong dependence on them.

2.1 Cross section for elastic collision

It is well known that the interaction between two particles of charges Z_1e and Z_2e is described by the following potential[7]:

energy, a semiempirical method[5] is used in this report, which relates the heat of chemisorption to the binding energy. The desorption cross section calculated from Winters and Sigmund's model are compared with the compiled experimental data[6]. It is found that the calculated results show good agreement with the experimental data for a few cases. For most of the cases, however, it is difficult to say that the experimental data can be quantitatively explained by the model.

In this report, we first review Winters and Sigmund's model and the physical quantities necessary to calculate the desorption cross section based on the model are briefly reviewed in chapter 2. Comparison of the experimental data with the model is presented in chapter 3. In chapter 4, we try to explain the data analytically on the basis of an elastic collisional model and consider other mechanisms responsible for desorption than Winters and Sigmund's model.

2. Theoretical considerations based on elastic collision

Studies of ion-impact desorption have been carried out on the surface covered with atoms and molecules which are different from the substrate atoms. The amount of adsorbed atoms is less than one monolayer in most of the IID experiments. It is expected that the process of ejection of adsorbed atoms differs from that of substrate atoms in a few points. For example, the emitted particle definitely comes only from the upper surface layer and changes in the kinematics of collision processes occurring at the surface due to the large mass difference betweeen adsorbate and substrate-atoms. The mass of substrate-atom is mostly heavier than that of adsorbed atom. The process of ejection was first investigated by Winters and Sigmund[2] for the specific case of a chemisorbed monolayer of nitrogen on tungsten. In section 2.1, the cross section for elastic collision is described. In section 2.2, Winters and Sigmund's model is outlined. In sections 2.3, 2.4 and 2.5, physical quantities involved in their model are presented from a standpoint of calculations of desorption cross sections, because the desorption cross section has very strong dependence on them.

2.1 Cross section for elastic collision

It is well known that the interaction between two particles of charges Z_1e and Z_2e is described by the following potential[7]:

$$V(r) = [Z_1 Z_2 e^2/r]\ \Phi_{TF}(r/a), \tag{2.1}$$

where $\Phi_{TF}(r/a)$ is the Thomas-Fermi screening function for an isolated atom and a is the screening length. The screening function $\Phi_{TF}(r/a)$ satisfies the nonlinear differential equation, which is derived by substituting, into Poisson's equation, the electron density calculated on the basis of Fermi-Dirac statistics. The differential equation for the Thomas-Fermi screening function cannot be solved analytically without some approximations, the solutions of which having been tabulated[8,9]. Depending on the regions of inter-nuclear separation, approximate solutions have been suggested[10]. Lindhard and his co-workers[11] have suggested that the screening function Φ_{TF} can be approximately expressed over the limited ranges of separation by a power form,

$$\Phi_{TF}(r/a) = (k_s/s)(a/r)^{s-1}, \tag{2.2}$$

where k_s is a numerical constant, depending on s. The value of s depends on the range of interaction distances. Using the inverse-power potential, we can easily obtain simple analytical expressions for the scattering cross section, the range distribution and the scattering angle. The differential scattering cross section $d\sigma$ can be derived through a standard method,

$$d\sigma = (C_m/E^m)(dT/T^{m+1})(de'/2\pi)\ \delta[e\ e'-\cos\Phi'], \tag{2.3}$$

with

$$C_m = (\pi/2)\lambda_m a_{12}^2 (M_1/M_2)^m (2Z_1 Z_2 e^2/a_{12})^{2m}, \tag{2.4}$$

$$a_{12} = 0.8853\ a_B (Z_1^{2/3} + Z_2^{2/3})^{-1/2}, \tag{2.5}$$

where $m = 1/s$, a_B is the Bohr radius, E the kinetic energy of incident particle, T the transferred energy, Φ' the laboratory scattering angle, e and e' the unit vectors parallel to the velocities of the particles and $\delta[e\ e'-\cos\Phi']$ a delta function. Geometry of a single-scattering event and physical quantities used in this section are shown in Figure 1. In eq. (2.4), λ_m is a matching parameter for the power approximation of the differential cross section and a dimensionless function of the parameter m which has values between 0 and 1. The values of λ_m vary slowly from m = 1 at

high energies down to m = 0 at low energies. Several values of m and λ_m are shown in Table 1. It is known that the Thomas-Fermi potential overestimates the interaction in the low-energy range 10 eV $\leqq$ E $\leqq$ 1 keV, where Born-Mayer potential is appropriate although little theoretical justification is found. The differential cross section for Born-Mayer interaction has been compared to that for Thomas-Fermi interaction by Sigmund[12] who has shown that eq. (2.3) becomes a reasonable approximation even if m is taken close to zero and that in the case of m = 0 eqs. (2.4) and (2.5) can be replaced by

$$C_0 = (\pi/2)\lambda_0 a_0^2, \; a_0 = 0.219 \text{ Å}, \quad \lambda_0 = 24, \tag{2.6}$$

which correspond to the parameters in a Born-Mayer potential. For m = 1, equation (2.3) corresponds to the differential cross section for Rutherford scattering.

Table 1 Coefficients of Power Potential*)

m	λ_m
1.00	0.50
0.50	0.327
0.333	1.309
0.191	2.92
0.055	15.0
0.0	24.0

*) K.B. Winterbon, P. Sigmund and J. B. Sanders; Mat. Fys. Medd. Dan. Vid. Selsk. 37, no.14, 1−73, (1970).

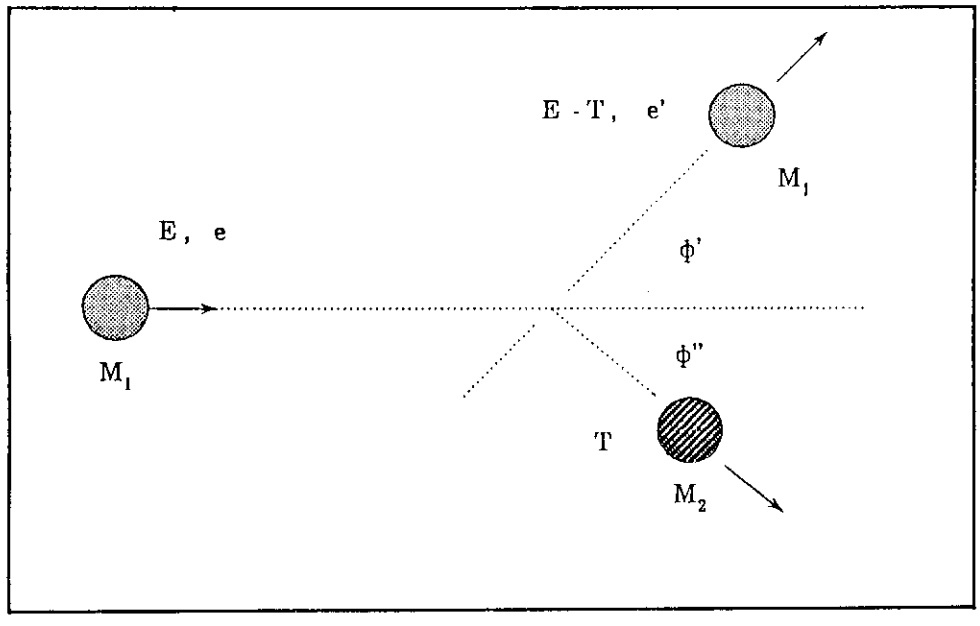

Fig. 1 Scattering geometry in an elastic collision

2.2 Winters and Sigmund's model

Winters and Sigmund[2] have proposed a model for the ejection of adatom due to ion-impact, based on energy and momentum transfer occurring between incoming ion, substrate atom and adsorbed atom. Namely, a chemisorbed nitrogen atom on tungsten is desorbed by the following processes:

(A) Direct knock-on by incident ion.

(B) Knock-on by reflected ion.

(C) Knock-on by sputtered substrate atom.

The processes (A) and (B) are basically equal to the collision of the ion with the adsorbate atom although the energy- and angular- distributions of ions are different between the two processes. These processes (A), (B) and (C) are schematically shown in Figs. 2, 3 and 4, where incidention, substrate atom and adsorbed atom are designated by numbers "1", "2" and "3", respectively. The energies of the particles and the directions of their motions are also shown in parentheses.

The desorption cross section for process (A) is given by,

$$\sigma_A = (1/\cos\theta)\int d\sigma_{13}(E,e,E_0,e_0)\int dE'\, de'\, R_{32}(E_0,e_0,E',e'), \tag{2.7}$$

where θ is is the incident angle measured from surface normal, E_0 the energy of adsorbed atom transferred from incident ion, e_0 the direction of motion of adsorbed atom, and $d\sigma_{13}$ the cross section for the collision of incident ion "1" with adsorbed atom "3". The integrand $R_{32}(E_0,e_0,E',e')$ shows the distribution in energy E' and direction e' of adsorbed atom after being reflected from the substrate atom "2" either directly or after some penetration. If an adatom is assumed to be bound isotropically and be reflected without energy loss, i.e.,

$$\int dE'\, de'\, R_{32}(E_0,e_0,E',e') = \Theta(E_0-U_3), \tag{2.8}$$

where U_3 is the binding energy of adsorbed atom and Θ the step function, equation (2.7) reads,

$$\sigma_A = (1/\cos\theta)(C_{13}/m_{13})(r_{13}^{m_{13}}/U_3^{2m_{13}})(X^{m_{13}}-1)/X^{2m_{13}}, \tag{2.9}$$

where m_{13} is defined by the interaction potential and $X = (r_{13}E)/U_3$. Equation (2.9) shows that σ_A depends on incident angle θ, binding energy U_3, exponent m_{13} and masses of both incident ion and adsorbate atom through energy transfer factor, $r_{13} = 4M_1M_3/(M_1+M_3)^2$. Coefficient C_{13} is given by,

$$C_{13} = (\pi/2)\lambda_{m_{13}}\, a_{13}^{2}(M_1/M_3)^{m_{13}}\,(2Z_1Z_3e^2/a_{13})^{2m_{13}}\ , \qquad (2.10)$$

where a_{13} is the Thomas-Femi screening length for the collision of ion "1" with adsorbate atom "3". When $m_{13} = 0$, the desorption cross section can be written, with the use of a relation; $\lim_{m_{13}\to 0}(X^{-m_{13}}-X^{-2m_{13}})/m_{13} = \ln X$,

$$\sigma_A = (12\pi\, a_0^{2}/\cos\theta)\,\ln(r_{13}E/U_3), \qquad (2.11)$$

where a_0 is a screening length defined eq. (2.6).

The desorption cross section for process (B) can be expressed by,

$$\sigma_B = \int dE_0\, de_0\, R_{12}(E,e,E_0,e_0) \int d\sigma_{13}(E_0,e_0,E',e')/\cos\theta_0\ , \qquad (2.12)$$

where θ_0 is the angle between the direction of the reflected ion and the surface normal. The function $R_{12}(E,e,E_0,e_0)$ is the energy- and angular-distribution of the reflected ions, which depends on various parameters; particle-solid combinations, incident energy and angle, exit energy and angle, etc. For a Maxwellian distribution of the incident particles[13], the energy distributions of reflected particles have an inclination to decrease exponentially as the energy increases. It has also been shown[3] that the angular distribution for the isotropic bombardment shows approximately a cosine distribution except at small exit angles. From these results of experiments and computer simulations, $R_{12}(E,e,E_0,e_0)$ can be assumed to be given by,

$$R_{12}(E,e,E_0,e_0) = C_R\, R(E,e)E_0^{\,2m_{12}-1}\,\cos\theta_0\ , \qquad (2.13)$$

where θ_0 is the polar angle measured with respect to the surface normal. The dependence on azimuthal exit angle in eq. (2.13) is assumed to be isotropic. The function R(E,e) is called the particle reflection coefficient, which is the ratio of the number of all backscattered particles to the number of incident particles. The value of exponent m_{12} in eq. (2.13) is defined by the interaction potential between the incident particle and the target atom. The factor C_R is a normalized constant and obtained from a relation,

$$\int dE_0\, de_0\, R_{12}(E,e,E_0,e_0) = R(E,e). \qquad (2.14)$$

Integrating eq. (2.12) with the use of eqs. (2.3), (2.13) and (2.14), we get

$$\sigma_B = 4(m_{12}/m_{13})C_{12}R(E,e)(r_{13}^{m_{13}}/U_3^{2m_{13}})\ G(X), \tag{2.15}$$

where G(X) depends on the exponents m_{12} and m_{13} and $X = r_{13}E/U_3$,

$$G(X) = \{[X^{2m_{12}-m_{13}}-1]/(2m_{12}-m_{13})-[X^{2(m_{12}-m_{13})}-1]/(2m_{12}-2m_{13})\}/X^{2m_{12}} \tag{2.16}$$

If $m_{12} = m_{13} = m$, equation (2.15) becomes

$$\sigma_B = 4C_{13}\ R(E,e)(r_{13}^{m}/U_3^{2m})[(X^m-1)/m-\ln(X)]/X^{2m}. \tag{2.17}$$

The desorption cross section for process (C) is given by,

$$\sigma_c = \int dE_0\ de_0\ S_{12}(E,e,E_0,e_0) \int d\sigma_{23}(E_0,e_0,E',e')/\cos\theta_0, \tag{2.18}$$

where $S_{12}(E,e,E_0,e_0)$ is the distribution in energy E_0 and direction e_0 of the sputtered target atoms. The $d\sigma_{23}$ is the differential cross section for the collision of the sputtered atom "2" with the adsorbate atom "3". The energy and angular distribution[14] of sputtered particles is assumed to be

$$S_{12}(E,e,E_0,e_0) = C_S\ S(E,e)[E_0/(E_0+U_2)^3]\ \cos\theta_0, \tag{2.19}$$

where S(E,e) is the sputtering yield and U_2 is the binding energy of substrate atom. The constant C_S is a normalized factor and given by a relation,

$$\int dE_0\ de_0\ S_{12}(E,e,E_0,e_0) = S(E,e). \tag{2.20}$$

With these equations (2.3), (2.18), (2.19) and (2.20), the desorption cross section for process (C) is,

$$\sigma_c = (4C_{m_{23}}/m_{23})S(E,e)(r_{23}U_2/U_3)F_{m_{23}}\{r_{12}r_{23}E/U_3, r_{23}U_2/U_3\}, \tag{2.21}$$

with

$$F_{m_{23}} = (r_{23}^{m_{23}}/U_3^{2m_{23}})\int dX(X^{-m_{23}+1}-X^{-2m_{23}+1})/(X+r_{23}U_2/U_3)^3, \tag{2.22}$$

where $X = r_{23}\ E/U_3$. In eq. (2.21), the exponent m_{23} is defined by the interaction potential between the target atom and adsorbate atom. If $m_{23} = 0$, then equation (2.21) becomes

$$\sigma_C = 48\pi a_0^2 S(E,e)(r_{23}U_2/U_3)F\{r_{12}r_{23}E/U_3, r_{23}U_2/U_3\}(1-U_2/r_{12}E)^{-2}, \quad (2.23)$$

with

$$F = \int dX\ X\ \ln(X)/(X + r_{23}\ U_2/U_3)^3. \quad (2.24)$$

In eqs. (2.21) and (2.24), the dependence of functions $F_{m_{23}}$ and F on $r_{12}r_{23}E/U_3$ is introduced from the upper limit of integrations, the region of which is from 1 to $r_{12}r_{23}E/U_3 - r_{23}U_2/U_3$.

From eqs. (2.9), (2.15) and (2.23), it is found that in the calculation of desorption cross section, σ_A, σ_B and σ_C the parameters m_{13} and m are very important and should be correctly chosen to describe the interactions among incident ions, substrate atoms and adatoms. In addition, the following parameters are significantly important:

incident energy and angle (E,θ)
atomic masses (M_1,M_2,M_3)
atomic numbers (Z_1,Z_2,Z_3)
binding energies (U_2,U_3)
reflection coefficient R(E,e)
sputtering yield S(E,e)

In the following sections, the physical quantities U_3, R(E,e) and S(E,e) are discussed.

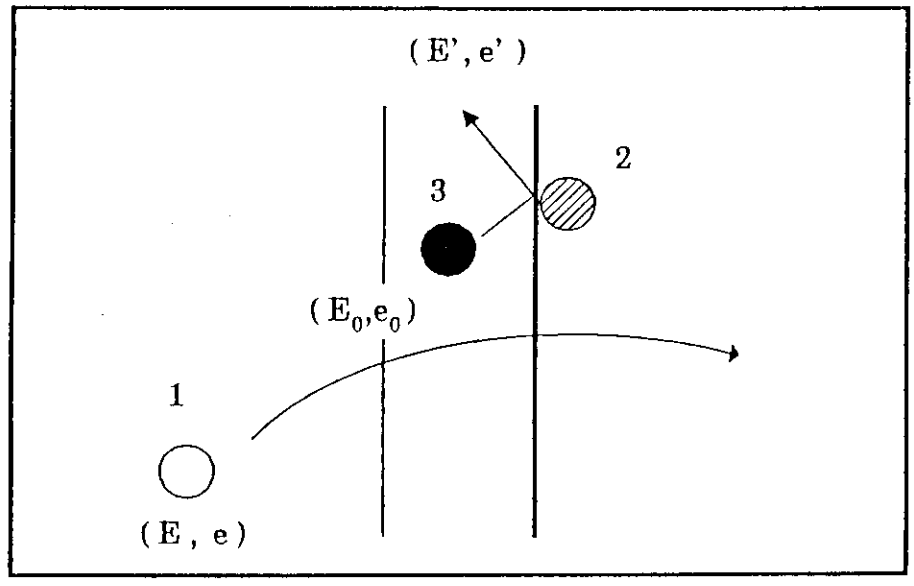

Fig. 2 Process (A) in ion impact desorption

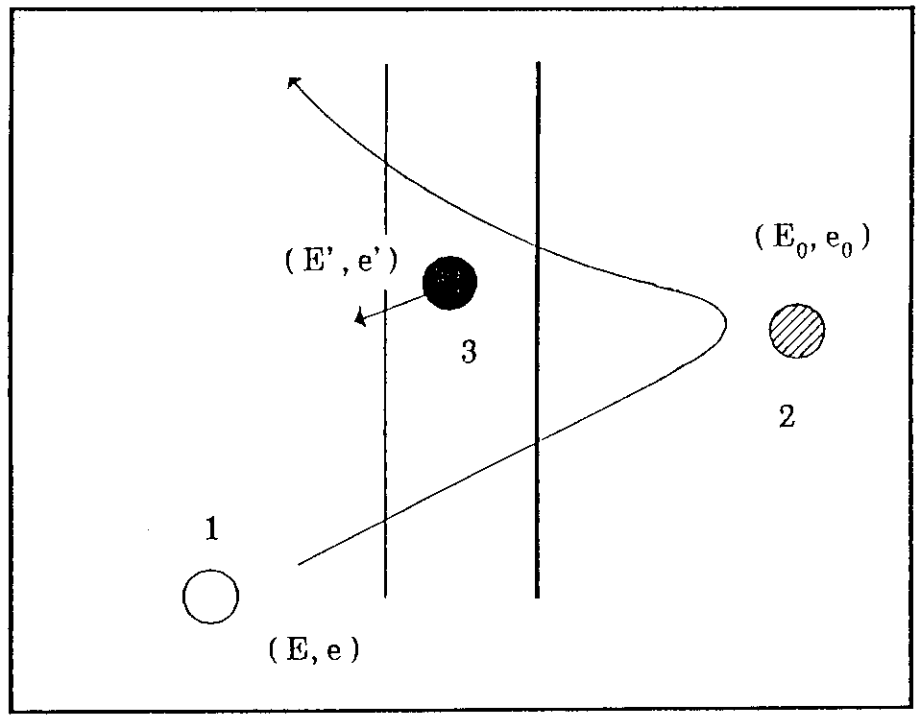

Fig. 3 Process (B) in ion impact desorption

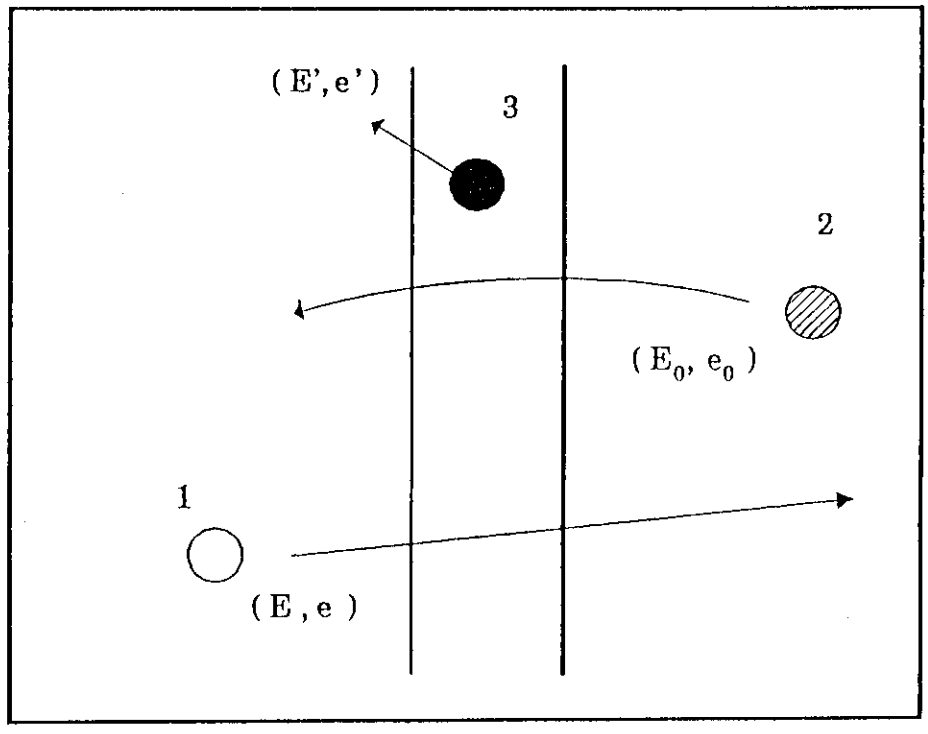

Fig. 4 Process (C) in ion impact desorption

2.3 Binding energy of adatom

In the preceeding section, it is shown that the binding energies U_2 and U_3 are very important parameters for estimation of desorption cross sections. Most of adsorption states, investigated in IID experiments, are the ones of chemisorption where typical binding energies between adatom and surface atom are several electron volts. The binding energies of molecularly adsorbed gases are lower than those of dissociatively adsorbed gases. Since the binding energies cannot be measured directly, they are usually estimated from the heat of vaporization or the surface energies. The binding energies for adsorbates are found to be generally lower than those for substrate atoms and have been estimated using the heat of adsorption. For the dissociative adsorption of A_2 molecule, the binding energy between adatom and surface atom can be related to the dissociation energy of the molecule D_{A_2} and the heat of adsorption Q,

$$(D_{A_2} + Q)/2 \ . \tag{2.25}$$

The dissociation energy for some gases relevant to this study D_{A_2} is shown in Table 2. Equation (2.25) is justified only for the case of either adsorption on clean surface, namely initial adsorption or adsorption where adatom binds to surface atom with two bonds, $M_S + A_2 \rightarrow 2M_S\text{-}A$, where M_S stands for a surface atom. With substituting the experimental data on heat of adsorption, the binding energies can be calculated from eq. (2.25). The calculated values, however, scatter due to the diversity in experimental data, possibly arising from different surface structures and surface temperatures. It is known that measurements on initial adsorption are difficult. Adatoms have been found to have a tendency to occupy sites with a high symmetry and to adsorb in ordered overlayers with a periodicity related to that of the surface atoms. In this report, we use eq. (2.25) for an estimation of the binding energies for S_2 adsorption. For H_2, O_2 and N_2 adsorption, semiempirical methods are used, which are described below.

Miyazaki and Yasumori[5] proposed a semiempirical method of evaluating the surface atom-adatom binding energy and heat of dissociative chemisorption, based on Pauling's formulation[15] for atom-atom bond energy. They assumed that the single bond energy between surface-atom M_S and adatom A, $E_{M_S\text{-}A,S}$ is related to the single bond energy $E_{M\text{-}A,S}$ between isolated atoms M and A by introducing a parameter k

$$E_{M_S\text{-}A,S} = k\, E_{M\text{-}A,S} \ , \tag{2.26}$$

where the subscript S stands for a single bond. On the other hand, when a molecule A_2 is dissociatively adsorbed on a surface composed of atoms M, the heat of chemisorption Q is approximately given by

$$Q = -D_{A_2} + 2E_{M_S-A,n} , \tag{2.27}$$

where $E_{M_S-A,n}$ is the energy of multiple-bond of order n between surface atom M_S and atom A. The order n is taken as 2 for oxygen and 3 for nitrogen. With an approximate relation, $E_{M_S-A,n} = nE_{M_S-A,S}$, we can get from eqs. (2.26) and (2.27),

$$(Q + D_{A_2})/2n = E_{M_S-A,S} = k\, E_{M-A,S} . \tag{2.28}$$

The single bond energy $E_{M-A,S}$ in eq. (2.28) can be estimated by the Pauling-Eley[16] formula with energy unit in kcal/mole,

$$E_{M-A,S} = (E_{M-M} + E_{A-A,S})/2 + 23(X_M - X_A)^2 , \tag{2.29}$$

where X_M and X_A are the electronegativities of the metal atom M and adatom A, respectively. Some values of X_M and X_A are shown in Table 3. In eq. (2.29), then E_{M-M} is the energy of the bond between metal atoms and $E_{A-A,S}$ is the energy of single bond of a molecule. The single bond energy $E_{A-A,S}$ is shown in Table 2. The value of E_{M-M} is obtained by multiplying the bulk heat of sublimation of the metal by a factor which accounts for the multiple bonding in the bulk metal. This factor is 1/4 for body-centered cubic metals and 1/6 for the other metals[17]. Miyazaki and Yasumori[5] plotted the quantity in the left side of eq. (2.28) against $E_{M-A,S}$ in the cases of oxygen and nitrogen adsorption on transition d-metals. They found the left hand side of eq. (2.28) is proportional to $E_{M-A,S}$ in both cases.

Their method is here applied to other kinds of solids, on which the molecules O_2 and N_2 adsorb dissociatively. We use the experimental data on heat of chemisorption for evaporated metal films. The experimental values of Q we compiled from the literature are shown in Appendix for O_2 and N_2 adsorption. Figure 5 shows our results. The left hand side of eq. (2.28) is proportional to $E_{M-A,S}$ for both O_2 and N_2 adsorption. The proportional constant, k in eq. (2.28), is found to be 0.67. This means that the single bond energies E_{M_S-A} between surface atom and adatom are less by about 30% than $E_{M-A,S}$ expected from eq. (2.29). Then the surface binding energy U_3 can be obtained from a relation,

$$0.67nE_{M-A,S} \ , \tag{2.30}$$

with known values of $E_{M-A,S}$.

For hydrogen adsorption[18], the heat of adsorption is given with energy unit in kcal/mole by,

$$q = E_{M-M} + 46.12(X_{M,S} - X_H)^2 \ , \tag{2.31}$$

where $X_{M,S}$ is the electronegativity of "solid" metals. $X_{M,S}$ is always lower than that of the corresponding isolated atom X_M which is shown in Table 3, and can be derived from a work function Φ, i.e., $X_{M,S} = 0.318\ \Phi$[19]. Using these relations, Trasatti[20] calculated the heat of adsorption and obtained results in satisfactory agreement with the experimental data for hydrogen adsorption on polycrystalline metal which are given in Appendix. A comparison of calculated q and experimental data on heat of hydrogen adsorption is shown in Fig. 6 which indicates that q has a roughly linear dependence on the experimental data except a few elements. The heat of adsorption obtained from this linear dependence is substituted into eq. (2.25) to get the binding energy. For CO adsorption, the binding energy may be roughly the same as the heat of adsorption because most of IID experiments on CO have been concerned with its molecular adsorption. The compiled data on heat of adsorption for CO and S_2 molecules are also shown in Appendix, together with for O_2 and N_2 adsorption. The binding energies obtained from above mentioned procedures are listed in Table 4.

Table 2 Dissociation energy and single bond energy of some gases in kcal/mol

Gases	Dissociation Energy D_{A_2}	Single Bond Energy $E_{A\text{-}A,S}$ *)
H_2	104.2	104.2
N_2	226.0	38
O_2	118	33.2
S_2	102	50.9
CO	256	84.0
NO	151	
CO_2	384	

*) L. Pauling; The Nature of the Chemical Bond (Cornell University Press, Ithaca, 1960).

Table 3 Work function and electronegativity of some element

Element	Work Function (eV) *)	Electronegativity**)
H		2.1
N		3.0
O		3.5
S		2.5
Ti	4.10	1.5
Cr	4.40	1.6
Mn	3.90	1.5
Fe	4.65	1.8
Co	4.70	1.8
Ni	4.73	1.8
Cu	4.70	1.9
Nb	4.20	1.6
Mo	4.30	1.6
Rh	4.80	2.2
Pd	5.00	2.2
Ta	4.22	1.5
W	4.55	1.7
Pt	5.40	2.2

*) S. Trasatti; J. Chem. Soc. Faraday Trans I, 68, 229-236 (1972).

**) L. Pauling; The Nature of the Chemical Bond (Cornell University, Ithaca, 1960).

Table 4 Binding energies for some adsorbate/substrate combinations

Adsorbate	Substrate	Binding state	Binding energy (eV)	Remark
N	Fe poly		5.53	1)
	Mo poly		6.51	1)
	W poly		7.35	1)
	W (110)	β_2	6.61	1)
	W (110)		6.61	1)
O	Si poly		5.41	1)
	Ti poly		6.85	1)
	Fe poly		5.54	1)
	Ni poly		5.32	1)
	Cu poly		4.82	1)
	Mo poly		6.09	1)
	Mo (110)		6.00	2)
	SiC		4.35	1)
	TiC		5.02	1)
S	Ni sponge		3.41	4)
	Ni poly		5.00	2)
	Mo (110)		3.34	4)
	Mo (110)		4.77	5)
	Mo (110)		4.12	5)
	Mo (110)		5.16	6)
	Mo (110)		4.60	2)
	Mo (111)		4.85	6)
Cl	W (100)		4.2	2)

Table 4 (continued)

Adsorbate	Substrate	Binding state	Binding energy (eV)	Remark
H	Ni poly		2.97	7)
	Ni poly		1.50	2)
	Ni (111)		2.74	8)
	Ni (100)		3.04	8)
	Mo poly		3.40	7)
	Mo (110)		1.50	2)
	Mo (100)	β_3	2.82	8)
	W poly		3.40	7)
	W (100)	β_2	2.99	6)
	W (110)	β_1	2.95	8)
	W (110)	β_1	2.80	8)
	W (111)	β_4	3.04	8)
D	SS316		0.5	9)
CO	Ti poly		6.72	10)
	Ni poly		1.82	10)
	Ni poly		1.30	2)
	Ni (100)		1.30	11)
	Ni (111)		1.17	11)
	Mo poly		3.25	10)
	Mo (100)	α	1.30	11)
	Mo (100)	β_1	2.70	11)
	Mo (100)	β_2	3.40	11)
	Mo (110)		3.00	2)

Table 4 (continued)

Adsorbate	Substrate	Binding state	Binding energy (eV)	Remark
CO	Rh poly		2.08	10)
	Rh (110)		1.30	12)
	SS304	α	0.9	13)
	SS304	β	1.55	13)
	SS304	γ	1.96	13)
	SS316L	α	1.2	13)
	SS316L	β	1.7	13)
	SS316L	γ	2.2	13)
S	SS316		0.5	

The binding energies used in the calcualtions are underlined.

1) From eq. (2-29) and (2-30).

2) A. Sagara, K. Akashi, K. Kamada and A. Miyahara; "ISS Studies on Sputtering of Chemisorbed Gases by Low-Energy Ions" J. Nucl. Mater. 103&104, 357 - 362 (1981).

3) B. Biedermann and H.W. Wassmuth; "Reaction- and Desorption Kinetics of Strontium and Chlorine on a Tungsten Surface" in Proc. 7th Intern. Vac. Conger. & 3 rd Intern. Conf. Solid Surfaces edited by R. Dobrozemsky et al. (F. Berger & Sohne, Vienna, 1977) p1097-1100.

4) From eq. (2-25) and Table A_5 in Appendix.

5) M.H. Farias, A.J. Gellman and G.A. Somorjai; "The CO Coadsorption and Reaction of Sulfer, Hydrogen and Oxygen on Clean and Suffided Mo (100) and MoS_2 (0001) Crystal Faces" Surf. Sci. 140, 181 - 196 (1984).

Table 4 (Continued)

6) Th. Baldinger and E. Bechtold; "Adsorption of Sulfer on a Molybdenum Field Emitter" Surf. Sci. 159, 406 - 424 (1985).

7) From eqs. (2-25) and (2-31) and Figure 6.

8) From eq. (2-25) and Table A_3 in Appendix.

9) R. Bastasz and L.G. Haggmark; "Ion Impact Desorption and Hydrogen Release" J. Nucl. Mater. 103&104, 499 - 502 (1981).

10) From eq. (2-25) and Table A_4 in Appendix.

11) L.D. Schmidt; "Chermisorption: Aspects of the Experimental Situation" in " Interactions on Meatal Surfaces " edited by R. Gomer (Springer, Berlin, 1975) p63 - 100.

12) R.A. Marbow and R.M Lambert; "Chemisorption, Surface Structure Chemistory, and Electron Impact Properties of Carbon Monoxide on Rhodium (110)" Surf. Sci. 67, 489 - 500 (1977).

13) A. Mathewson, R. Calder, A. Grillot and P. Verbeek; "Thermal Desorption of CO from Some Stainless Steels" in Proc. 7th Intern. Vac. Conger. & 3rd Intern. Conf. Solid Surfaces edited by R. Dobrozemsky et al. (F. Berger & Sohne, Vienna, 1977) p1027 - 1030.

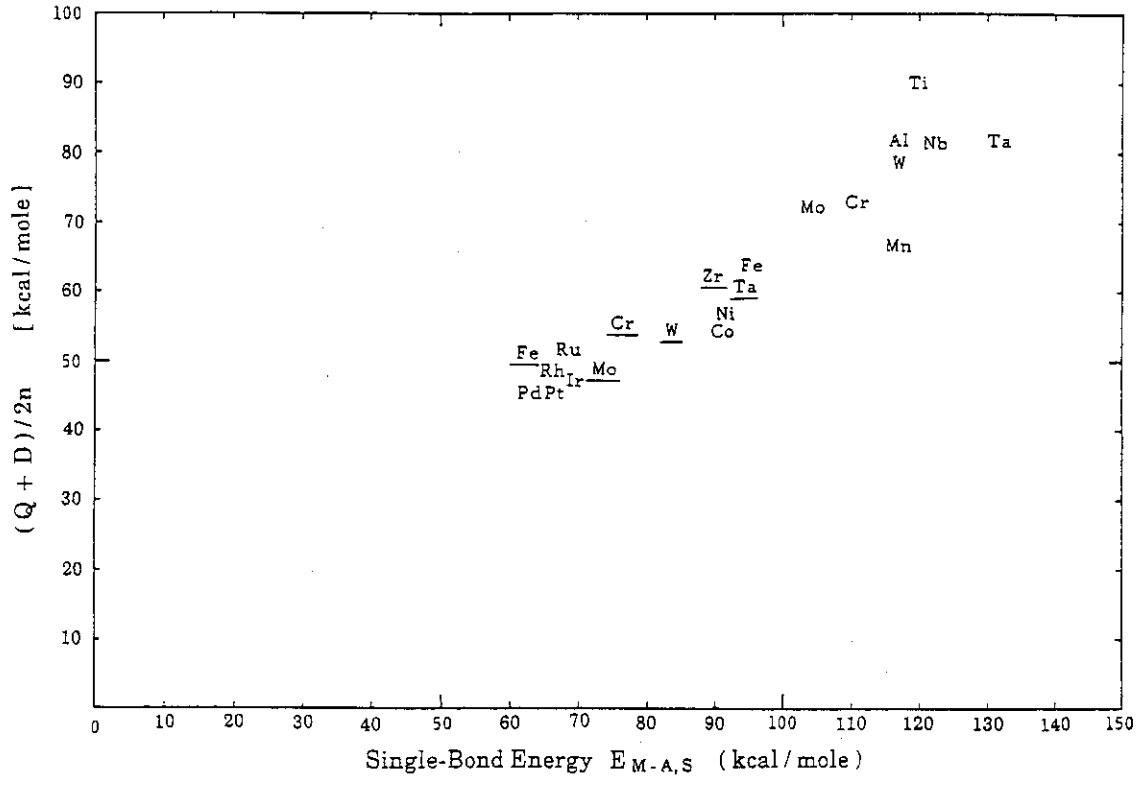

Fig. 5 Adsorption of O_2 and N_2 on various elements. The underline stands for N_2 adsorption.

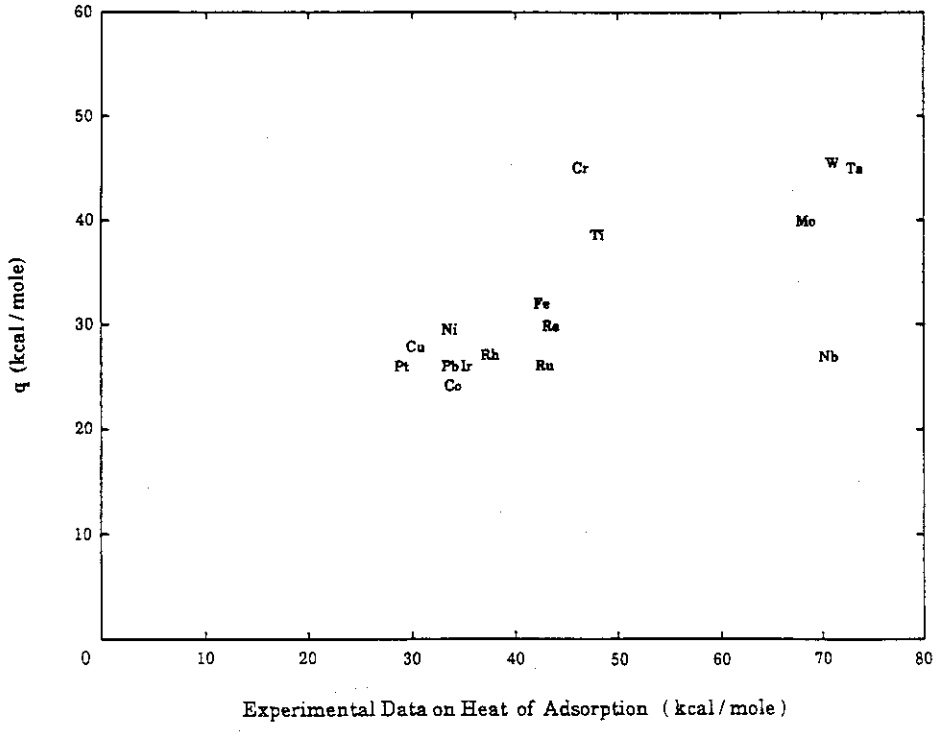

Fig. 6 Comparison of calculated and experimental data on heat of H_2 adsorption

2.4 Reflection of ions from solid surfaces

When a solid is bombarded with ions, some of the ions are backscattered from the surface. Others penetrate the target and lose energy due to collisions with target atoms and electrons. Some of the penetrating particles change in the direction of their motion by single or multiple collision and finally leave the target surface. This process is called reflection and its quantitative treatment is of great importance in the present day fusion technology. As well known, the reflection process of H_2, D_2 and H_3 from the wall of fusion devices is one of the processes determining the balance of particles and energy in plasma. In this section only brief summary, which is necessary to discuss the mechanisms of desorption, is described. The reader is referred to a few reviews[21,22] for detailed discussions of reflection processes, i.e., the reflection coefficients, the distributions in charge, and the angle and energy of the reflected particles.

The energy and angular-distributions of reflected particles are usually measured in a specific solid angle at definite exit angle and often only for the charged particles. The measured distributions are thus by no means characteristic of the total reflected fluxes. More systematic researches have often been given by computer simulations which provide the general characteristics of energy and angular distributions of reflected light ions for keV incident ions. The energy distribution depends strongly on incident energy. At low energies only a single peak with an energy characteristic of a single collision is observed, the energy of the peak being shifted to lower energies relative to the incident energy as the incident energy increases. At high incident energies, a broader energy spectrum can be observed, which indicates that the ions penetrate the target and lose a wide range of energies. The spectrum measured is cut off at lower energies because of the increasing probability of neutralization. At high energies, the spectrum shows a monotonous decrease because of the decrease of neutralization probability with energy. The energy distributions also depend on target materials to show spectra different in shape and height at the same incident energy and at normal incidence. On the other hand, the angular distributions also depend on various parameters. For normal incidence, the distribution is a cosine distribution except at higher energies and at small exit angles. At large angles of incidence, the distribution becomes strongly peaked around the direction corresponding to specular reflection. It is impossible to describe these dependerces in an analytical form.

We can define the particle reflection coefficient by the energy and angular distributions $f(E,e,E_0,e_0)$,

$$R(E,e) = N/N_0 = \int dE_0\ de_0\ f(E,e,E_0,e_0), \tag{2.32}$$

where N and N_0 are numbers of the reflected and incident particles respectively. The function $f(E,e,E_0,e_0)$ is roughly approximated by eq. (2.13) when the energy distribution of incident particles is a Maxwellian distribution and the angular distribution of incident particles is isotropic[3]. The particle reflection coefficients R(E,e) have been directly measured with various experimental methods. But there are the same difficulties in measurement as those for energy and angle distributions.

Eckstein and Verbeek[3] obtained the reflection coefficients of hydrogen and helium isotopes on iron and nickel targets by computer simulation. They have proposed, through a curve fitting, an analytical experession for the reflection coefficients for normal incidence over a wide range of reduced energies,

$$R(E,1) = [(1+3.2116\varepsilon^{0.34334})^{3/2}+(1.3288\varepsilon^{3/2})^{3/2}]^{-2/3} \tag{2.33}$$

with

$$\varepsilon = E/E_{TF} = [M_2/(M_1+M_2)][a_{12}\ E/(Z_1Z_2e^2)]. \tag{2.34}$$

where Z_1, M_1 and Z_2, M_2 are the nuclear charges and masses of the incident particle and target atoms, respectively, and E_{TF} is the Thomas Fermi energy in the center-of-mass system for a head-on collision (see Table 5). The value of R(E,1) approaches 1 as the energy decreases and is proportional to $E^{-3/2}$ in the energy range $10 \leqq \varepsilon \leqq 10^2$. These features are in reasonable agreement with the data of theoretical and experimental results. For non-normal incidence, it was reported[23] that the reflection coefficient R(E,e) is roughly approximated by substituting $\varepsilon(\cos\theta)^2$ for ε in eq. (2.33). It can be expected from eq. (2.33) that the reflection coefficients decrease with increase of the incident energy and increase with increase of atomic number of targets. The available data for the reflection coefficients have been found to be in reasonable agreement with this relation. In the case of non-normal incidence, the reflection coefficient R(E,e) is a little larger than that for normal incidence. The results calculated from eq. (2.33) are listed in Tables 6~10 as a function of projectile energy for various ion-

target combinations. Figures 7 and 8 show the reflection coefficients for Ni and Mo targets.

Table 5 Thomas-Fermi energy E_{TF} (keV) for ion-target combinations*)

Target	H^+	D^+	$^3He^+$	$^4He^+$	Ne^+	Ar^+	Xe^+
Si	1.16	1.20	2.59	2.67	23.92	66.83	591.39
Ti	2.05	2.09	4.42	4.50	33.98	85.68	642.45
Fe	2.54	2.59	5.43	5.51	39.88	97.63	694.18
Ni	2.80	2.84	5.95	6.05	43.08	104.46	728.91
Cu	2.93	2.97	6.20	6.30	44.09	105.57	777.77
Mo	4.54	4.58	9.85	9.95	63.93	143.34	848.23
Rh	5.16	5.21	10.75	10.85	68.83	152.75	881.83
W	9.86	9.92	20.28	20.39	119.2	246.75	1189.9

*) $E_{TF} = (1 + M_1/M_2)(Z_1 Z_2 e^2 / a_{TF})$

$= 30.75(1 + M_1/M_2)[Z_1 Z_2 (Z_1^{2/3} + Z_2^{2/3})^{1/2}]$ (eV)

Table 5 (continued)*)

Compound	Z_2^c	M_2^c	H^+	D^+	$^4He^+$	Ne^+	Ar^+
SiC	10	20.05	0.77	0.80	1.84	18.78	56.19
TiC	14	29.96	1.16	1.20	2.65	23.27	64.38
SS304[1)]	25.766	55.272	2.52	2.56	5.46	39.54	97.01
SS316[2)]	26.178	56.272	2.57	2.61	5.56	40.12	98.12

*) This table lists E_{TF} for some composite materials with average atomic number Z_2^c and mass M_2^c:

$$E_{TF} = 30.75(1 + M_1/M_2^c)[Z_1 Z_2^c (Z_1^{2/3} + Z_2^{c\,2/3})^{1/2}] \quad (eV)$$

$$M_2^c = (x M_A + y M_B)/(x+y), \quad Z_2^c = (x Z_A + y Z_B)/(x+y) \quad \text{for } A_x B_y$$

1) SS304: Fe(68.35%) + C(0.02%) + Mn(1.50%) + Si(0.6%) + Cr(18.33%) + Ni(11.2%)

2) SS316: Fe(66.5%) + C(0.1%) + Mn(2.2%) + Si(0.4%) + Cr(16.4%) + Ni(12.2%) + Mo(2.2%)

Table 6 Reflection coefficients of H^+ ions for various targets

Energy (eV)	Ni	Ti	TiC
50		0.5271	0.4781
100	0.4942	0.4676	0.4189
200	0.4348	0.4086	0.3612
300	0.4006	0.3748	0.3281
400	0.3766	0.3512	0.3046
500	0.3582	0.3330	0.2862
600	0.3433	0.3181	0.2710
700	0.3307	0.3055	0.2578
800	0.3199	0.2946	0.2461
900	0.3103	0.2848	0.2354
1000	0.3016	0.2760	0.2257
1200	0.2866	0.2605	0.2083
1400	0.2737	0.2471	0.1929
1600	0.2624	0.2350	0.1791
1800	0.2522	0.2241	0.1667
2000	0.2428	0.2141	0.1555
2200	0.2342	0.2048	0.1452
2400	0.2262	0.1961	0.1358
2600	0.2186	0.1880	0.1273
2800	0.2115	0.1803	0.1195
3000	0.2047	0.1731	0.1123
3500	0.1892	0.1567	0.0969
4000	0.1754	0.1423	0.0843
4500	0.1629	0.1297	0.0741
5000	0.1516	0.1185	0.0656

Table 7 Reflection coefficients of He^+ ions for various targets

Energy (eV)	Ni	Mo	Rh	W
50	0.6177	0.6571	0.6638	0.7099
100	0.5601	0.6017	0.6088	0.6586
200	0.5008	0.5435	0.5509	0.6033
300	0.4660	0.5088	0.5162	0.5695
400	0.4414	0.4840	0.4915	0.5451
500	0.4224	0.4649	0.4723	0.5260
600	0.4071	0.4493	0.4567	0.5104
700	0.3941	0.4361	0.4435	0.4971
800	0.3830	0.4248	0.4321	0.4857
900	0.3733	0.4148	0.4222	0.4755
1000	0.3646	0.4060	0.4133	0.4665
1200	0.3496	0.3907	0.3980	0.4509
1400	0.3371	0.3779	0.3851	0.4377
1600	0.3262	0.3669	0.3740	0.4264
1800	0.3166	0.3572	0.3643	0.4164
2000	0.3080	0.3486	0.3557	0.4076
2200	0.3002	0.3408	0.3479	0.3996
2400	0.2930	0.3337	0.3408	0.3923
2600	0.2864	0.3272	0.3342	0.3856
2800	0.2802	0.3211	0.3282	0.3795
3000	0.2745	0.3155	0.3226	0.3738
3500	0.2613	0.3029	0.3100	0.3611
4000	0.2497	0.2920	0.2991	0.3501
4500	0.2392	0.2822	0.2894	0.3405
5000	0.2296	0.2734	0.2806	0.3319

Table 8 Reflection coefficients of Ne^+ ions for various targets

Energy (eV)	Ni	Cu	Mo	Rh
50	0.7602	0.7617	0.7840	0.7883
100	0.7142	0.7158	0.7410	0.7459
200	0.6633	0.6650	0.6928	0.6982
300	0.6315	0.6333	0.6624	0.6681
400	0.6082	0.6101	0.6400	0.6458
500	0.5898	0.5917	0.6222	0.6281
600	0.5746	0.5765	0.6073	0.6134
700	0.5616	0.5635	0.5947	0.6007
800	0.5503	0.5522	0.5835	0.5879
900	0.5402	0.5422	0.5737	0.5799
1000	0.5312	0.5332	0.5648	0.5710
1200	0.5156	0.5176	0.5493	0.5556
1400	0.5023	0.5043	0.5362	0.5425
1600	0.4909	0.4929	0.5248	0.5311
1800	0.4807	0.4827	0.5147	0.5210
2000	0.4717	0.4737	0.5056	0.5120
2200	0.4635	0.4655	0.4974	0.5038
2400	0.4560	0.4580	0.4899	0.4963
2600	0.4492	0.4512	0.4831	0.4894
2800	0.4429	0.4449	0.4767	0.4830
3000	0.4370	0.4390	0.4708	0.4771
3500	0.4239	0.4259	0.4575	0.4639
4000	0.4126	0.4146	0.4461	0.4524
4500	0.4027	0.4047	0.4361	0.4424
5000	0.3939	0.3959	0.4271	0.4334

Table 9 Reflection coefficients of Ar^+ ions for various targets

Energy (eV)	Ti	Ni	Cu	Mo	W
50	0.8006	0.8112	0.8118	0.8273	0.8523
100	0.7599	0.7721	0.7727	0.7906	0.8198
200	0.7138	0.7275	0.7282	0.7485	0.7820
300	0.6845	0.6990	0.6998	0.7214	0.7573
400	0.6628	0.6779	0.6787	0.7011	0.7387
500	0.6455	0.6609	0.6617	0.6848	0.7236
600	0.6310	0.6467	0.6476	0.6711	0.7109
700	0.6186	0.6346	0.6354	0.6594	0.6999
800	0.6078	0.6239	0.6247	0.6490	0.6902
900	0.5981	0.6143	0.6152	0.6397	0.6815
1000	0.5893	0.6057	0.6066	0.6313	0.6736
1200	0.5741	0.5907	0.5915	0.6167	0.6597
1400	0.5611	0.5778	0.5787	0.6041	0.6477
1600	0.5498	0.5666	0.5675	0.5930	0.6372
1800	0.5398	0.5566	0.5575	0.5833	0.6278
2000	0.5307	0.5477	0.5486	0.5744	0.6193
2200	0.5226	0.5395	0.5404	0.5664	0.6115
2400	0.5151	0.5321	0.5330	0.5591	0.6044
2600	0.5082	0.5253	0.5262	0.5523	0.5978
2800	0.5019	0.5189	0.5198	0.5460	0.5917
3000	0.4959	0.5130	0.5139	0.5401	0.5860
3500	0.4827	0.5997	0.5006	0.5269	0.5830
4000	0.4712	0.4882	0.4891	0.5154	0.5618
4500	0.4611	0.4781	0.4790	0.5053	0.5518
5000	0.4521	0.4691	0.4700	0.4963	0.5428

Table 10 Reflection coefficients of Xe^+ ions for various targets

Energy (eV)	Fe	Mo	W
50	0.8903	0.8982	0.9083
100	0.8648	0.8742	0.8865
200	0.8344	0.8457	0.8602
300	0.8143	0.8266	0.8426
400	0.7989	0.8120	0.8291
500	0.7863	0.8000	0.8180
600	0.7756	0.7898	0.8085
700	0.7662	0.7809	0.8001
800	0.7579	0.7730	0.7927
900	0.7504	0.7658	0.7860
1000	0.7436	0.7592	0.7798
1200	0.7315	0.7476	0.7689
1400	0.7210	0.7375	0.7594
1600	0.7116	0.7285	0.7509
1800	0.7033	0.7204	0.7432
2000	0.6957	0.7131	0.7363
2200	0.6887	0.7064	0.7299
2400	0.6823	0.7001	0.7239
2600	0.6767	0.6943	0.7184
2800	0.6707	0.6889	0.7132
3000	0.6654	0.6838	0.7084
3500	0.6536	0.6722	0.6973
4000	0.6431	0.6621	0.6875
4500	0.6338	0.6529	0.6788
5000	0.6253	0.6447	0.6709

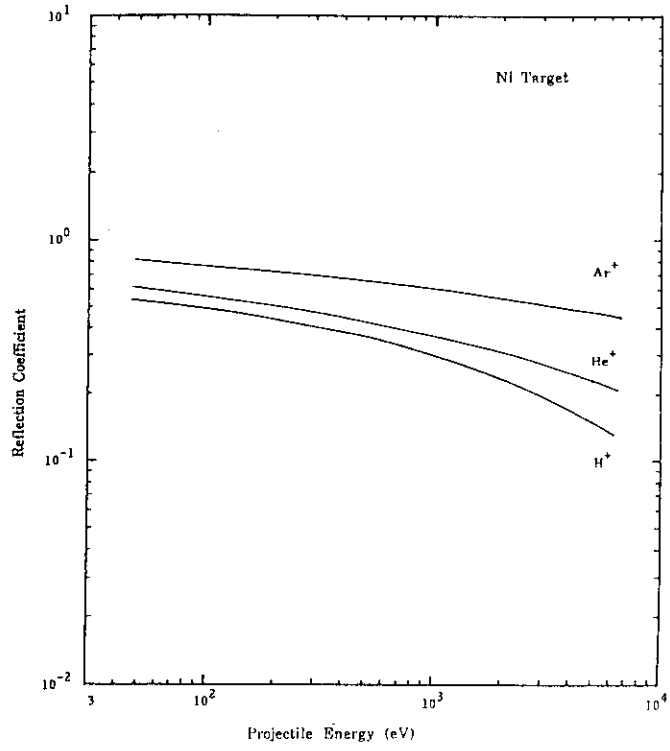

Fig. 7 Reflection Coefficients of H^+, He^+ and Ar^+ ions

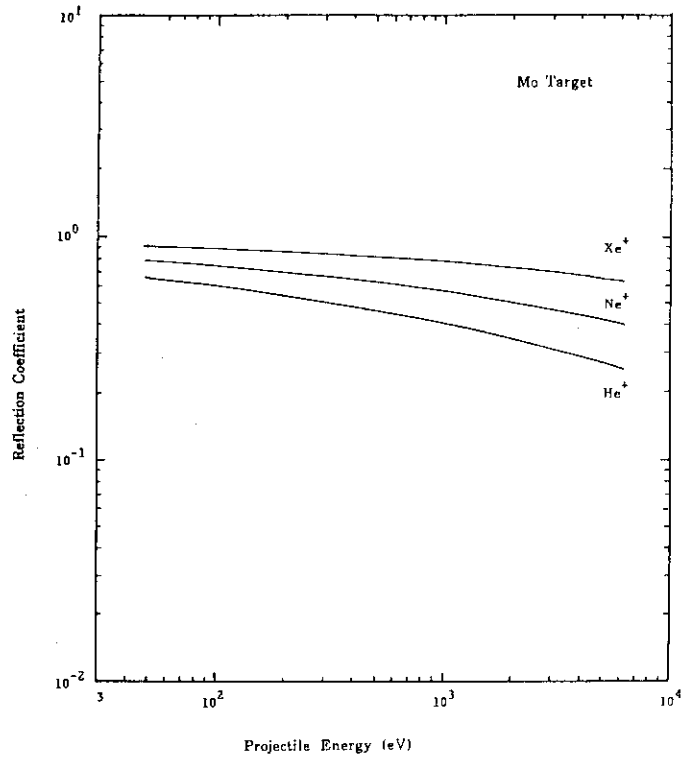

Fig. 8 Reflection Coefficients of He^+, Ne^+ and Xe^+ ions

2.5 Sputtering

Sputtering has been widely studied both for the physical understanding of the collisional processes involved and for various practical reasons such as sputter surface cleaning, high resolution depth profiling (SIMS) and plasma-wall interaction problems in fusion devices. There are many reports[24~26] written from various points of view. A comprehensive and detailed theory of sputtering has been given by Sigmund[12,27,28]. The theory is based on random collision processes which are described by a linearized Boltzman equation, and enables us to predict the details of sputtering and absolute sputtering yields as a function of incident energy. It is a consequence of the theory that the sputtering yield is directly proportional to the deposited energy at the solid surfaces. The deposited energy is proportional to the nuclear stopping cross section $S_n(E)$. Then the sputtering yield at normal incidence $Y(E,0)$ can be written by

$$Y(E,0) = [0.042/U_2]\ a(M_2/M_1)S_n(E)\ , \tag{2.35}$$

where $a(M_2/M_1)$ is a function of mass ratio between target M_2 and projectile M_1 and U_2 the surface binding energy. Derivations of universal expressions[29,30] for sputtering yield have been attempted on the basis of eq. (2.35). The universal behaviour is due to the fact that the energy dependence of $S_n(E)$ can be described by a universal function $s_n(\varepsilon)$ depending only on reduced energy ε,

$$S_n(E) = r_{12}\ \pi\ a_{12}^2\ E_{TF}\ s_n(\varepsilon), \tag{2.36}$$

where $s_n(\varepsilon)$ is common to all projectile-target combinations. An analytical expression[30] for $s_n(\varepsilon)$ has been published and approximates to the exact numerical results[11] within a few percents.

$$s_n(\varepsilon) = [3.441\varepsilon^{1/2}\ln(\varepsilon+2.718)]/[1+6.355\varepsilon^{1/2}+\varepsilon(6.882\varepsilon^{1/2}-1.708)]. \tag{2.37}$$

Equation (2.35) has been applied to a number of practical cases. The agreement with experimental data for heavy ions is fairly good in many cases. However, it has been found that eq. (2.35) is only valid for heavy ion sputtering at energies well above the threshold energy. For heavy ion sputtering at low energies as well as light-ion sputtering, a significant fraction of the total yield is found to be due to backscattered ions[31,32].

In the last few years, several modification[33,34] of eq. (2.35) have been made in order to cover light ion and also low-energy heavy ion sputtering. Bohdansky[4] has derived an expression for normal incidence which shows good agreement with experimental data at ion energies below 5 keV.

$$Y(E,0) = [0.042/U_2]\, a(M_2/M_1)[R_p/R]\, S_n(E) g(\varepsilon'), \tag{2.38}$$

where R_p/R is the ratio of projected range R_p to average path length R and given by

$$R_p/R = K(M_2/M_1) + 1, \tag{2.39}$$

which means a surface-correction term, i.e., the average number of surface crossings. This term is introduced to get the correct deposited energy for a real surface, which is obtained roughly from dividing $aS_n(E)$ by R/R_p. In eq. (2.39), then K is only a weak function of ε with an average value $K = 0.4$ if inelastic collisions are not taken into account. In eq. (2.38), a function of $g(\varepsilon')$ is introduced in order to modify eq. (2.35) in the threshold region;

$$g(\varepsilon') = (1 - \varepsilon'^{-2/3})(1 - \varepsilon'^{-1})^2, \tag{2.40}$$

with $\varepsilon' = E/E_{th}$ where E_{th} is the threshold energy for sputtering. The threshold energy is sometimes obtained from experimental data by linear extrapolation of the yield-versus-energy curve to zero yield[35]. It is found that sputtering yields for different ion-target combinations at low energies have a similar energy dependence and are expressed by a normalized function. By use of this function, normalized threshold energies E_{th}/U_2 for 16 different target materials are derived and plotted as a function of M_1/M_2. The threshold energies E_{th} obtained are shown in Table 11. With use of eq. (2.36), then eq. (2.38) can be written as follows,

$$Y(E,0) = Q\, S_n(\varepsilon) g(\varepsilon'), \tag{2.41}$$

where Q depends only on masses of projectile and target and is independent of projectile energy,

$$Q = (0.042/U_2)\, a^*\, r_{12}\, \pi\, a_{12}^2\, E_{TF}, \tag{2.42}$$

with $a^* = a(R_p/R)$. The values of a^* are read from the graph published by Bohdansky[34] and are shown in Table 11, with the values of U_2. Sputtering yields calculated from eq. (2.41) are shown in Fig. 9 for tungsten target and in Tables 12~16 for various targets.

The sputtering yields also depend on the angle of incidence in a complicated way. Theoretical investigations[12] on angular dependence of sputtering yields show $(\cos\theta)^{-f}$ dependence at not-too-oblique incidence, where $1 \leq f \leq 2$. Most of the experimental data for not-too-oblique incidence show that the yield increases to a maximum at 70° ~ 80° with $(\cos\theta)^{-1}$ dependence and then decreases to zero at glancing incidence. The angle which gives the maximum, shifts to higher values with increase of incident energy. An empirical formula for incident-angular dependence has been obtained[36]. In this report, the sputtering yield is approximated by

$$S(E,e) = Y(E,0)(\cos\theta)^{-1} \tag{2.43}$$

The energy and angular distributoins of sputtered particles have also been widely investigated. Measured energy spectra for heavy-ion sputtering are found to obey approximately the predicted inverse square relation in the energy range between U_2 and incident energy. Furthermore, there is a maximum in the distribution at an energy close to the surface binding energy. However, it is known that the energy spectrum shows in its tail some deviations from an E^{-2} dependence which is predicted by the theory. This deviation is considered to be due to the anistropy of the momentum distribution of the sputtered particles. Such effect is important in light-ion and non-normal sputtering and can be considered to cause the spectrum to be either sharper of flatter than the inverse square dependence. The angular distribution of sputtered atoms is predicted to obey a cosine law for amorphous targets at normal incidence. An "over-cosine" distributoin is, however, found for the case where the mass of the projectile is smaller than that of the target. It is known in this case that the contribution from reflected particles to sputtering is dominant. Many experimental data for non-normal incidences show disagreement with a cosine law, some being "under-cosine" and others being "over-cosine". Computer simulations show that primary recoils contribute predominantly to sputtering in cases where large deviations from the cosine distribution are found. However, the modification of the distribution function may not play an important role in the present calculations of desorption cross sections.

Table 11 Parameters for sputtering yield

Ion	Target	α^*	U_2(eV)	E_{th}
Xe^+	Fe	0.20	4.28	45.5
	Ni	0.21	4.44	46.4
	Mo	0.24	6.82	49.8
	W	0.32	8.90	70.3
Ar^+	Ti	0.28	4.85	33.5
	Ni	0.32	4.44	31.1
	Cu	0.32	3.49	27.9
	Mo	0.43	6.82	33.4
	W	0.42	8.90	37.4
	TiC	0.24	5.02	44.2
	SiC	0.21	4.35	43.9
	SS304	0.3	4.32	30.9
Ne^+	Ni	0.44	4.44	25.8
	Cu	0.43	3.49	35.2
	Mo	0.51	6.82	29.3
	Rh	0.5	5.75	30.2
	W	0.52	8.90	31.2
	SS304	0.46	4.32	24.6

Table 11 (continued)

Ion	Target	α^*	U_2 (eV)	E_{th}
He^+	Ti	0.42	4.85	47.5
	Ni	0.61	4.44	22.2
	Mo	0.52	6.82	40.9
	Rh	0.53	5.75	46.0
	W	0.35	8.90	102.4
	SS304	0.56	4.32	23.1
$^3He^+$	W	0.58	8.90	151.3
D^+	TiC	0.75	5.02	27.8
	SiC	0.71	4.35	19.6
	SS304	0.53	4.32	34.6
H^+	Ti	0.42	4.85	47.5
	Ni	0.40	4.44	48.8
	TiC	0.73	5.02	45.6
	SS316	0.47	4.33	66.9
	SS304	0.47	4.32	66.7

Table 12 Sputtering yields of H^+ ions incident on various targets

Energy (eV)	Ni ×0.1	Ti ×0.1	TiC ×0.1
50		*.****	*.****
100	0.0142	0.0163	0.0153
200	0.0575	0.0618	0.0667
300	0.0869	0.0914	0.0994
400	0.1067	0.1105	0.1194
500	0.1206	0.1235	0.1318
600	0.1307	0.1325	0.1396
700	0.1383	0.1390	0.1445
800	0.1440	0.1436	0.1474
900	0.1484	0.1469	0.1490
1000	0.1517	0.1492	0.1496
1200	0.1562	0.1517	0.1490
1400	0.1586	0.1523	0.1469
1600	0.1596	0.1519	0.1442
1800	0.1597	0.1507	0.1410
2000	0.1592	0.1490	0.1377
2200	0.1583	0.1471	0.1344
2400	0.1570	0.1450	0.1311
2600	0.1556	0.1428	0.1279
2800	0.1539	0.1406	0.1249
3000	0.1522	0.1383	0.1219
3500	0.1477	0.1327	0.1151
4000	0.1431	0.1274	0.1089
4500	0.1386	0.1224	0.1035
5000	0.1345	0.1178	0.0986

Table 13 Sputtering yields of He^+ ions incident on various targets

Energy (eV)	Ni	Mo	Rh	W
50	0.0137	0.0002	*.****	*.****
100	0.0503	0.0082	0.0071	*.****
200	0.0956	0.0266	0.0276	0.0003
300	0.1217	0.0392	0.0424	0.0027
400	0.1392	0.0481	0.0532	0.0060
500	0.1518	0.0549	0.0614	0.0093
600	0.1614	0.0603	0.0679	0.0122
700	0.1690	0.0646	0.0732	0.0149
800	0.1751	0.0682	0.0775	0.0172
900	0.1801	0.0713	0.0814	0.0193
1000	0.1843	0.0739	0.0846	0.0211
1200	0.1906	0.0781	0.0899	0.0243
1400	0.1950	0.0814	0.0941	0.0269
1600	0.1982	0.0840	0.0974	0.0291
1800	0.2004	0.0861	0.1000	0.0310
2000	0.2018	0.0878	0.1022	0.0326
2200	0.2027	0.0892	0.1040	0.0341
2400	0.2032	0.0900	0.1055	0.0353
2600	0.2033	0.0912	0.1067	0.0364
2800	0.2031	0.0919	0.1078	0.0374
3000	0.2027	0.0925	0.1086	0.0383
3500	0.2010	0.0934	0.1101	0.0401
4000	0.2985	0.0938	0.1109	0.0415
4500	0.1957	0.0939	0.1112	0.0427
5000	0.1926	0.0937	0.1112	0.0435

Table 14 Sputtering yields of Ne^+ ions incident on various targets

Energy (eV)	Ni ×10	Cu ×10	Mo ×10	Rh ×10
50	0.0055	0.0014	0.0020	0.0020
100	0.0284	0.0217	0.0145	0.0156
200	0.0631	0.0620	0.0356	0.0393
300	0.0864	0.0907	0.0503	0.0560
400	0.1035	0.1123	0.0614	0.0686
500	0.1170	0.1293	0.0702	0.0787
600	0.1281	0.1433	0.0776	0.0870
700	0.1375	0.1552	0.0838	0.0942
800	0.1456	0.1655	0.0893	0.1004
900	0.1528	0.1745	0.0941	0.1060
1000	0.1592	0.1826	0.0984	0.1109
1200	0.1701	0.1964	0.1059	0.1195
1400	0.1792	0.2079	0.1122	0.1267
1600	0.1870	0.2177	0.1176	0.1330
1800	0.1938	0.2262	0.1224	0.1385
2000	0.1997	0.2337	0.1266	0.1434
2200	0.2050	0.2404	0.1304	0.1478
2400	0.2098	0.2464	0.1338	0.1517
2600	0.2141	0.2518	0.1369	0.1553
2800	0.2180	0.2567	0.1398	0.1587
3000	0.2216	0.2612	0.1424	0.1617
3500	0.2293	0.2710	0.1482	0.1685
4000	0.2357	0.2790	0.1531	0.1742
4500	0.2411	0.2858	0.1572	0.1791
5000	0.2457	0.2916	0.1609	0.1833

Table 15 Sputtering yields of Ar^+ ions incident on various targets

Energy (eV)	Ti ×10	Ni ×10	Cu ×10	Mo ×10	W ×10
50	0.0018	0.0034	0.0067	0.0017	0.0004
100	0.0214	0.0299	0.0430	0.0205	0.0094
200	0.0594	0.0782	0.0136	0.0576	0.0298
300	0.0869	0.1129	0.1464	0.0850	0.0457
400	0.1080	0.1394	0.1790	0.1063	0.0582
500	0.1249	0.1610	0.2054	0.1237	0.0686
600	0.1391	0.1790	0.2275	0.1384	0.0775
700	0.1513	0.1946	0.2466	0.1511	0.0852
800	0.1619	0.2082	0.2634	0.1623	0.0922
900	0.1714	0.2204	0.2783	0.1724	0.0984
1000	0.1799	0.2314	0.2918	0.1815	0.1041
1200	0.1947	0.2506	0.3154	0.1975	0.1141
1400	0.2073	0.2669	0.3355	0.2111	0.1228
1600	0.2181	0.2811	0.3530	0.2231	0.1305
1800	0.2277	0.2937	0.3684	0.2337	0.1373
2000	0.2362	0.3049	0.3823	0.2433	0.1435
2200	0.2439	0.3151	0.3948	0.2520	0.1492
2400	0.2509	0.3243	0.4062	0.2599	0.1544
2600	0.2573	0.3328	0.4167	0.2672	0.1593
2800	0.2632	0.3407	0.4264	0.2740	0.1638
3000	0.2687	0.3480	0.4354	0.2803	0.1680
3500	0.2807	0.3641	0.4554	0.2944	0.1775
4000	0.2910	0.3780	0.4725	0.3065	0.1857
4500	0.2998	0.3900	0.4874	0.3172	0.1930
5000	0.3076	0.4006	0.5006	0.3267	0.1996

Table 16 Sputtering yields of Xe^+ ions incident on various targets

Energy (eV)	Fe ×10	Mo ×10	W ×10
50	*.****	*.****	*.****
100	0.0158	0.0105	0.0021
200	0.0666	0.0525	0.0328
300	0.1096	0.0898	0.0680
400	0.1450	0.1209	0.0994
500	0.1750	0.1474	0.1269
600	0.2011	0.1706	0.1513
700	0.2242	0.1912	0.1732
800	0.2450	0.2098	0.1930
900	0.2639	0.2268	0.2113
1000	0.2813	0.2424	0.2281
1200	0.3125	0.2705	0.2585
1400	0.3400	0.2953	0.2853
1600	0.3645	0.3175	0.3094
1800	0.3866	0.3376	0.3314
2000	0.4070	0.3561	0.3516
2200	0.4257	0.3732	0.3703
2400	0.4431	0.3891	0.3877
2600	0.4593	0.4040	0.4041
2800	0.4746	0.4179	0.4195
3000	0.4890	0.4331	0.4340
3500	0.5217	0.4613	0.4673
4000	0.5507	0.4880	0.4970
4500	0.5768	0.4121	0.5238
5000	0.6005	0.5341	0.5483

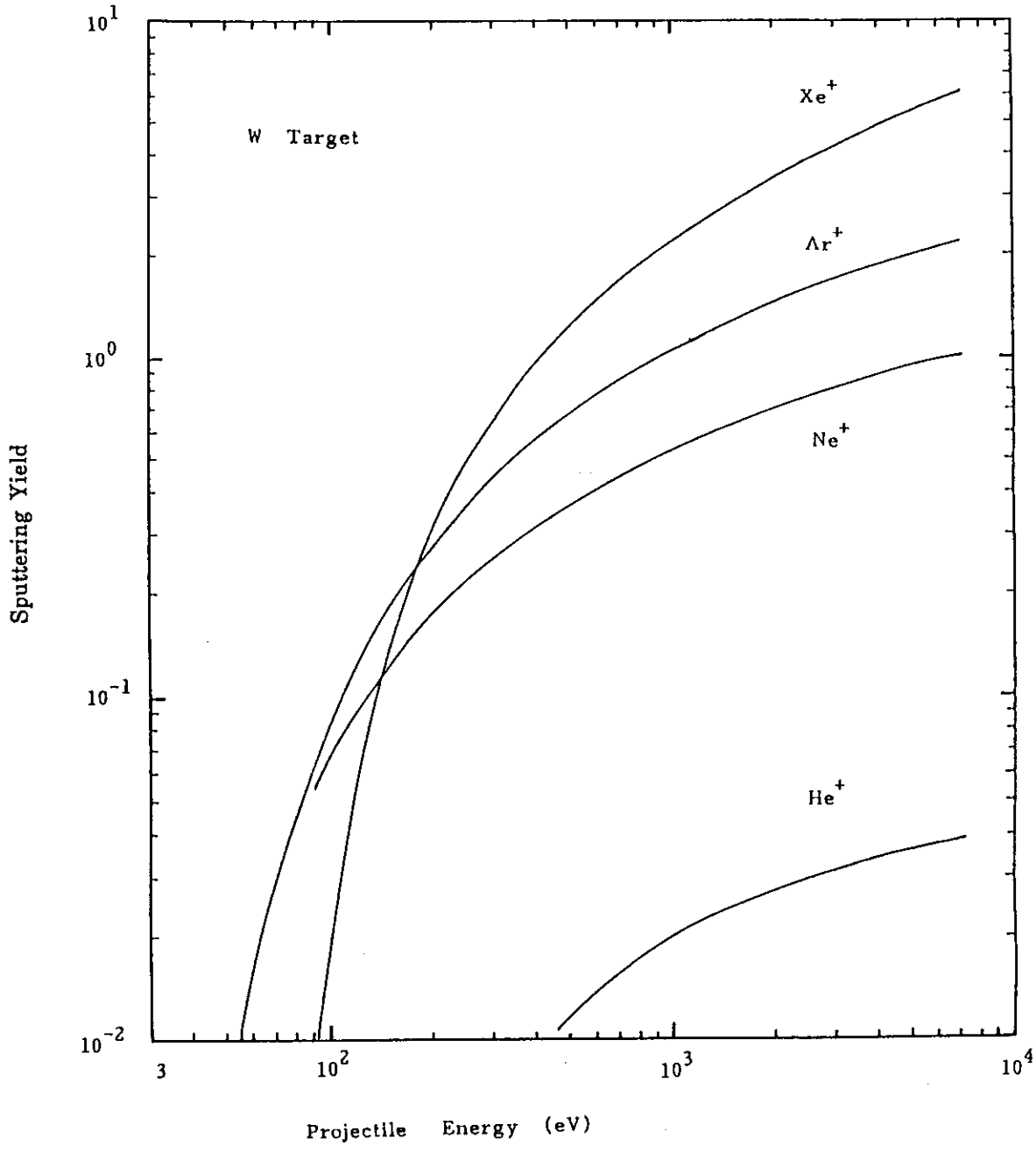

Fig. 9 Dependence of sputtering yield on projectile energy

3. Experimental data and comparison with theoretical model

3.1 Experimental data on desorption cross section

We have compiled the data on the desorption cross sections and yields for various adsorbate-target combinations. The compiled data have already been reported in a JAERI-M report[6]. Among the compiled data, we have chosen only the desorption cross sections and rearranged them as functions of projectile energy and projectile-ion species. The desorption cross sections for light ions are shown in Figs. 10 ~ 12. For light ions such as H^+, D^+ and He^+ ions, the desorption cross sections are in the range of 10^{-17} cm^2 except for a few cases corresponding to molecular adsorption and decrease slowly as the projectile energy increases in the energy range studied. In contrast, the desorption cross sections for heavier ions such as Ne^+, Ar^+ and Xe^+, which are an order of magnitude larger than those for light ions increase slowly with increasing energy as shown in Figs. 13 ~ 16. In cases of Ne^+ and Ar^+ ions, some of the desorption cross sections seem to have no dependence on projectile energy and costant in the energy region. Figures 17 ~ 22 show the cases where the desorption cross sections rapidly increase as the projectile energy increases regardless of projectile ion species. The desorption cross section has a maximum near a few thousand eV for a case where an oxygen atom adsorbs on Cu surfaces. Figure 23 shows the data which have been obtained in the low energy region. The desorption cross section shows an initial decrease as the projectile energy increases and then increases with increasing energy. Figure 24 shows dependence of desorption cross section on the angle of incidence θ relative to the surface normal. The solid curve shows $(\cos\theta)^{-1}$ distribution. In most cases, a maximum is found near 60°, the value of which is larger within a factor of 3 than the value measured at 20°. The variation of desorption cross section with incident angle is smaller than that of sputtering yield.

Judging from the experimental data in Figs. 11 ~ 22, the desorption cross section in the energy range studied is, in a first approximation, considered to have a linear dependence on projectile energy, when the desorption cross section is plotted against the projectile energy on log scales. Namely, the desorption cross section can be written as;

$$\sigma = Q_{exp} E^a \qquad (3.1)$$

where Q_{exp} and a are fitting parameters. These values of Q_{exp} and a are shown in Table 17.

Table 17 Values of a and Q_{exp} obtained from experimental data

Ion	Adsorabate	Substrate	a	Q_{exp}
H^+	O	Ti	-0.447	7.032×10^{-16}
	S	Ni (110)	1.632	5.266×10^{-22}
D^+	O	Si (111)	-0.887	9.512×10^{-14}
$^3He^+$	H	W(100)	1.786	3.209×10^{-21}
$^4He^+$	H	Mo (110)	-0.425	2.701×10^{-15}
	O	Ni (110)	-1.280	3.701×10^{-13}
	O	Mo (110)	-0.532	1.930×10^{-15}
	O	Mo poly	0.070	1.283×10^{-17}
	S	Ni (110)	0.566	1.839×10^{-17}
	S	Mo (110)	-0.384	1.284×10^{-15}
	CO	Ni (110)	1.150	4.391×10^{-19}
	CO	Ni poly	-0.240	2.665×10^{-15}
	CO	Mo(110)	-0.344	6.836×10^{-16}
	CO	Mo poly	0.754	2.188×10^{-19}
	CO	Rh (001)	0.942	1.591×10^{-18}
Ne^+	O	Ni (110)	2.050	3.128×10^{-22}
	O	Cu (110)	1.080	6.353×10^{-19}
	O	Mo (110)	0.204	1.538×10^{-16}

Table 17 (continued)

Ion	Adsorabate	Substrate	a	Q_{exp}
Ne^+	S	Ni poly	0.061	5.057×10^{-16}
	S	Ni single	2.050	2.325×10^{-21}
	S	Mo (110)	0.162	2.824×10^{-16}
	CO	Ni poly	0.084	1.288×10^{-15}
	CO	Rh (001)	2.356	1.094×10^{-22}
	CO	Mo (110)	0.066	4.493×10^{-16}
Ar^+	C	Ni (111)	2.938	7.545×10^{-25}
	N	Mo (100)	0.105	3.298×10^{-16}
	N	W (100)	-0.017	1.095×10^{-15}
	O	Ti	0.079	8.050×10^{-17}
	O	Ni (110)	0.929	7.617×10^{-18}
	O	Mo (110)	0.575	2.033×10^{-17}
	O	Cu (110)	0.830	1.002×10^{-17}
	S	Ni (110)	2.246	8.615×10^{-22}
	S	Mo (110)	0.296	1.507×10^{-16}
	Cl	Ni (111)	0.926	2.868×10^{-18}
	CO	Mo (110)	-0.017	1.097×10^{-15}
Xe^+	N	Mo (100)	0.392	5.738×10^{-17}
	N	W (100)	0.283	2.096×10^{-16}

Table 17 (continued)

Ion	Adsorbate	Substrate	a	Q_{exp}
H^+	O	TiC	-0.404	5.910×10^{-16}
	D	SS316	-0.606	5.120×10^{-15}
	S	SS316	-0.135	5.833×10^{-17}
	CO	SS304	-1.528	5.576×10^{-15}
D^+	O	SiC	-0.637	4.277×10^{-15}
	O	TiC	-0.916	3.141×10^{-14}
	CO	SS304	1.028	8.224×10^{-21}
$^4He^+$	CO	SS304	0.907	3.925×10^{-20}
Ne^+	CO	SS304	0.781	1.278×10^{-19}
Ar^+	O	SiC	0.035	4.871×10^{-16}
	O	TiC	0.231	8.565×10^{-17}
	CO	SS304	1.632	9.892×10^{-22}

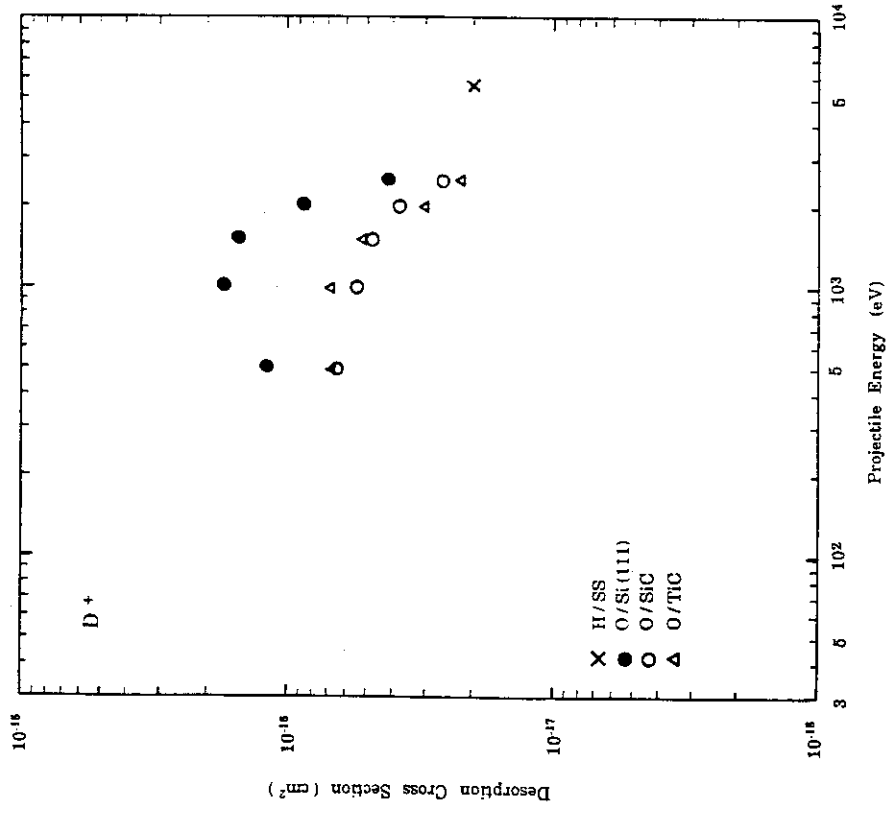

Fig. 11 Desorption cross section as a function of projectile energy

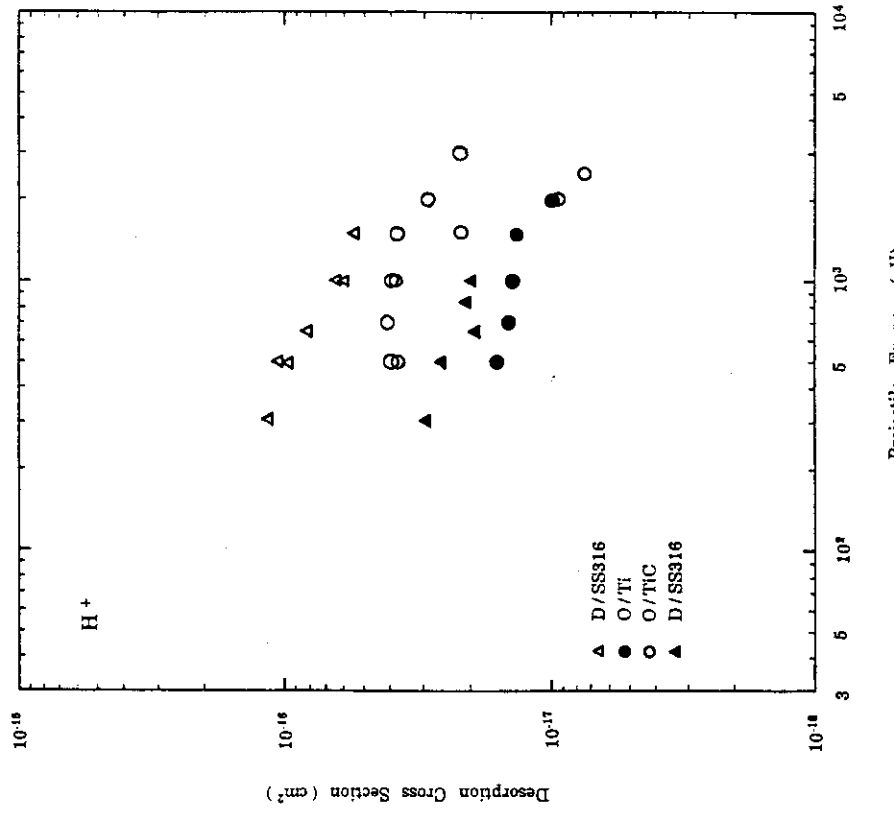

Fig. 10 Desorption cross section as a function of projectile energy

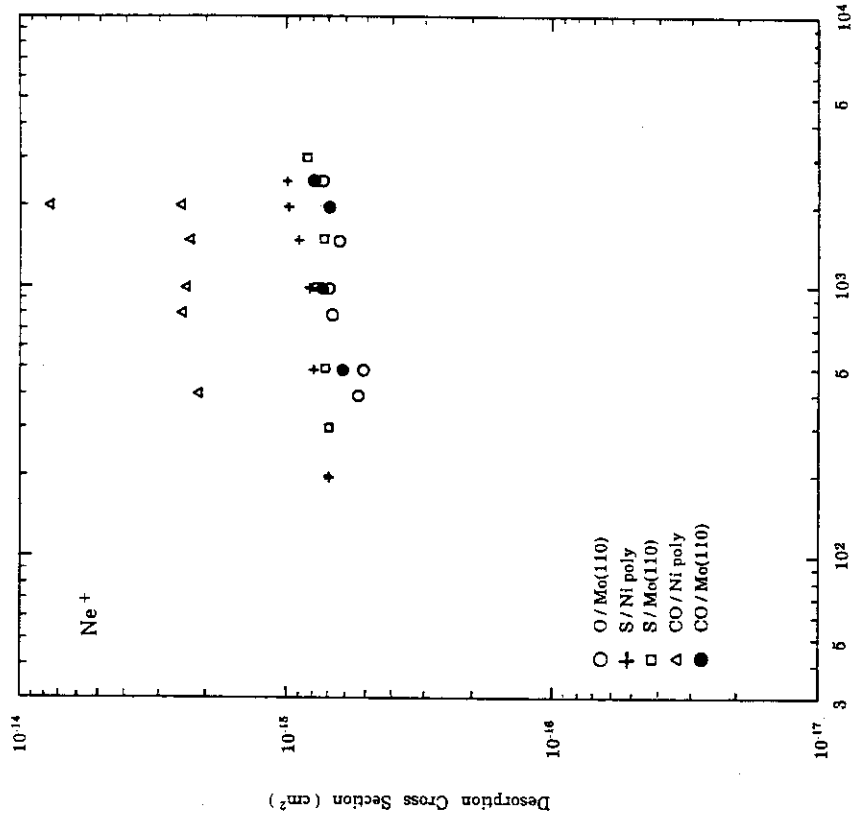

Fig. 13 Desorption cross section as a function of projectile energy

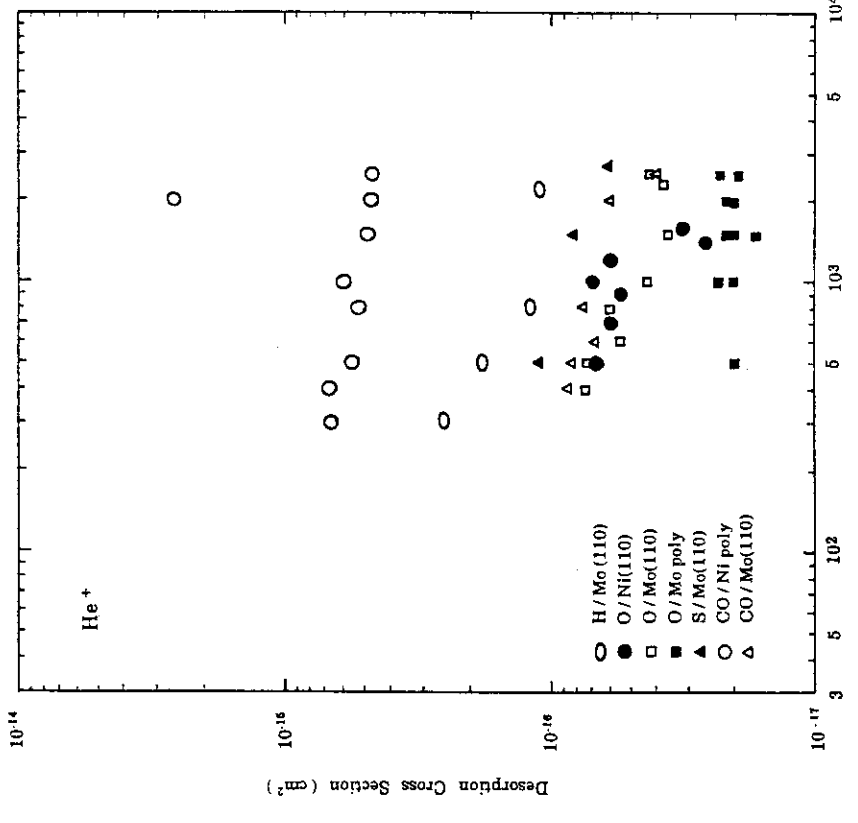

Fig. 12 Desorption cross section as a function of projectile energy

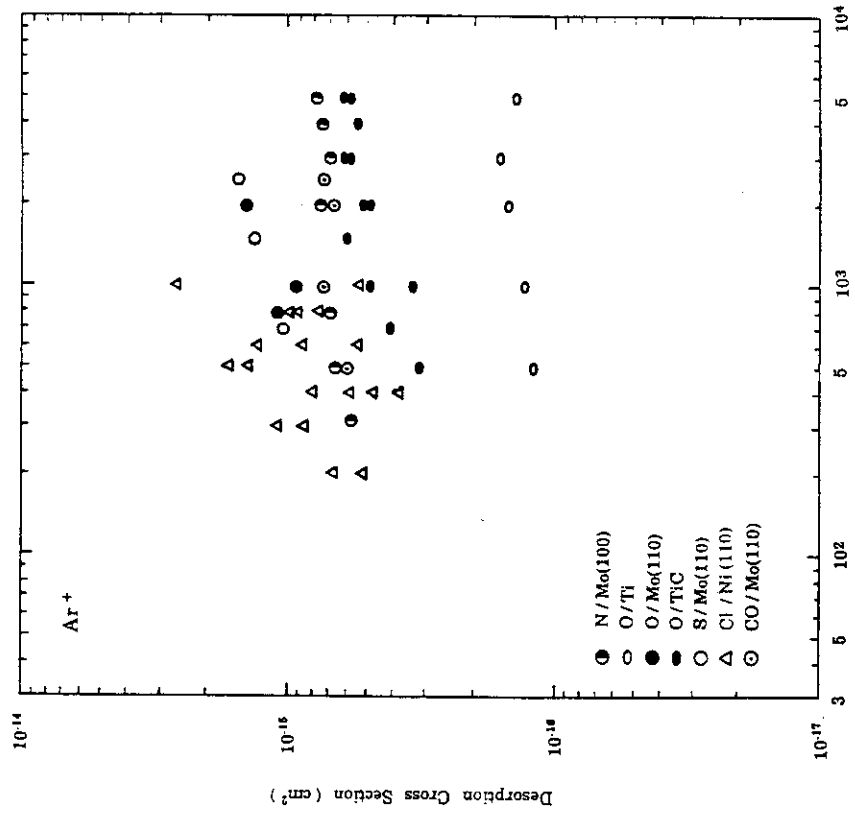

Fig. 15 Desorption cross section as a function of projectile energy

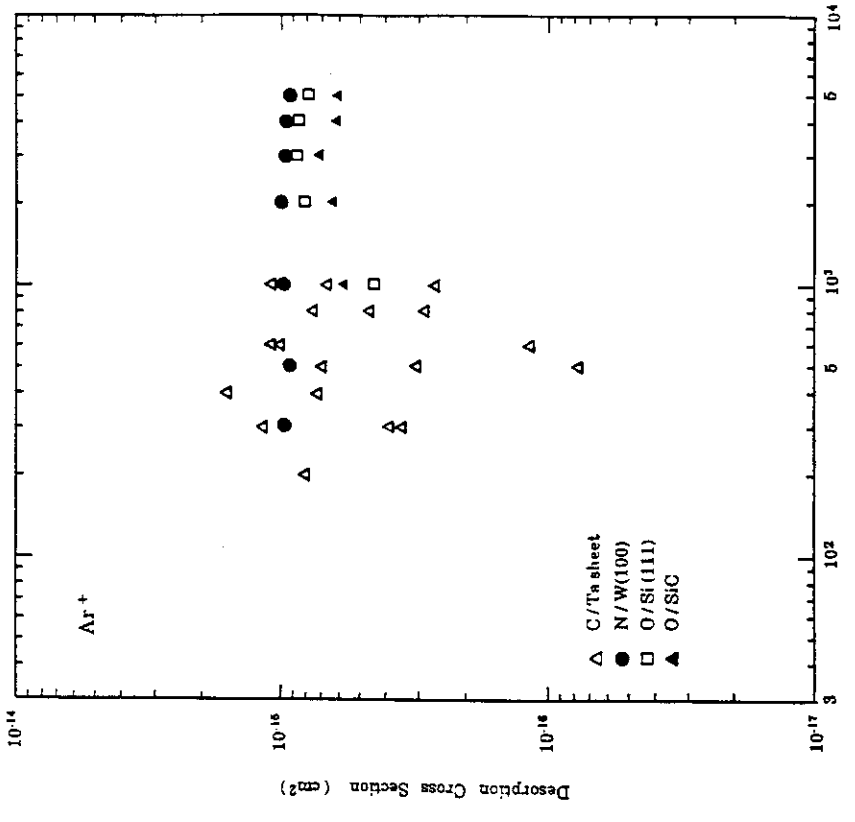

Fig. 14 Desorption cross section as a function of projectile energy

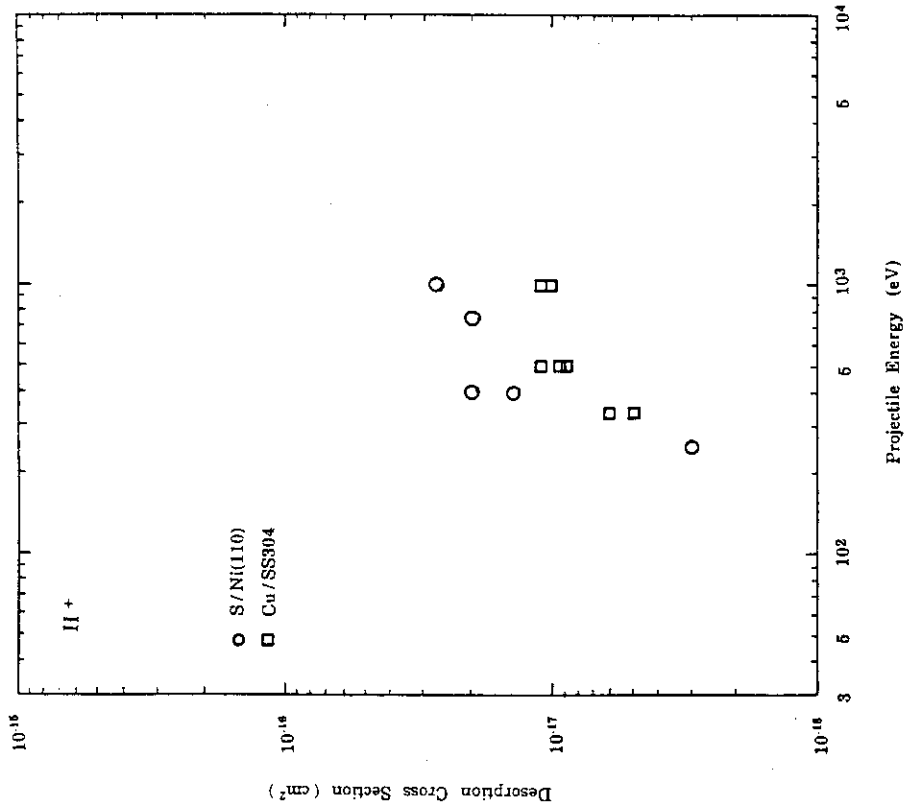

Fig. 17 Desorption cross section as a function of projectile energy

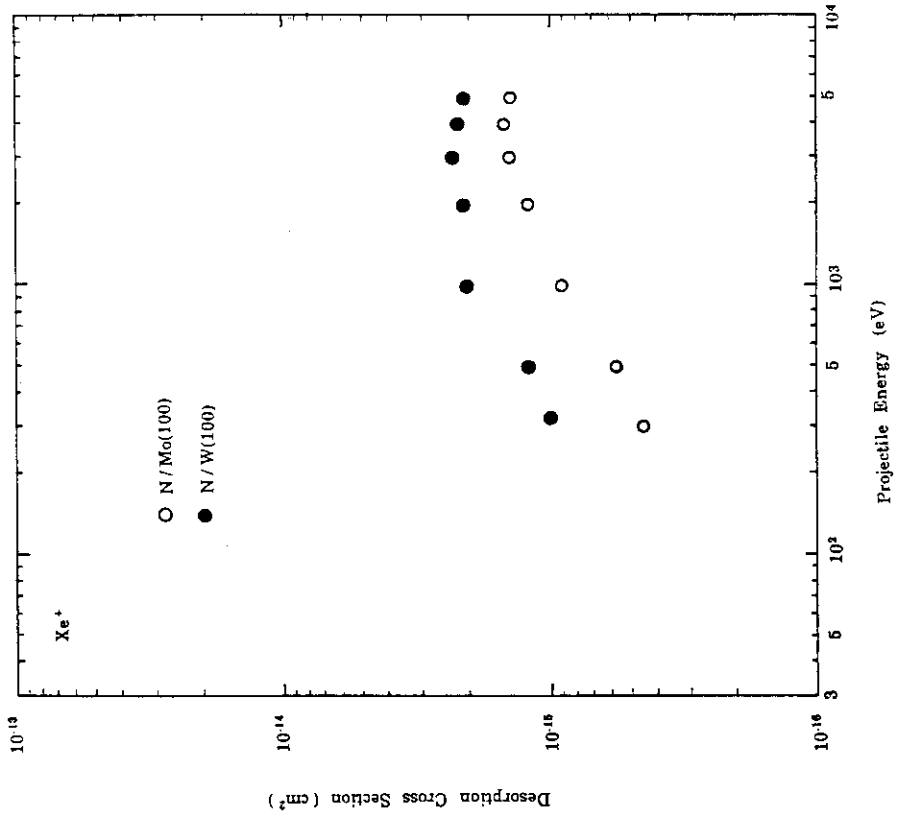

Fig. 16 Desorption cross section as a function of projectile energy

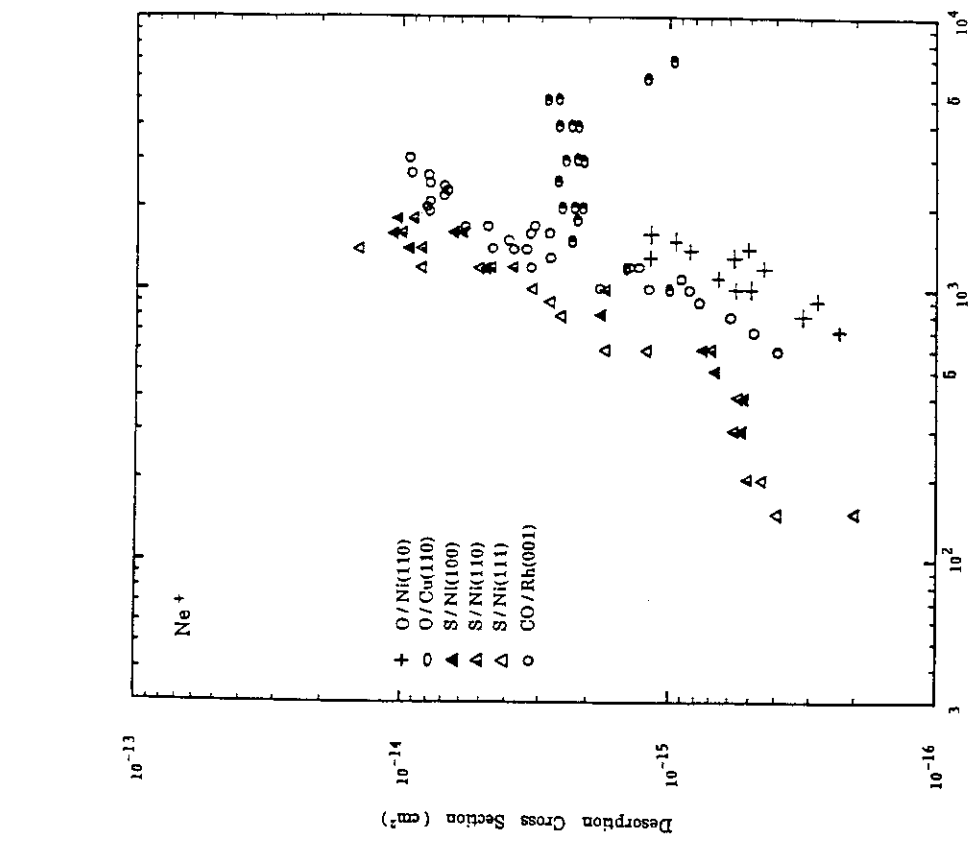

Fig. 19 Desorption cross section as a function of projectile energy

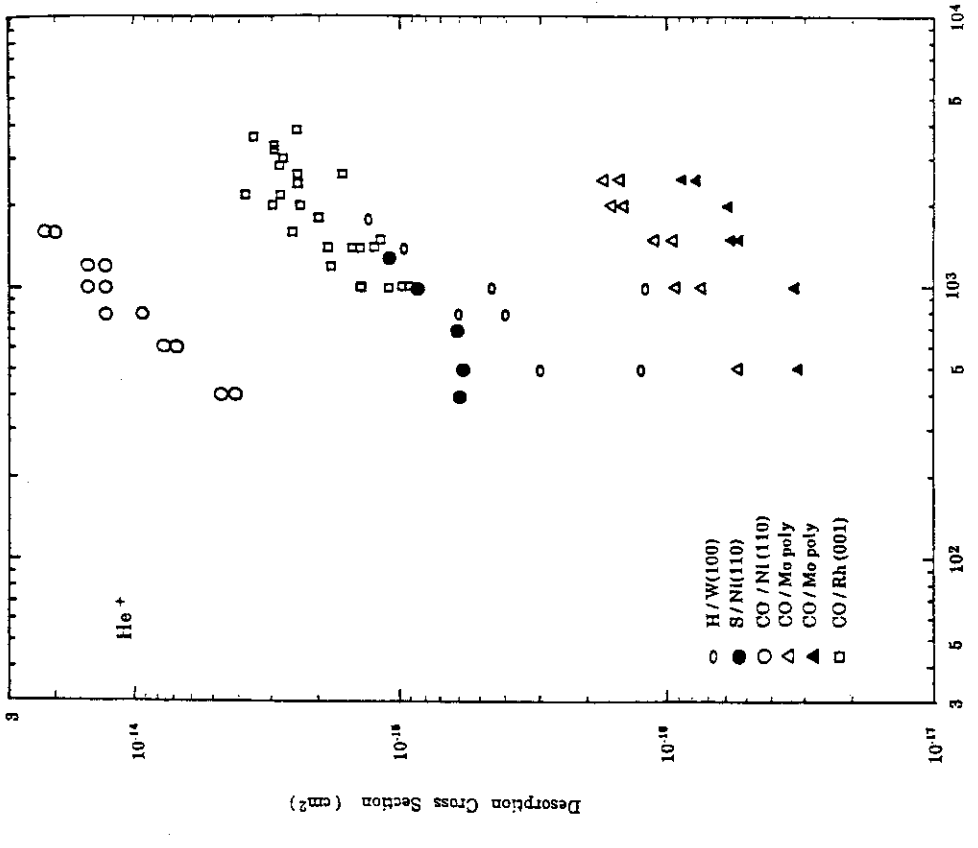

Fig. 18 Desorption cross section as a function of projectile energy

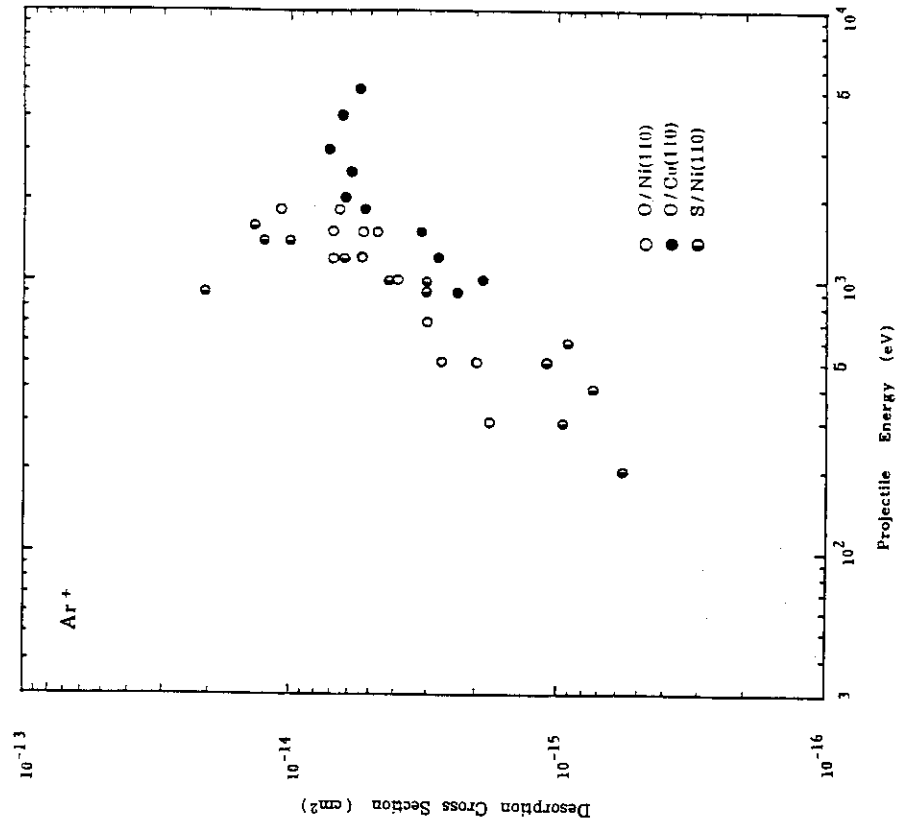

Fig. 21 Desorption cross section as a function of projectile energy

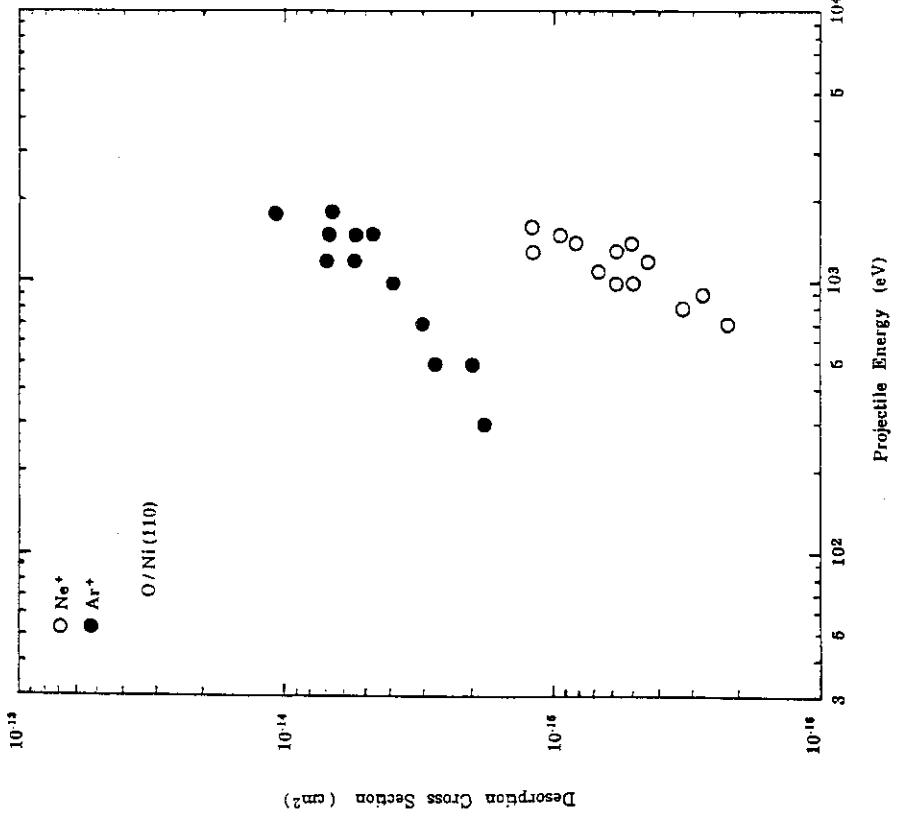

Fig. 20 Desorption cross section as a function of projectile energy

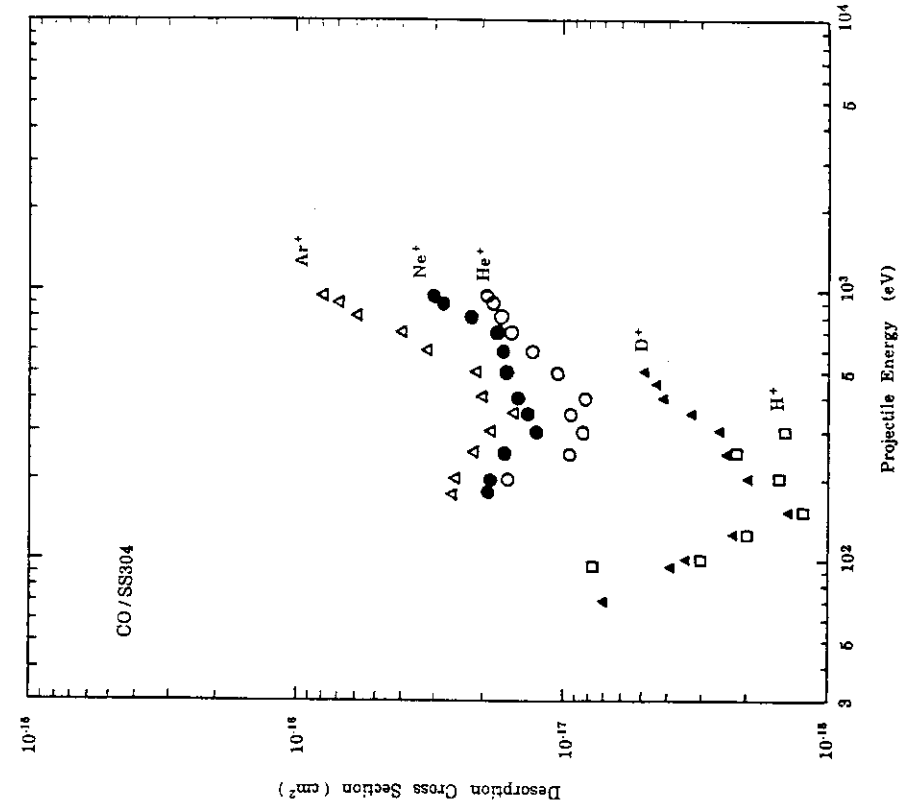

Fig. 23 Desorption cross section as a function of projectile energy

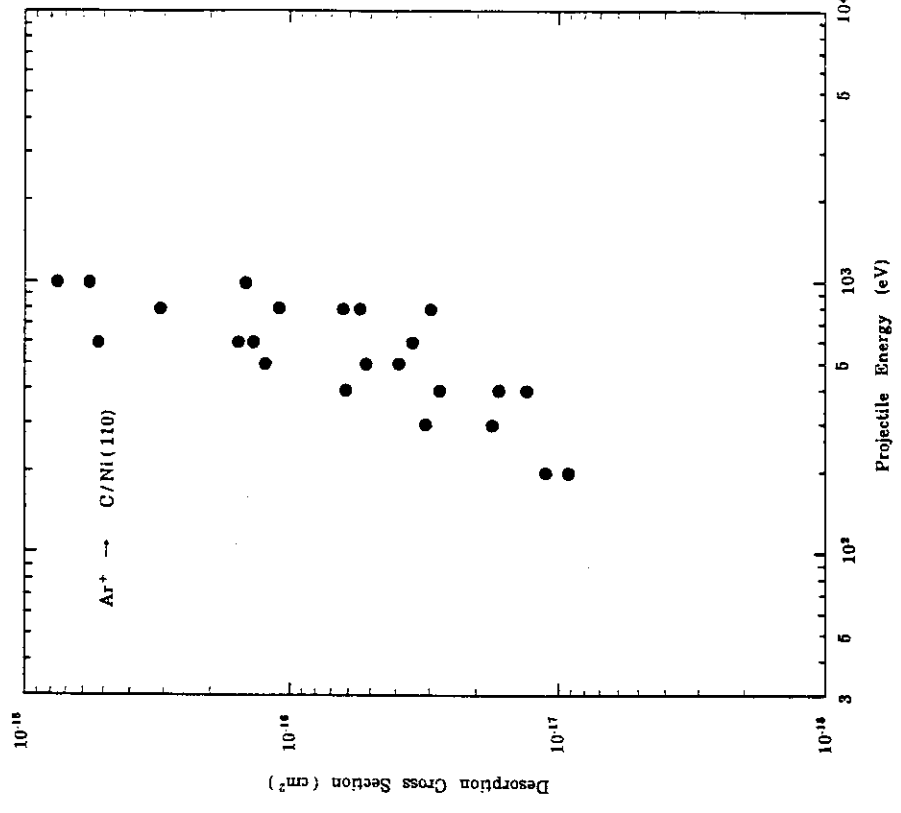

Fig. 22 Desorption cross section as a function of projectile energy

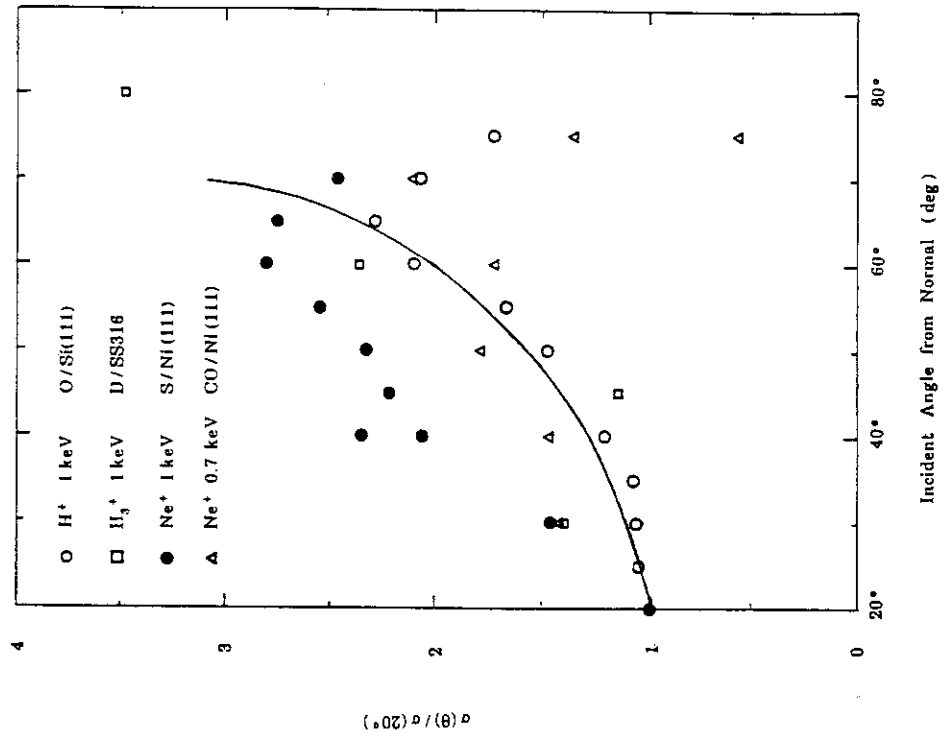

Fig. 24 Dependence on incident angle θ measured from surface normal

3.2 Comparisons with Winters and Sigmund's model

According to the Winters and Sigmund model[2], the total desorption cross section σ_D is given by the sum of cross sections for the processes (A), (B) and (C) which have already been discussed in section 2.2.

$$\sigma_D = \sigma_A + \sigma_B + \sigma_C \ . \tag{3.2}$$

Relative importance of three contributions is shown for the cases of D^+ and Ar^+ ions in Figs. 25 and 26. It is found that the contributions from σ_A and σ_B dominate for D^+ ion and low energy Ar^+ ion. Especially, the contribution from σ_B is very important for D^+ ion. As can be seen in eqs. (2.9) and (2.17), the desorption cross sections σ_A and σ_B depend on m_{13} and m, respectively, which are defined by interaction potential assumed. The large values of m_{13} and m tend to overestimate the contributions from σ_A and σ_B in the low energy region in comparison with experimental data. In the calculations of desorption cross sections, appropriate values of m_{13} and m have been chosen among the values in Table 1 by fitting the calculated results to the experimental data. The exponents m_{13} and m used in the calculations are shown in Table 18. It can be seen that the exponents for light ions are larger than those for heavier ions. This is a reasonable and predicted result. When appropriate fitting parameters of m_{13} and m cannot be found, mark (+ +) is used in the Table 18. About half of the experimental data are found to be explained by the model proposed by Winters and Sigmund. Comparisons of the calculated results with the experimental data are shown in Figs. 27 ~ 34 for light ions and in Figs. 35 ~ 47 for heavy ions. As can be seen from these figures, the dependences of calculated data on projectile energy agree well with those of experimental data in almost all cases although quantitative agreement is poor except for a few cases. Especially, the agreement is remarkably poor in the cases in Figs. 33, 37 and 40. These correspond to the cases marked by (+ +) in Table 18. It might be possible that in these cases different mechanisms may exist in the desorption process from Winters and Sigmund's theory.

Table 18 Exponents m_{13} and m used in the calculations of desorption cross section

Ion	Adsorabate	Substrate	m_{13}	m
H^+	O	Si (111)	1.0	1.0
	O	Ti	0.5	0.5
	S	Ni (110)	+ +	+ +
D^+	O	Si (111)	0.5	1.0
$^3He^+$	H	W(100)	+ +	+ +
$^4He^+$	H	Mo (110)	0.5	0.5*)
	O	Ni (110)	1.0	0.5
	O	Mo (110)	0.5	0.5
	O	Mo poly	0.5	0.5
	S	Ni (110)	+ +	+ +
	S	Mo (110)	0.5	0.5
	CO	Mo(110)	0.5	0.5
	CO	Ni poly	0.5	0.5
	CO	Ni (110)	+ +	+ +
	CO	Mo poly	+ +	+ +
	CO	Rh (001)	+ +	+ +
Ne^+	O	Ni (110)	+ +	+ +
	O	Cu (110)	+ +	+ +
	O	Mo (110)	0.055	0.055*)

*) Agreement with the experimental data is excellent.

Table 18 (continued)

Ion	Adsorabate	Substrate	m_{13}	m
Ne^+	S	Ni poly	0.0	0.191
	S	Ni single	++	++
	S	Mo (110)	0.0	0.055
	CO	Ni poly	0.191	0.191
	CO	Mo (110)	0.191	0.191
	CO	Rh (001)	++	++
Ar^+	C	Ni (111)	++	++
	O	Si (111)	0.0	0.055
	O	Ti	0.0	0.191
	O	Ni (110)	++	++
	O	Cu (110)	++	++
	O	Mo (110)	0.0	0.055
	N	W (100)	0.0	0.191
	N	Mo (100)	0.0	0.191
	S	Ni (110)	++	++
	S	Mo (110)	0.0	0.191
	CO	Mo (110)	0.0	0.333
Xe^+	N	Mo(100)	0.0	0.191
	N	W (100)	0.0	0.191

Table 18 (continued)

Ion	Adsorabate	Substrate	m_{13}	m
H^+	O	TiC	0.5	0.5
	D	SS316	0.5	0.5
	S	SS316	0.5	0.5
	CO	SS304	++	++
D^+	O	SiC	0.5	0.5
	O	TiC	0.5	0.5
	CO	SS304	++	++
$^4He^+$	CO	SS304	++	++
Ne^+	CO	SS304	++	++
Ar^+	O	SiC	0.191	0.055
	O	TiC	0.0	0.055
	CO	SS304	++	++

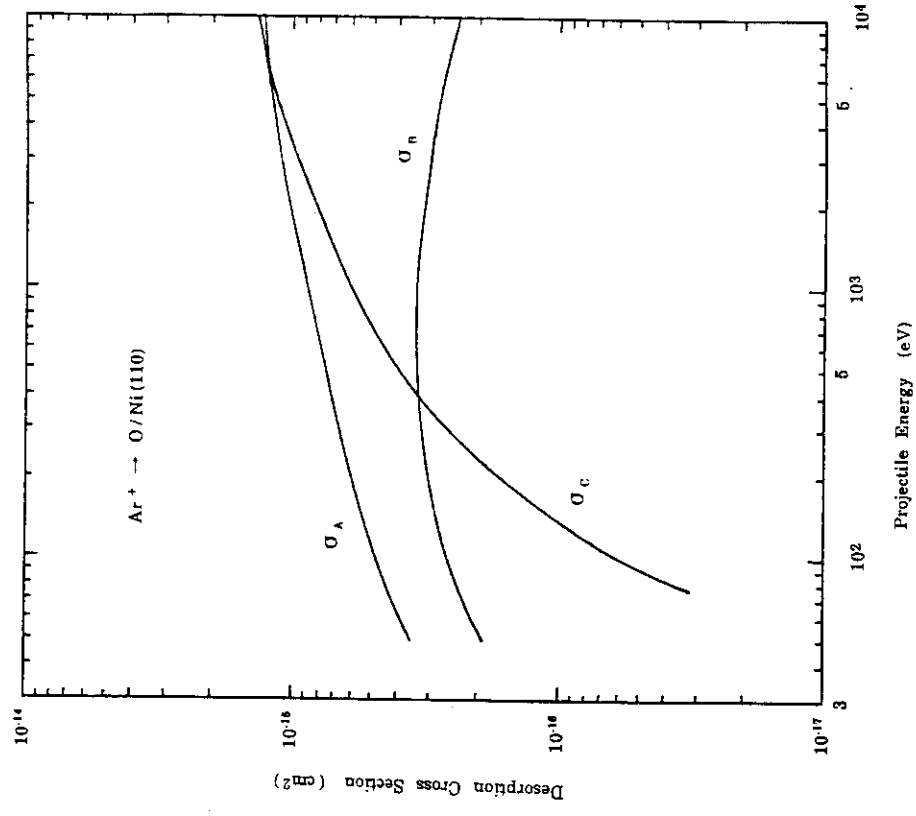

Fig. 26 Relative contributions from σ_A, σ_B and σ_C. The exponents m_{13} and m used in the calculations are 0.0 and 0.191, respectively.

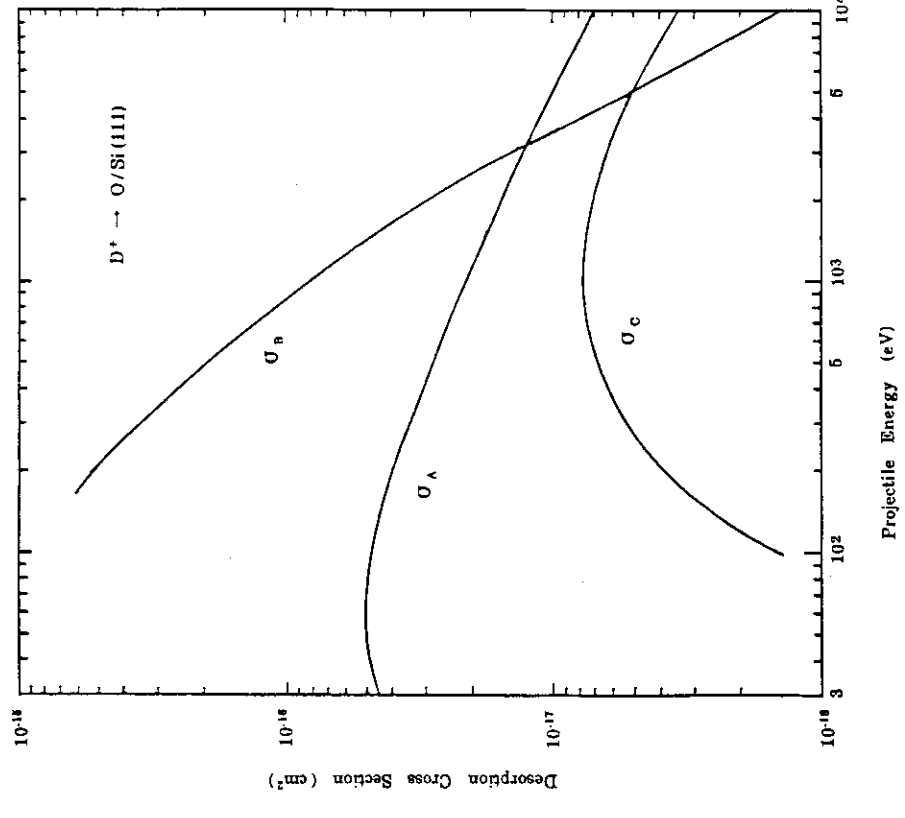

Fig. 25 Relative contributions from σ_A, σ_B and σ_C. The exponents m_{13} and m used in the calculations are 0.5 and 1.0, respectively.

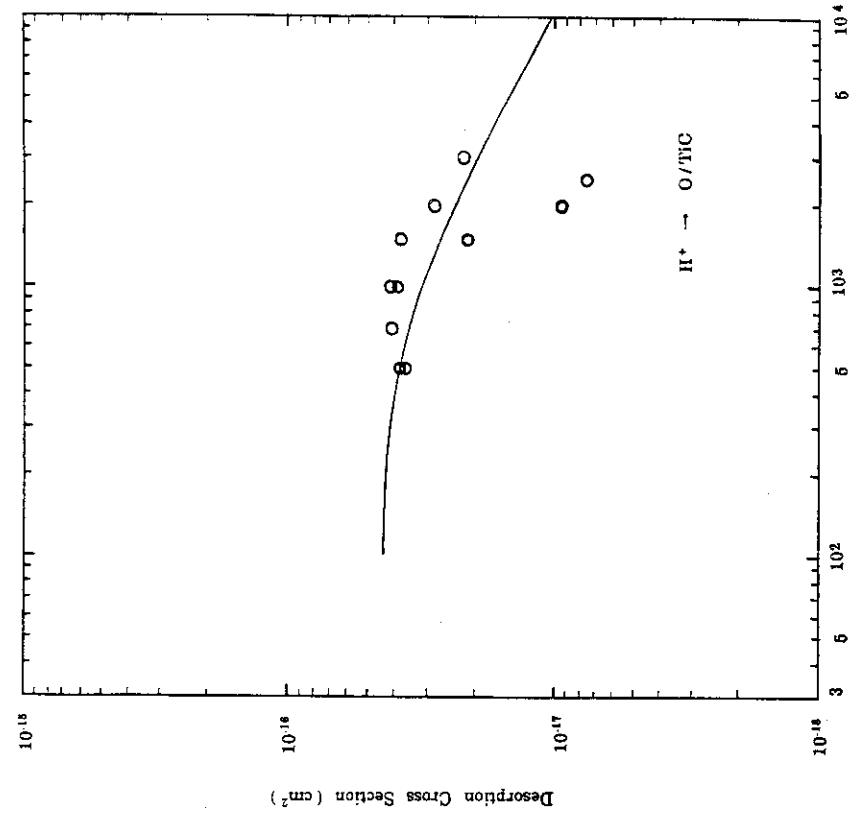

Fig. 28 Comparison of experimental and calculated desorption cross sections. The exponents m_{13} and m used in the calculations are shown in Table 18.

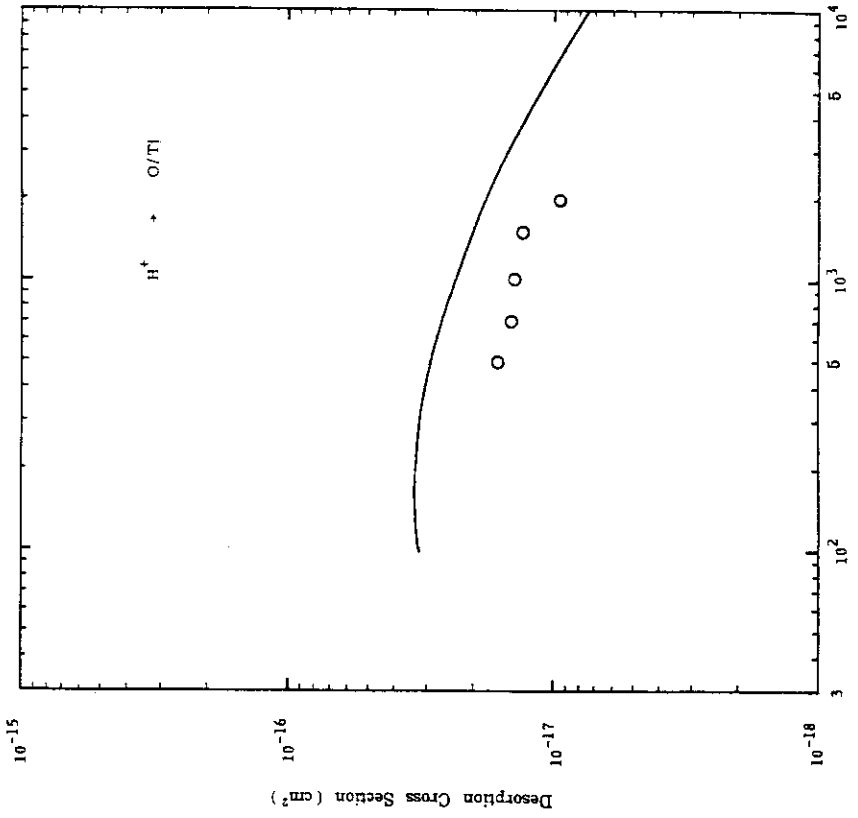

Fig. 27 Comparison of experimental and calculated desorption cross sections. The exponents m_{13} and m used in the calculations are shown in Table 18.

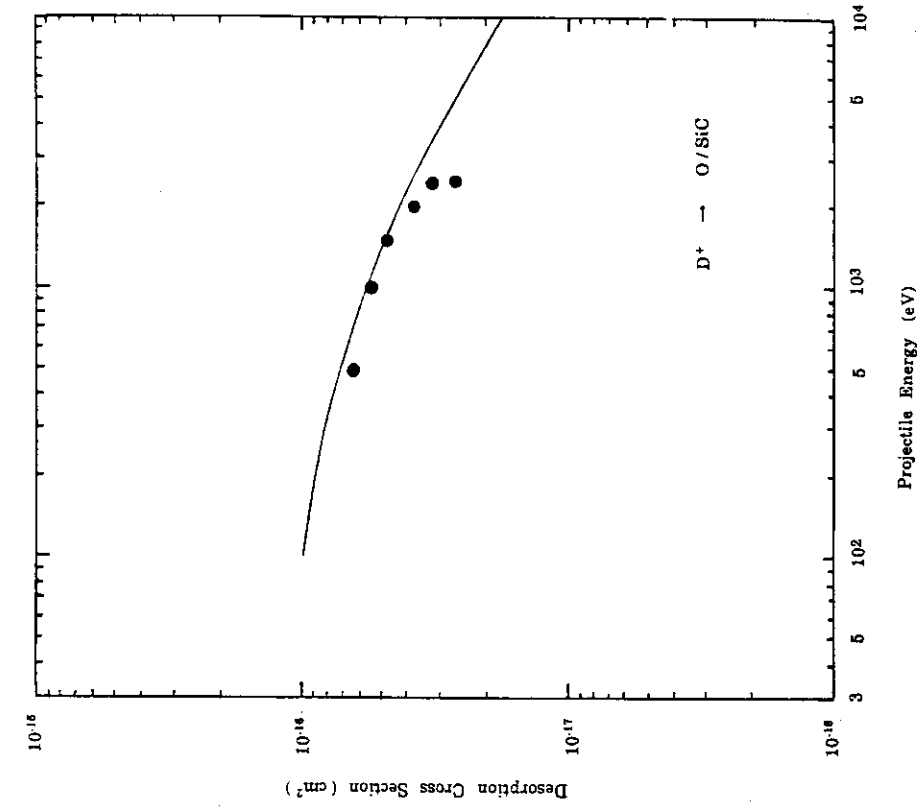

Fig. 30 Comparison of experimental and calculated desorption cross sections. The exponents m_{13} and m used in the calculations are shown in Table 18.

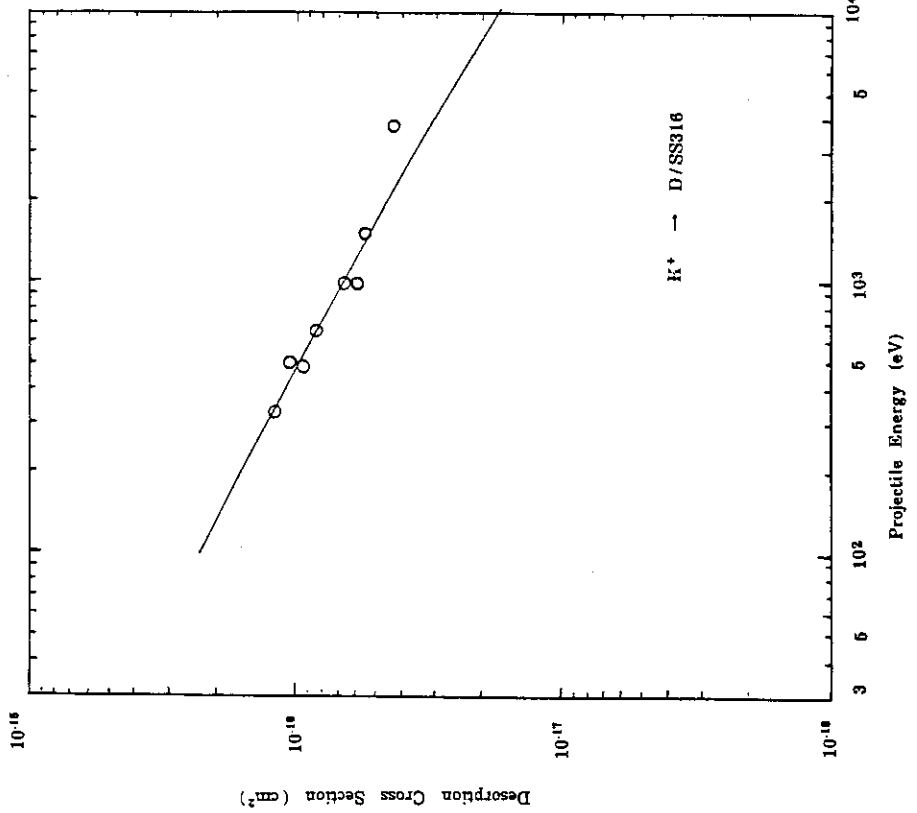

Fig. 29 Comparison of experimental and calculated desorption cross sections. The exponents m_{13} and m used in the calculations are shown in Table 18.

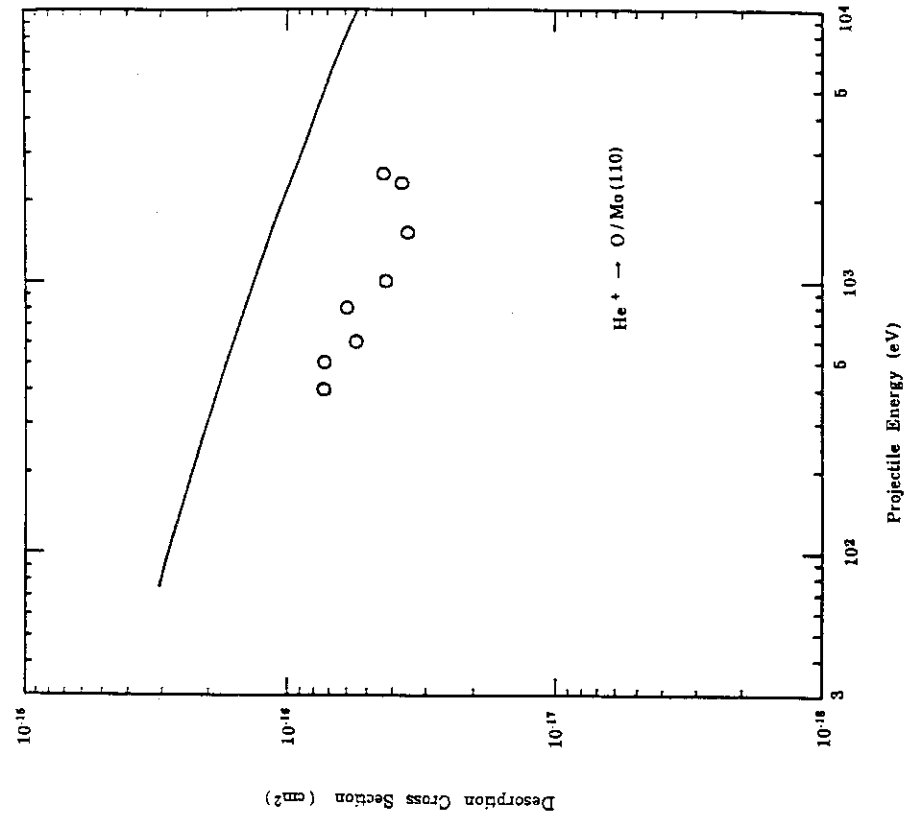

Fig. 32 Comparison of experimental and calculated desorption cross sections. The exponents m_{13} and m used in the calculations are shown in Table 18.

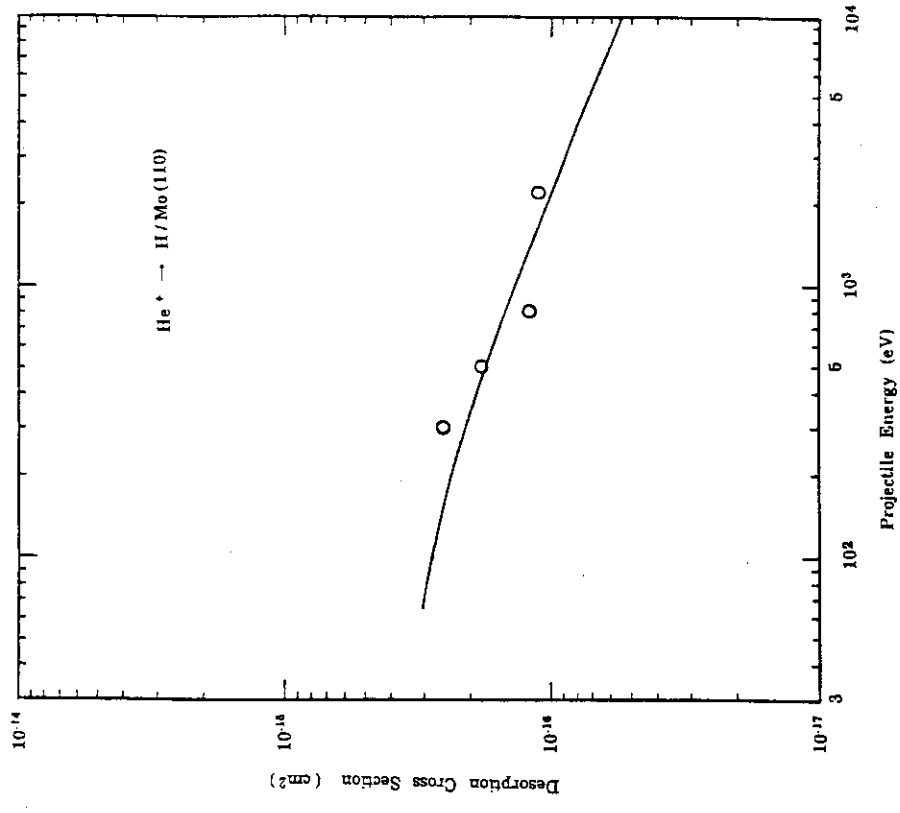

Fig. 31 Comparison of experimental and calculated desorption cross sections. The exponents m_{13} and m used in the calculations are shown in Table 18.

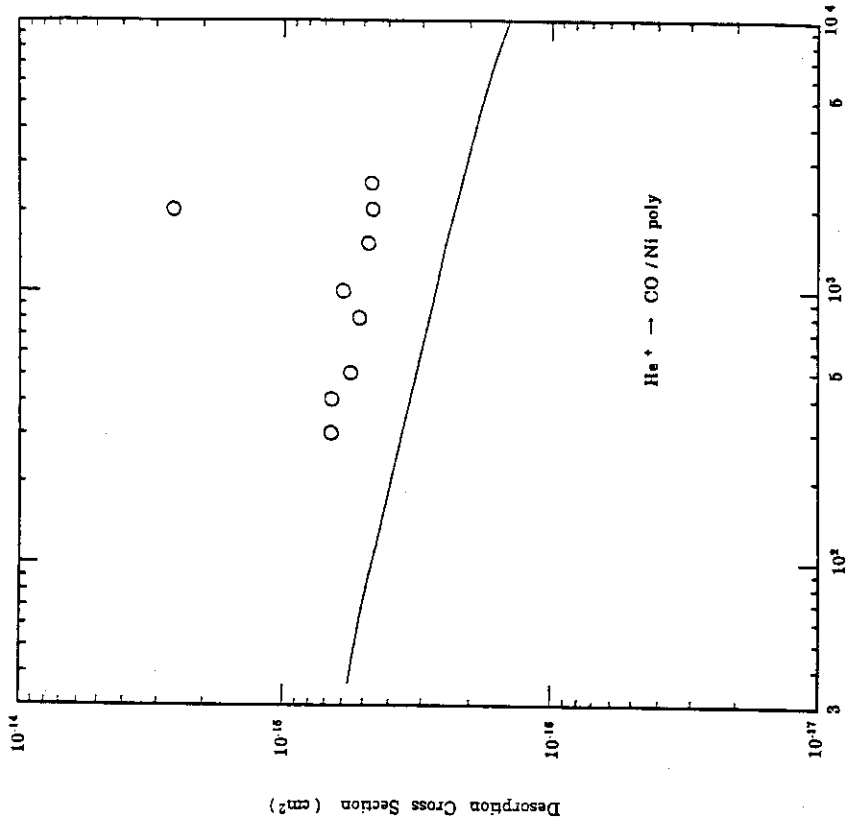

Fig. 34 Comparison of experimental and calculated desorption cross sections. The exponents m_{13} and m used in the calculations are shown in Table 18.

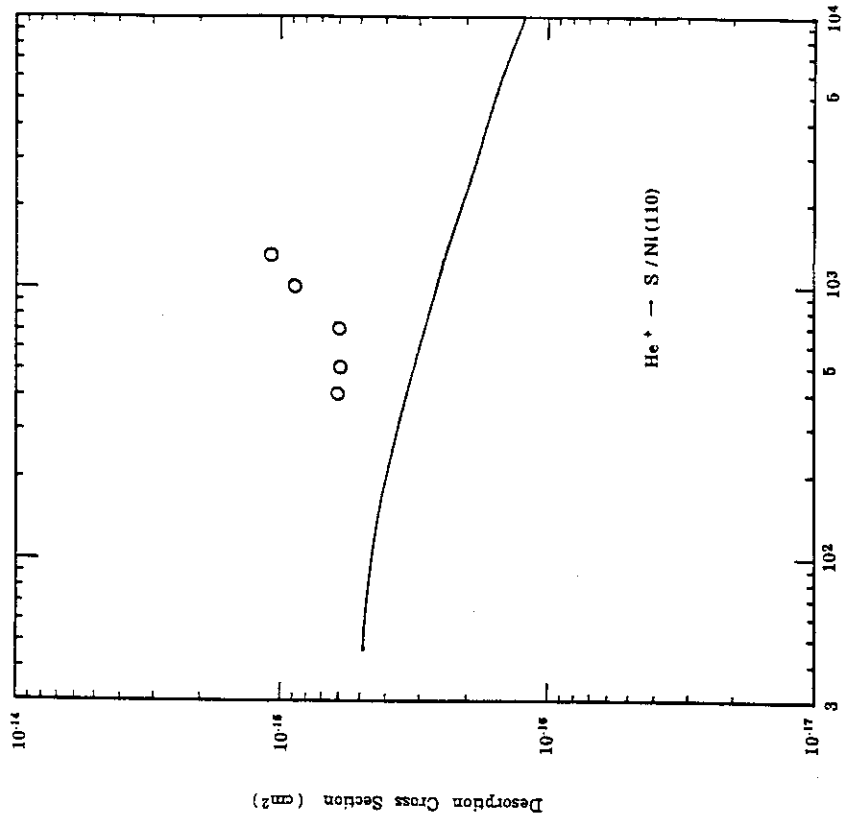

Fig. 33 Comparison of experimental and calculated desorption cross sections. The exponents m_{13} and m used in the calculations are 0.5 and 0.5, respectively.

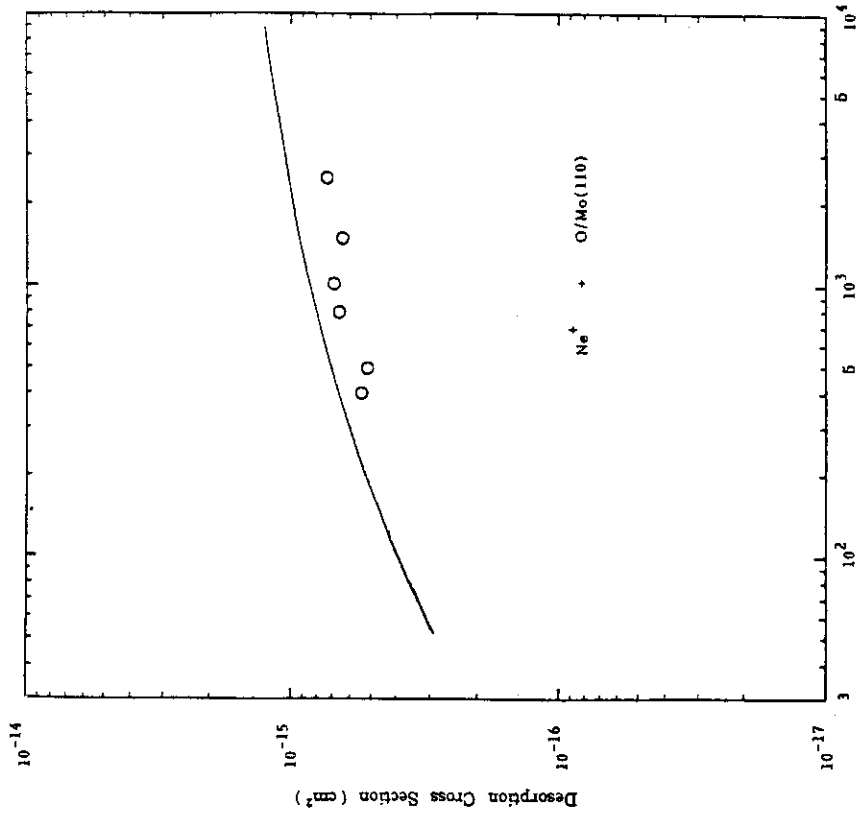

Fig. 36 Comparison of experimental and calculated desorption cross sections. The exponents m_{13} and m used in the calculations are shown in Table 18.

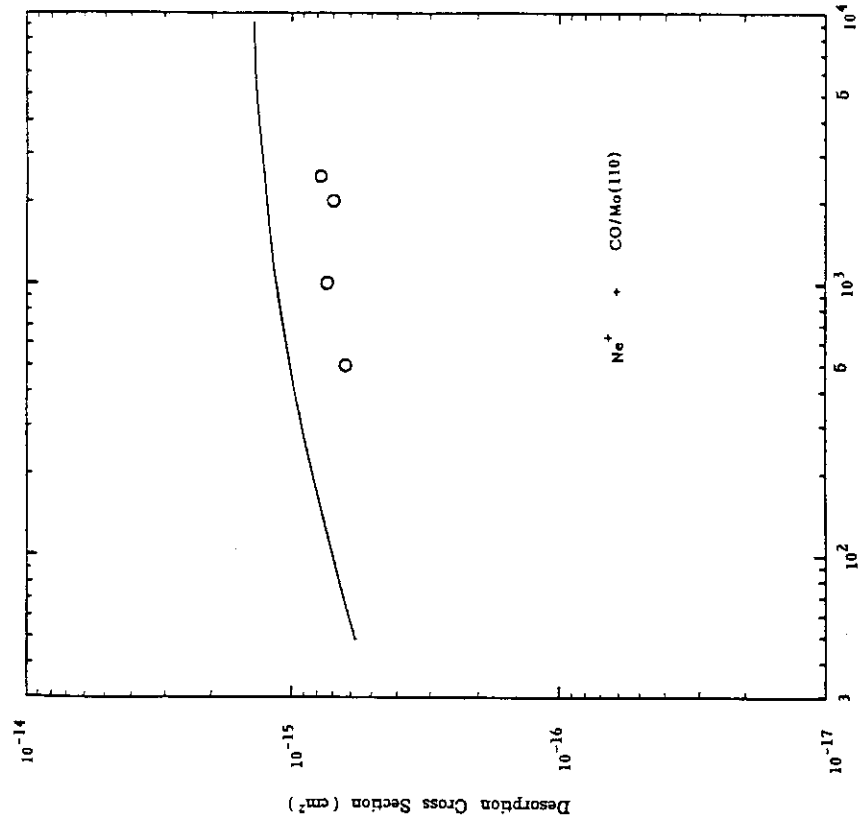

Fig. 35 Comparison of experimental and calculated desorption cross sections. The exponents m_{13} and m used in the calculations are shown in Table 18.

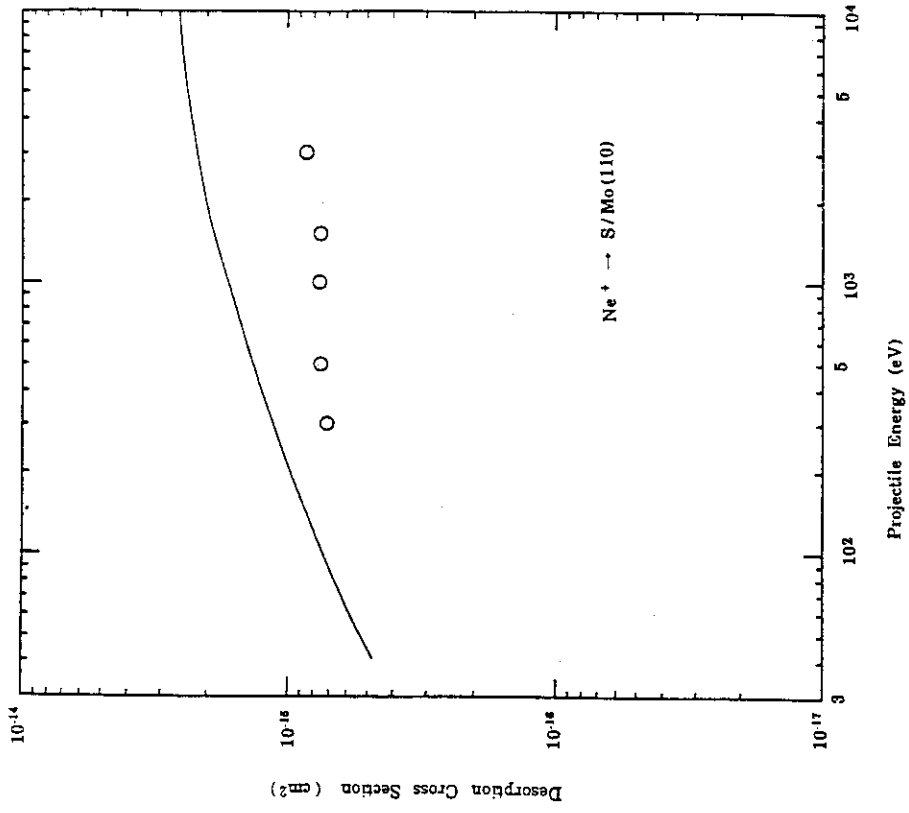

Fig. 38 Comparison of experimental and calculated desorption cross sections. The exponents m_{13} and m used in the calculations are shown in Table 18.

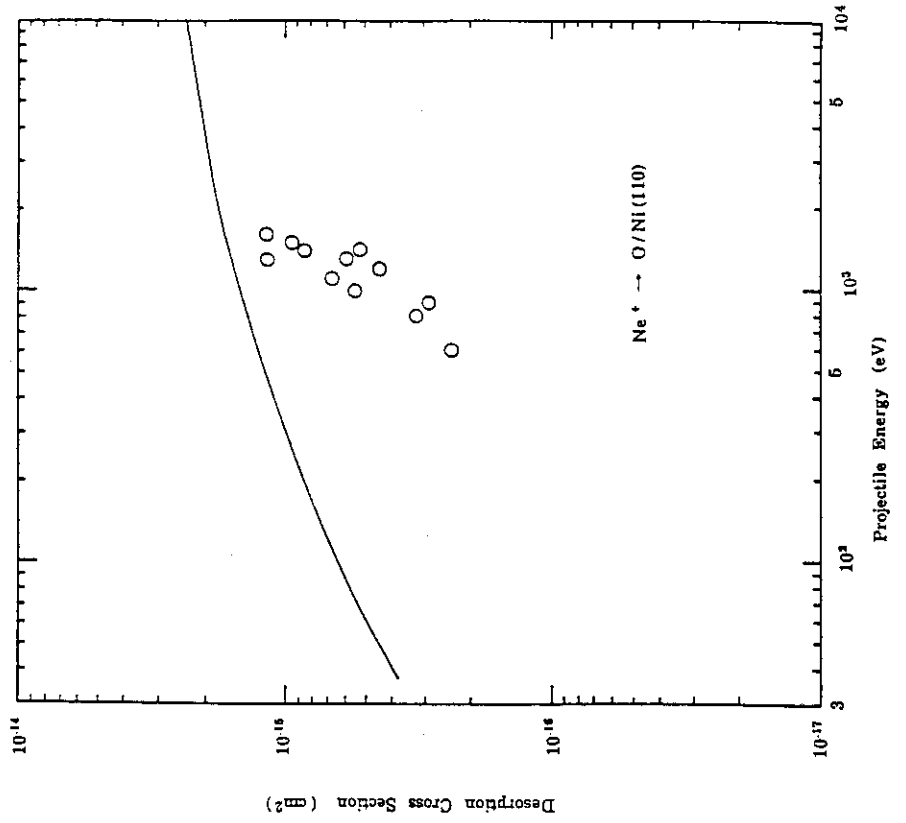

Fig. 37 Comparison of experimental and calculated desorption cross sections. The exponents m_{13} and m used in the calculations are 0.0 and 0.055, respectively.

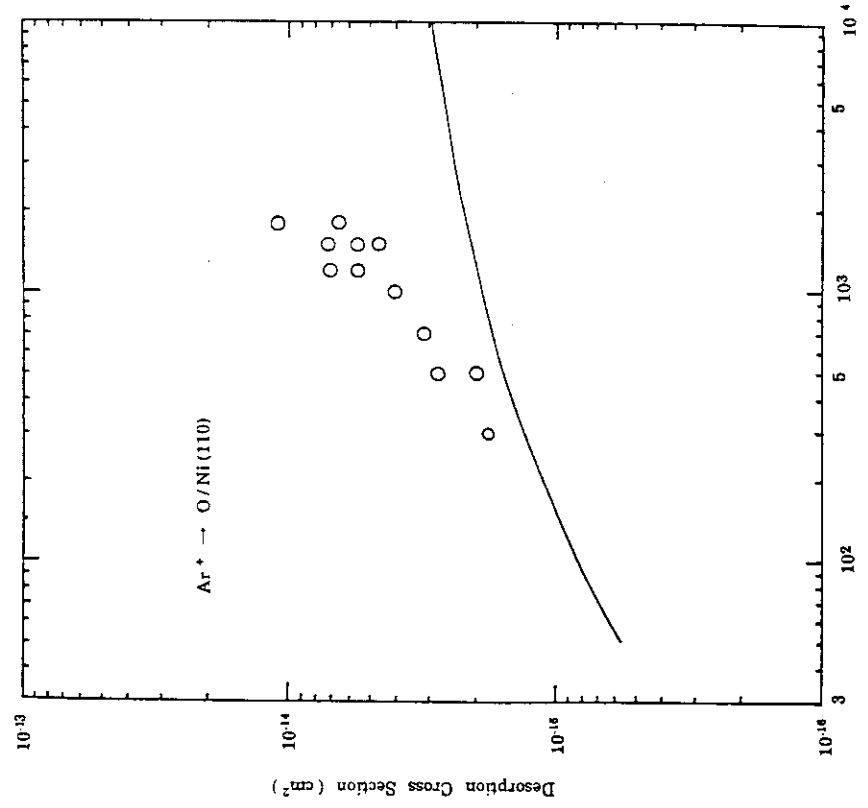

Fig. 40 Comparison of experimental and calculated desorption cross sections. The exponents m_{13} and m used in the calculations are 0.0 and 0.191, respectively.

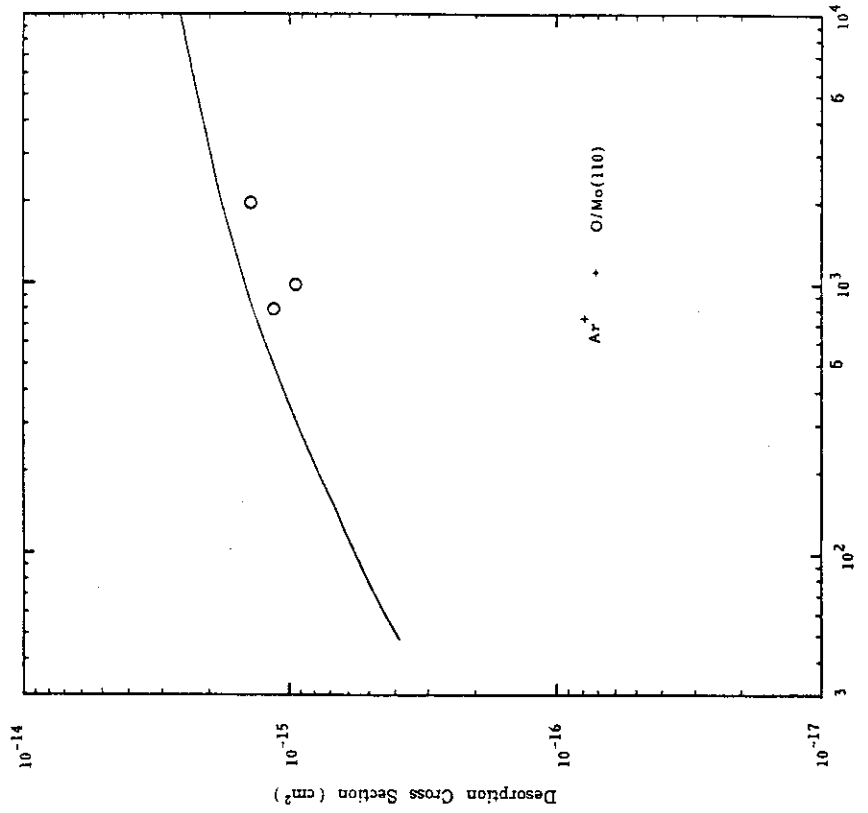

Fig. 39 Comparison of experimental and calculated desorption cross sections. The exponents m_{13} and m used in the calculations are shown in Table 18.

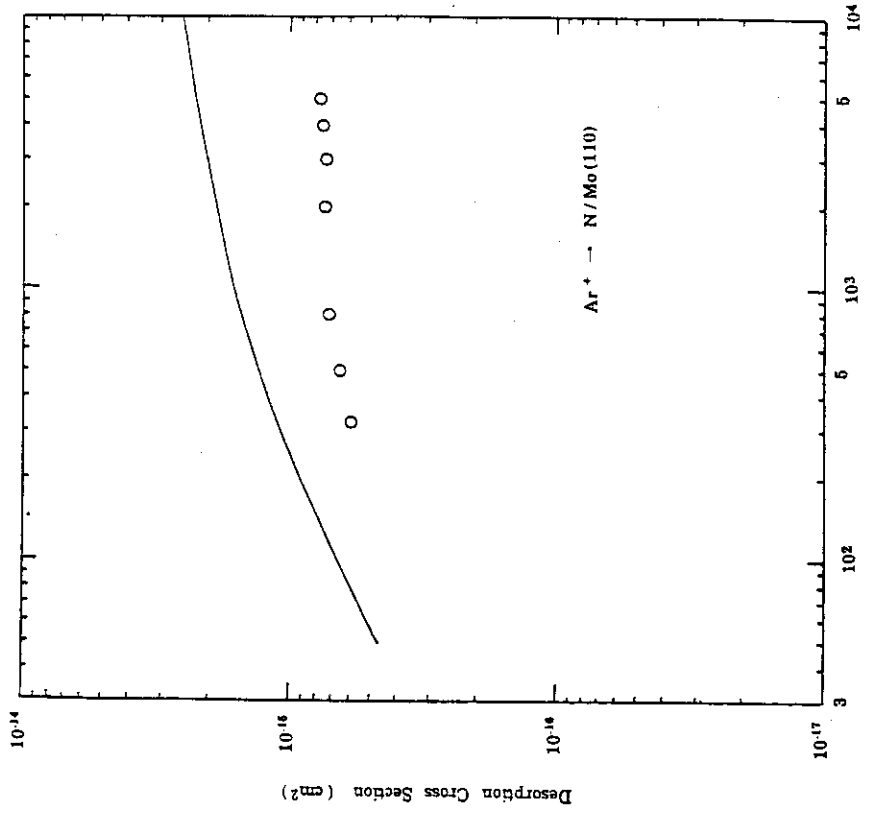

Fig. 42 Comparison of experimental and calculated desorption cross sections. The exponents m_{13} and m used in the calculations are shown in Table 18.

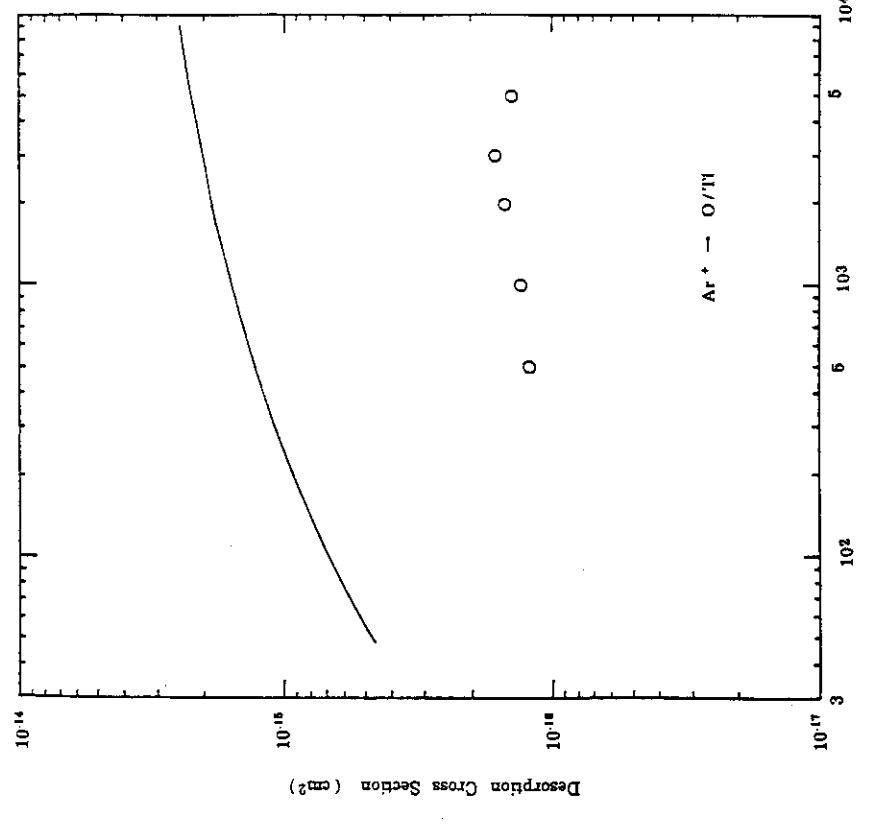

Fig. 41 Comparison of experimental and calculated desorption cross sections. The exponents m_{13} and m used in the calculations are shown in Table 18.

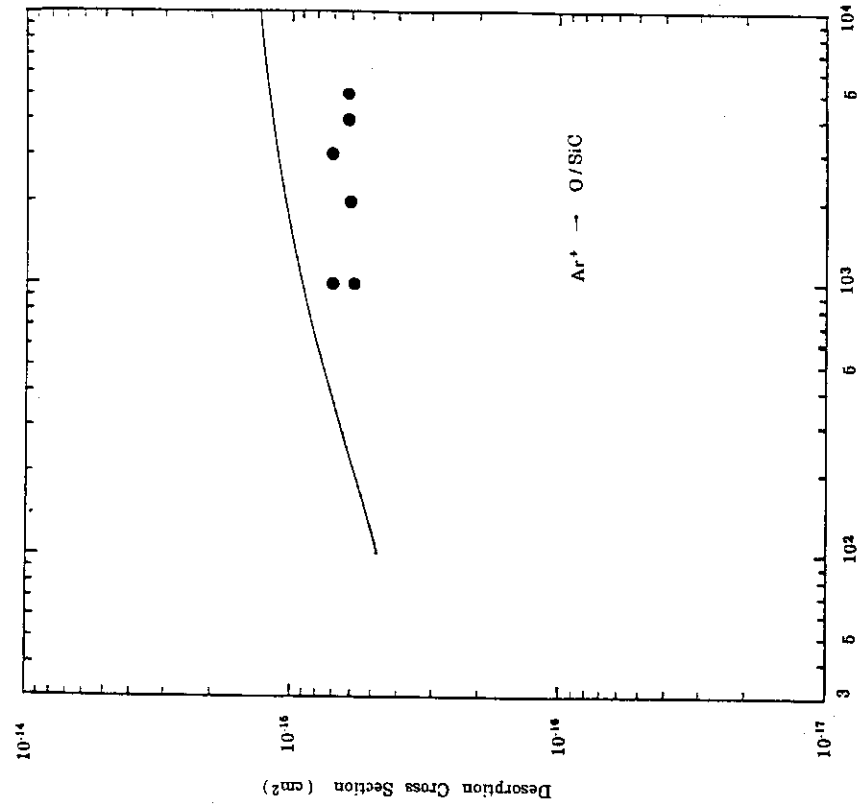

Fig. 44 Comparison of experimental and calculated desorption cross sections. The exponents m_{13} and m used in the calculations are shown in Table 18.

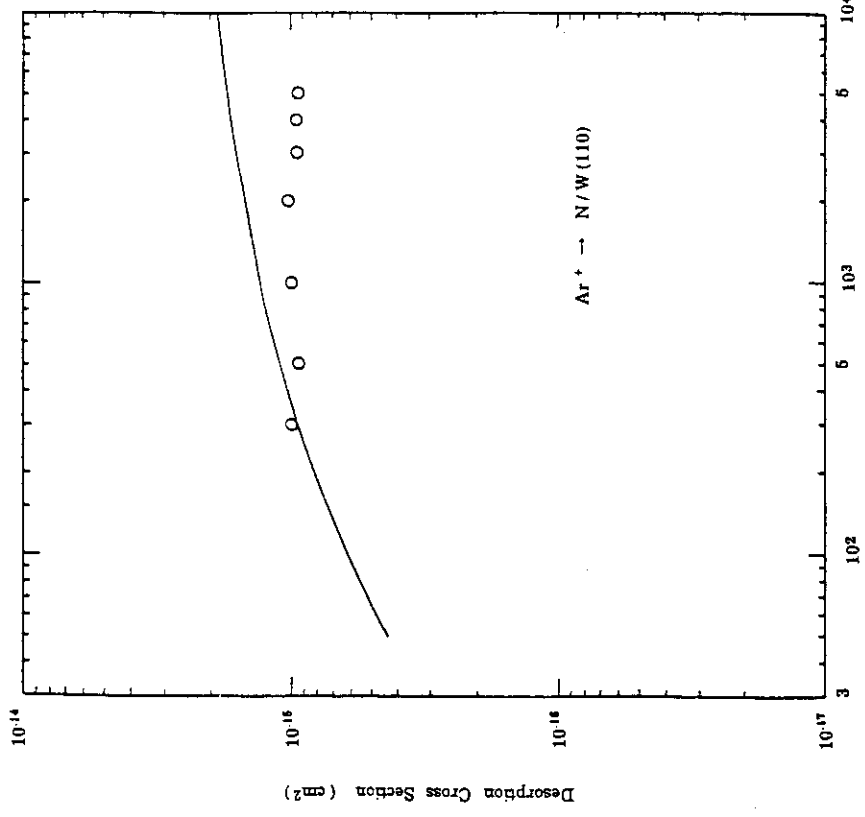

Fig. 43 Comparison of experimental and calculated desorption cross sections. The exponents m_{13} and m used in the calculations are shown in Table 18.

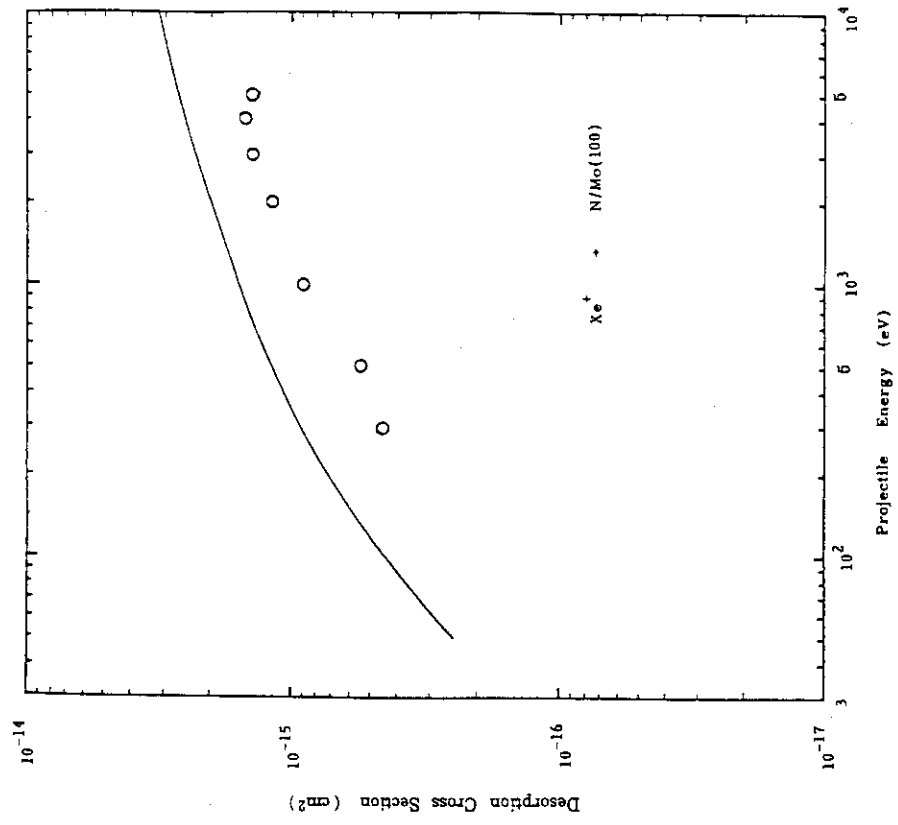

Fig. 46 Comparison of experimental and calculated desorption cross sections. The exponents $m_{1\,3}$ and m used in the calculations are shown in Table 18.

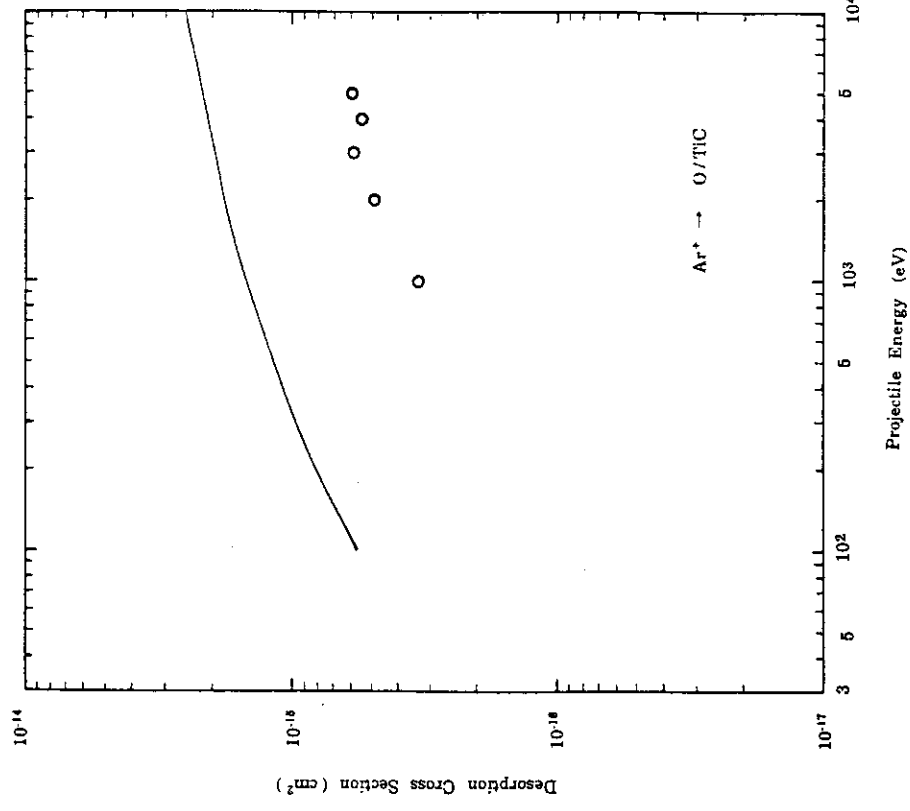

Fig. 45 Comparison of experimental and calculated desorption cross sections. The exponents $m_{1\,3}$ and m used in the calculations are shown in Table 18.

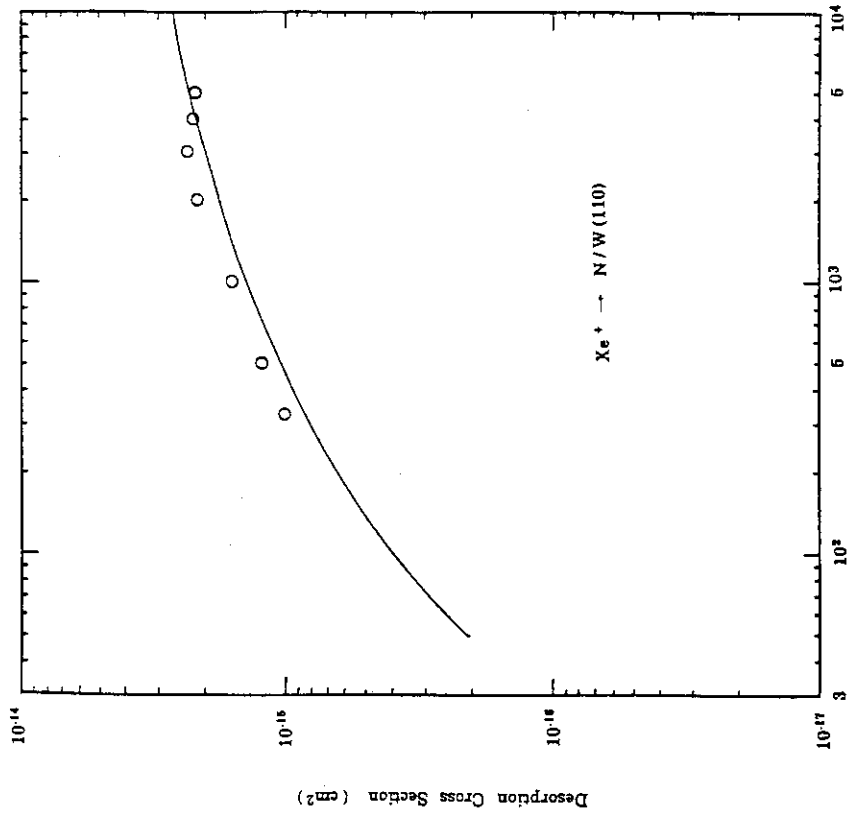

Fig. 47 Comparison of experimental and calculated desorption cross sections. The exponents m_{13} and m used in the calculations are shown in Table 18.

4. Discussion

In the preceding section, calculated desorption cross sections have been compared with experimental data. It is found that although Winters and Sigmund's model can explain some data, it fails to explain the other data. Here we first discuss the energy dependence of those data that are explainable by the model. Then we discuss the other desorption cross sections that are not explainable by the model and try to derive an empirical analytical curve for them.

4.1 Detailed studies of sputtering with TRIM.SP[37,38]

Computer simulation has been widely used in order to get a better understanding of the collisional processes. One of the advantages of computer simulation is that physical processes can be described without introducing special assumptions which are necessary in an analytical theory. Another advantage is that computer simulation permits us to study physical processes which are difficult to be experimentally carried out. Eckstein and Biersack[37] have improved Monte Carlo TRIM code and got a new code called TRIM.SP. In this code, four different collisional processes giving rise to sputtered atom have been taken into account and their relative contributions to the sputtering yields have been calculated. The sputtered atoms consist of primary knock-on and secondary knock-on atoms, both of which are created by either inward or outward (reflected) moving incident ions, as shown in Fig. 48. Eckstein and Biersack have studied the sputtering of carbon, nickel and molybdenum bombarded with H^+, D^+, He^+, Ne^+, Ar^+ and Xe^+ ions. The incident energy of ions ranges from 30 eV to 200 keV. A few results of their simulations are shown in Figs. 49, 50 and 51. All these results are obtained for normal incidence of ions. Figure 49 shows the ratio of primary and secondary knock-on atoms to all the sputtered atoms from Ni by H^+ ions. It is found that the primary and secondary knock-on atoms created by the reflected ions are dominant at low energies. At high energies $E \gg 10$ keV, the secondary knock-on atoms created by inward moving ions are dominant. The contribution from the primary knock-on atoms due to inward moving ions is small over the entire energy region. On the other hand, as can be seen from Fig. 50 which shows for Ar^+ ion that the relative contribution of secondary knock-on atoms created by inward moving ions is always dominant for heavier incident ions. This process has been treated with the transport theory proposed by

Sigmund[12]. Figure 51 shows an intermediate case, where the contribution from primary knock-on atoms is dominant at low energies and that from secondary knock-on atoms becomes important as the incident energy increases. By referring to these results, we attempt to interpret the energy dependence of experimental desorption cross sections in the following sections. For light ions, the desorption cross sections are related to the reflection coefficient by assuming that the desorption is caused by only reflected ions. Contributions from inward moving ions is completely neglected. For heavy ions, on the other hand, the desorption cross section are calculated by assuming that the desorption is caused by collision between sputtered atoms and adsorbed atom.

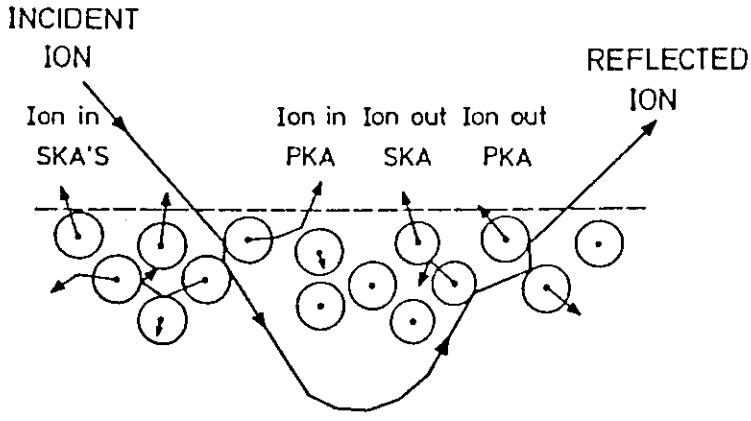

Fig. 48 Four possible sputtering events. SKA: secondary knock on atom, PKA: primary knock on atom[38)]

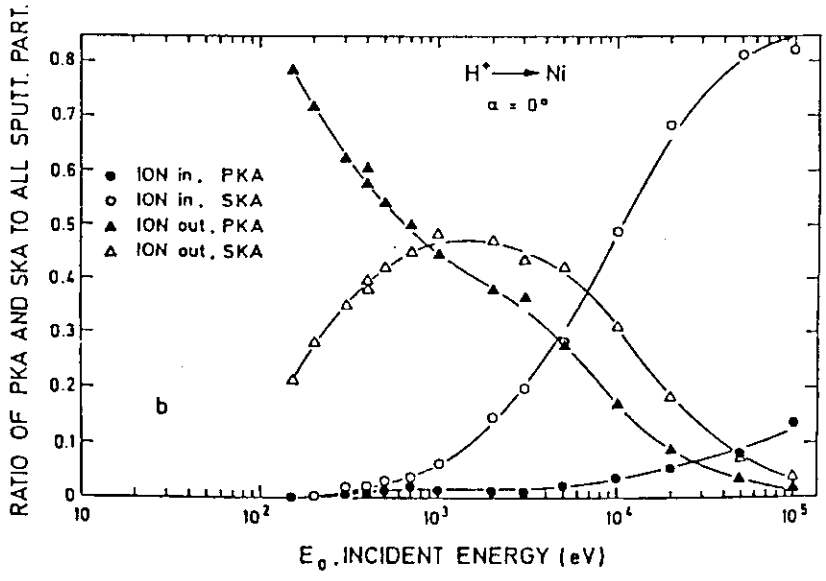

Fig. 49 Relative contribution from primary knock-on atom and secondary knock-on atom to sputtered yield[38)]

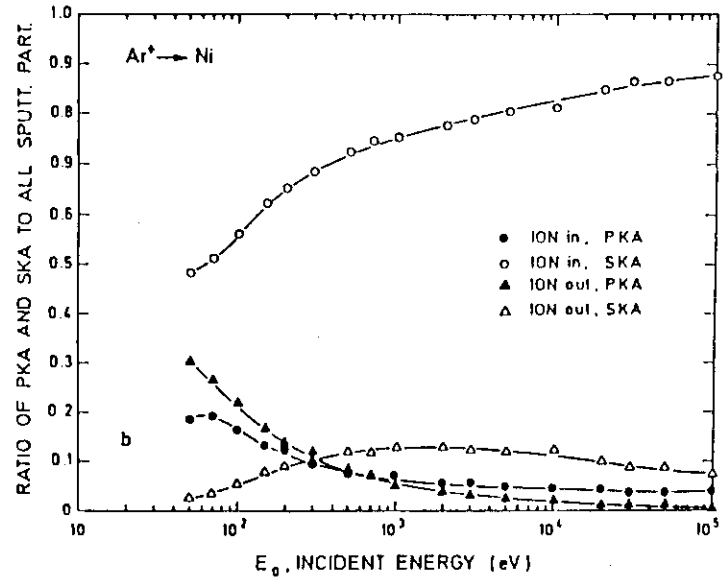

Fig. 50 Relative contribution from primary knock-on atom and secondary knock-on atom to sputtered yield[38)]

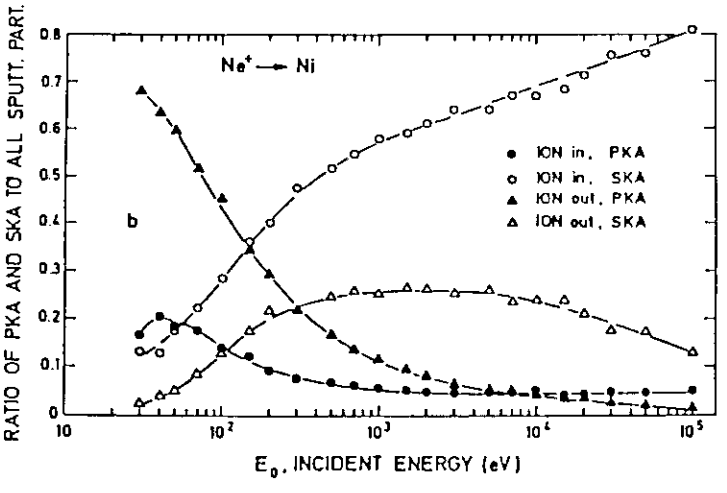

Fig. 51 Relative contribution from primary knock-on atom and secondary knock-on atom to sputtered yield[38)]

4.2 Reflection process based on single collision model

In the last 15 years, the reflection process of light ions from random sclids has been widely investigated, because of its great importance in nuclear fusion research. Various theoretical approaches have also been performed. These approaches are based on an elastic binary collisions of ions with target atoms. One of the approaches is called a single collision model. It is assumed in this model that a particle moves along straight line in the target, losing its energy, until it undergoes a single and large angle scattering with a target atom and then it returns to the surface without further scattering. This approach first proposed by McCracken and Freeman[39] is applicable to description of the scattering of light particles of sufficiently high energies. As the energy of particles decreases, the assumption of straight path before and after the collision becomes less and less valid. In the low energy region, the processes of ion penetration and reflection are described on the basis of statistical transport theory.

Derivation of an analytical expression for reflection coefficients of light ions is attempted using a single collision model. An ion with initial energy E is incident at an angle θ with respect to the surface normal and penetrates the target. The geometry of single collision model is shown in Figure 52. The slowing down process is assumed to be described by a friction-like electronic energy loss. The rate of energy loss is given by

$$- dE/d_{\tau} = N S_e(E) , \tag{4.1}$$

where N is the atomic density of the target atom and $S_e(E)$ is the electronic stopping power. The electronic stopping power is assumed to be proportional to the velocity of ion according to the theory of Lindhard and Scharff[40]. Using eq.(4.1), the energy of the ion for any distance τ travelled within the solid is obtained by

$$E(\tau) = E(1 - \tau/\tau_T)^2 , \tag{4.2}$$

where E is the incident energy and τ_T is the total path length. The energy after the nuclear collision is given by $k^2E(\tau)$, where $E(\tau)$ is the energy before collision and k^2 is given by the usual expression for elastic collisions calculated from the conservation of energy and momentum. Namely,

$$k = [\cos a + (\mu^2 - \sin a)^{1/2}] / (1 + \mu) , \tag{4.3}$$

where a is the scattering angle and μ is the ratio of the mass of target atom to that of incident ions, $\mu = M_2/M_1$. In the case of $\mu \gg 1$, recoil energy loss can be neglected, namely $k \simeq 1$. After the collision, the ion moves to the surface and again loses energy due to the electronic collision. The emerging energy E_0 of the ion is given by the same procedure which led to eq.(4.2),

$$E_0 = E[k - (\tau/\tau_T)(k + \cos\theta/\cos\beta)]^2 . \tag{4.4}$$

The probability $f(E,E_0,\theta,\beta,\Phi)dE_0\ d\Omega$ for backscattering of an ion into a solid angle $d\Omega(=\sin\beta\ d\beta\ d\Phi)$ and an energy interval dE_0 is given by

$$f(E,E_0,\theta,\beta,\Phi)dE_0\ d\Omega = N\ d\sigma[E(\tau)]d\tau , \tag{4.5}$$

where $d\sigma$ is the differential cross section for deflection in the laboratory system. The cross section in the center of mass system, using the inverse power approximation to Thomas-Fermi screening function, is expressed by

$$d\sigma_c = \pi\ a_{12}^2\ \lambda_m[E_{TF}/E(\tau)]^{2m}\ d(-\cos\theta_0)/(\sin\theta_0/2)^{2m+2} , \tag{4.6}$$

Equation (4.6) is an alternative expression of eq.(2.3) where θ_0 is the scattering angle in the center of mass system. Equation (4.6) is dependent on the path length τ through $E(\tau)$. It is known[41,42] in the case of large angle scattering that eq.(4.6) very closely approximates to the Thomas-Fermi cross section when the exponent m and the matching parameter λ_m are given by

$$m(\varepsilon) = 1/3 + (2/3)[1 + (2\lambda\varepsilon^{4/3})^{-2/3}]^{-1} , \tag{4.7}$$

$$\lambda_m(\varepsilon) = f(\varepsilon)/\varepsilon^{1-2m} , \tag{4.8}$$

$$f(\varepsilon) = \lambda\varepsilon^{1/3}[1 + (2\lambda\varepsilon^{4/3})^{2/3}]^{-3/2} , \tag{4.9}$$

where $f(\varepsilon)$ is Lindhard's scattering function, ε is the incident energy in Thomas-Fermi unit, $\varepsilon = E_0/E_{TF}$ and $\lambda = 1.309$. Equation (4.7) shows that the exponent m increases gradually toward 1 as the energy increases and equals

to 1/3 at low energy limit. The dependences of m and λ_m on reduced energy ε are shown in Fig. 53. The laboratory cross section $d\sigma$ can be derived from $d\sigma_c$ by the standard procedure[43] and is given by

$$d\sigma = \{a_{12}^2 \lambda_m 2^{m-2} [E_{TF}/E(\tau)]^{2m}\} F(a,\mu,m) d\Omega \ , \tag{4.10}$$

with

$$F(a,\mu,m) = [\mu/(1+\mu)^2]^m \cdot \{\mu \cos a + [\mu^2-(\sin a)^2]^{1/2}\}^2 \times \{\mu+(\sin a)^2+[\mu^2-(\sin a)^2]^{1/2} \cos a\}^{m-1} \times [\mu^2-(\sin a)^2]^{-1/2} (\sin a)^{-2m-2} \ . \tag{4.11}$$

If the Mass of incident ion is much smaller than that of the target $1 \ll \mu$, equation (4.11) becomes $(1-\cos a)^{-m-1}$ and then eq.(4.10) can be written as follows,

$$d\sigma = \{a_{12}^2 \lambda_m 2^{m-2} [E_{TF}/E(\tau)]^{2m}\} (1-\cos a)^{-m-1} d\Omega \ . \tag{4.12}$$

Substituting eq.(4.12) into (4.5), the probability of the reflected ions becomes

$$f(E,E_0,\theta,\beta,\Phi) = \{a_{12}^2 \lambda_m 2^{m-2} E_{TF}^2 / [E_0^2 S_e(E_0)]\} (1-\cos a)^{-(m+1)} \times \cos\beta(\cos\beta+\cos\theta)^{4m-1} [\cos\beta+(E/E_0)^{1/2} \cos\theta]^{-4m} \ . \tag{4.13}$$

where $d\tau$ in eq.(4.5) is derived from eq.(4.4). The scattering angle a is connected with the angles of incidence θ and emergence (β,Φ) through

$$\cos a = -\cos\theta \cos\beta + \sin\theta \sin\beta \cos\Phi \ . \tag{4.14}$$

The particle reflection coefficient is defined by integration of eq. (4.13) over the exit-angle (β,Φ) and-energy E_0 of the reflected particle,

$$R(E,\cos\theta) = \int dE_0 \, d\Omega \, f(E,E_0,\theta,\beta,\Phi) \ . \tag{4.15}$$

By substituting eq.(4.13) into eq.(4.15) and integrating, we can get[44],

$$R(E,\cos\theta) = [\lambda_m 2^m(1+\mu)^2\mu^{-1}\varepsilon_0^{-(2m-1)}](\cos a)^{-(4m-1)}[4(4m-1)\gamma\varepsilon_0^{1/2}]^{-1}$$

$$\times \int d(\cos\beta)\{[(\cos\beta+\cos\theta)^{4m-1}-(\cos\theta)^{4m-1}]/(\cos\theta+\cos\beta)^{m+1}$$

$$P_m[(1+\cos\theta\ \cos\beta)/(\cos\theta+\cos\beta)]\} \ , \qquad (4.16)$$

where P_m is the Legendre function of the first kind expressed as

$$P_m(z) = (1/\pi) \int d\Phi/[z+(z^2-1)^{1/2}\cos\Phi]^{m+1} \qquad (4.17)$$

In equation (4.16), the $y\varepsilon_0^{1/2}$ is the electronic stopping power expressed by dimensionless unit and γ is defined as

$$\gamma = 0.07953\ Z_1^{1/2}Z_2^{1/2}(Z_1^{2/3}+Z_2^{2/3})^{-3/4}(A_1+A_2)^{3/2}A_1^{3/2}A_2^{1/2} \ , \qquad (4.18)$$

where A_1 and A_2 are the masses of the projectile ion and target atom, Z_1 and Z_2 are the atomic numbers of the projectile ion and target atom. If $A_1 \ll A_2$ and $Z_1 \ll Z_2$, then equation (4.18) becomes $0.07953\ Z_1^{2/3}A_1^{-1/2}\mu$. In the case of normal incidence, the reflection coefficient $R(E,1)$ is given by

$$R(E,1) = [f(\varepsilon)/\varepsilon^{1/2}](\mu/\gamma)I(m) \ , \qquad (4.19)$$

with

$$I(m) = [(3m-1)-(4m-1)2^m+m2^{4m-1}]/[4m(4m-1)(3m-1)] \ . \qquad (4.20)$$

The energy dependence of I(m) is shown in Fig. 53. The reflection coefficient $R(E,\cos\theta)$ at oblique incidence[44] can be approximated by that of normal incidence such as,

$$R(E,\cos\theta) = R(E,1)[\cos\theta]^{-3+2(1-m)} \ . \qquad (4.21)$$

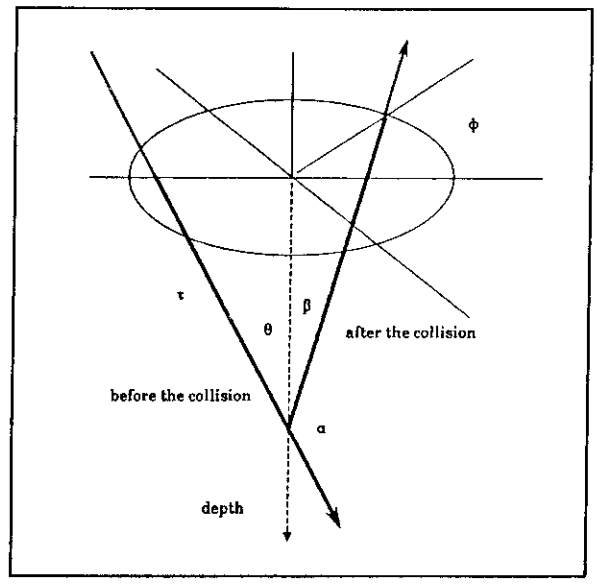

Fig. 52 Single collision model of reflection process

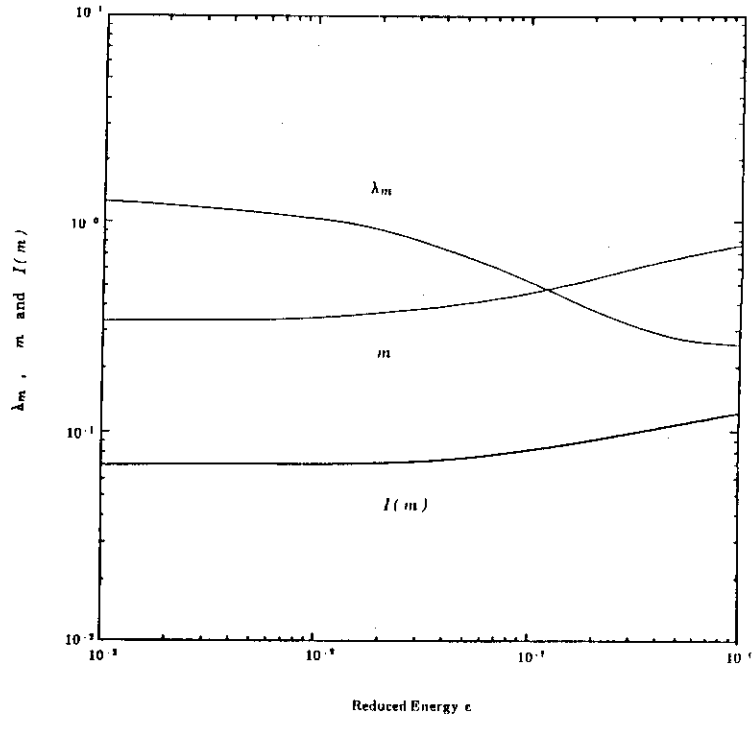

Fig. 53 Dependence of λ , m and I(m) on reduced energy ε

4.3 Contributions of the reflected ions to desorption process

In this section, the collision of the reflected ion with the adsorbate atom is analytically treated using the reflection coefficient derived in section 4.2. The desorption cross section due to this process has already been derived in section 2.2. If the incident energy E is larger than U_3/r_{13}, them equation (2.17) becomes

$$\sigma_B = [8\ C_{13}/U_3^{1/2}][R(E,e)/E^{1/2}] \ , \tag{4.22}$$

with

$$C_{13} = (\pi/2)\lambda_{1/2}a_{13}^2(M_1/M_3)^{1/2}(2Z_1Z_3e^2/a_{13}) \ . \tag{4.23}$$

where the exponent m is equal to 1/2 as shown in section 3-2. Substituting eq. (4.21) into (4.22) and expressing the incident energy E by the Thomas-Fermi unit, we can get,

$$\sigma_B = [G(A_1,A_3,Z_1,Z_2,Z_3)/U_3^{1/2}][(\cos\theta)^{-3+2(1-m)}I(m)][f(\varepsilon)/\varepsilon] \ , \tag{4.24}$$

with

$$G(A_1,A_3,Z_1,Z_2,Z_3) = 126A_1A_3^{-1/2}Z_1^{-1/6}Z_2^{-2/3}Z_3(Z_1^{2/3}+Z_3^{2/3})^{-1/2} \ , \tag{4.25}$$

where A_3 and Z_3 are mass number and atomic number of the adsorbate atom. Here the desorption cross section is expressed by $(\text{angstrom})^2$ unit. To facilitate comparisons of the experimental data for different ions, the desorption cross sections for H^+, D^+ and He^+ ions are plotted as a function of ε as shown in Figure 54. It is found that most of the cross sections gradually decrease as ε increases. To derive the energy-dependence of the desorption cross section, which is independent of incident ion, target atom and adsorbate atom, the experimental data are divided by $G(A_1,A_3,Z_1,Z_2,Z_3)U_3^{-1/2}(\cos\theta)^{-3+2(1-m)}$ I(m) and the results are shown in Fig. 55. The energy dependence of $f(\varepsilon)/\varepsilon$, which is included in eq.(4.24), is also shown in Fig. 55. It can be seen that the energy dependence of the normalized cross sections is similar to that of $f(\varepsilon)/\varepsilon$ for the case of H^+ and D^+ ions especially in the high energy region. This suggests that desorption process for H^+ and D^+ ions is induced by the collision of the reflected ions with the adsorbate atoms. For He^+ ion,

the energy-dependence of the experimental data deviates significantly from $f(\varepsilon)/\varepsilon$. The increase in the deviation with decreasing energy may be due to the fact that the collision of primary recoil atoms created by the reflected ions with the adsorbate atom is not taken into account in eq. (4.24). However, it is difficult to treat analytically this process because of the lack of correct information available on the energy- and angular- distribution of the reflected ions. There are only a few works[45,46,47] dealing with this process.

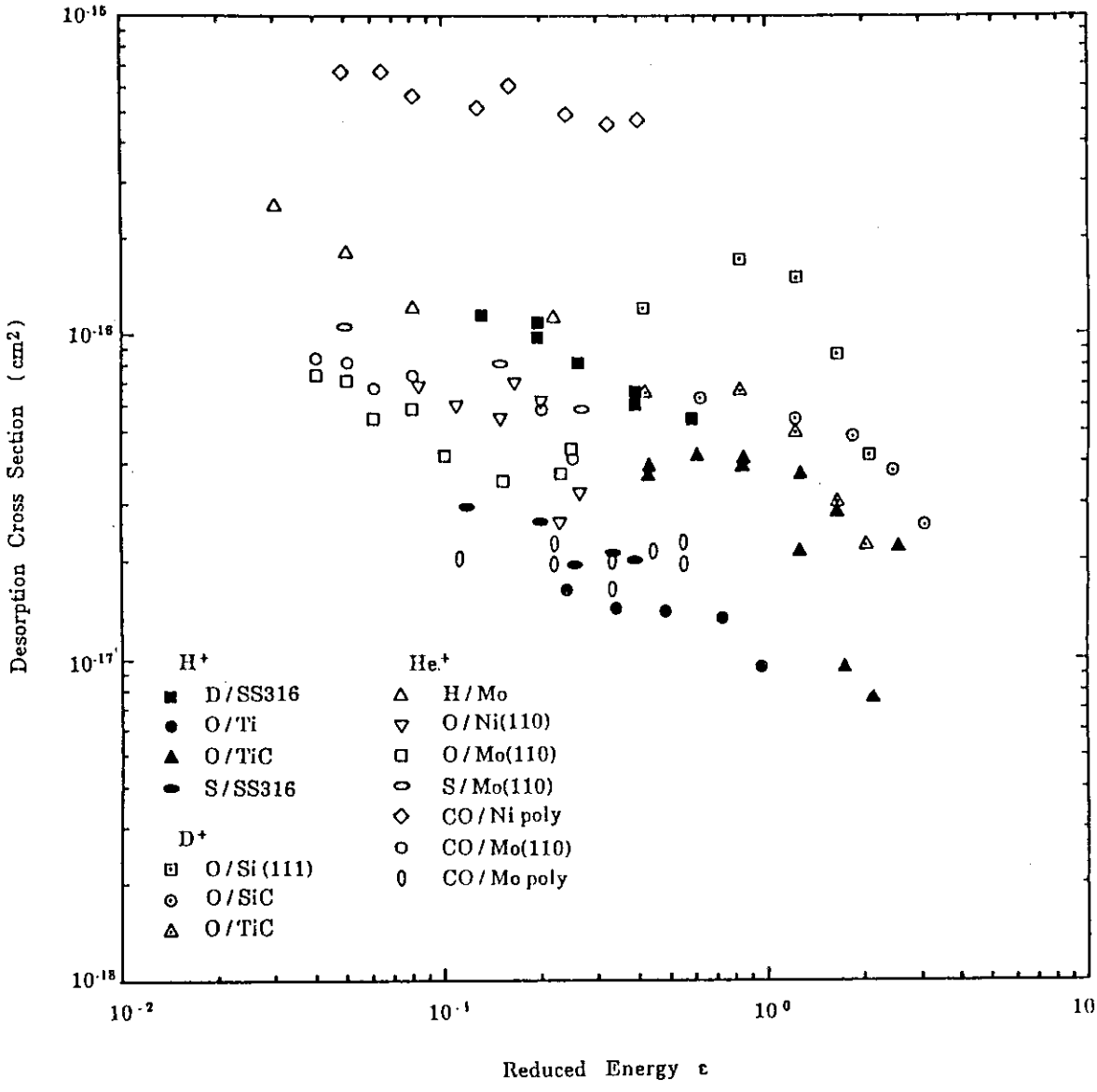

Fig. 54 Desorption cross section as a function of reduced energy ε

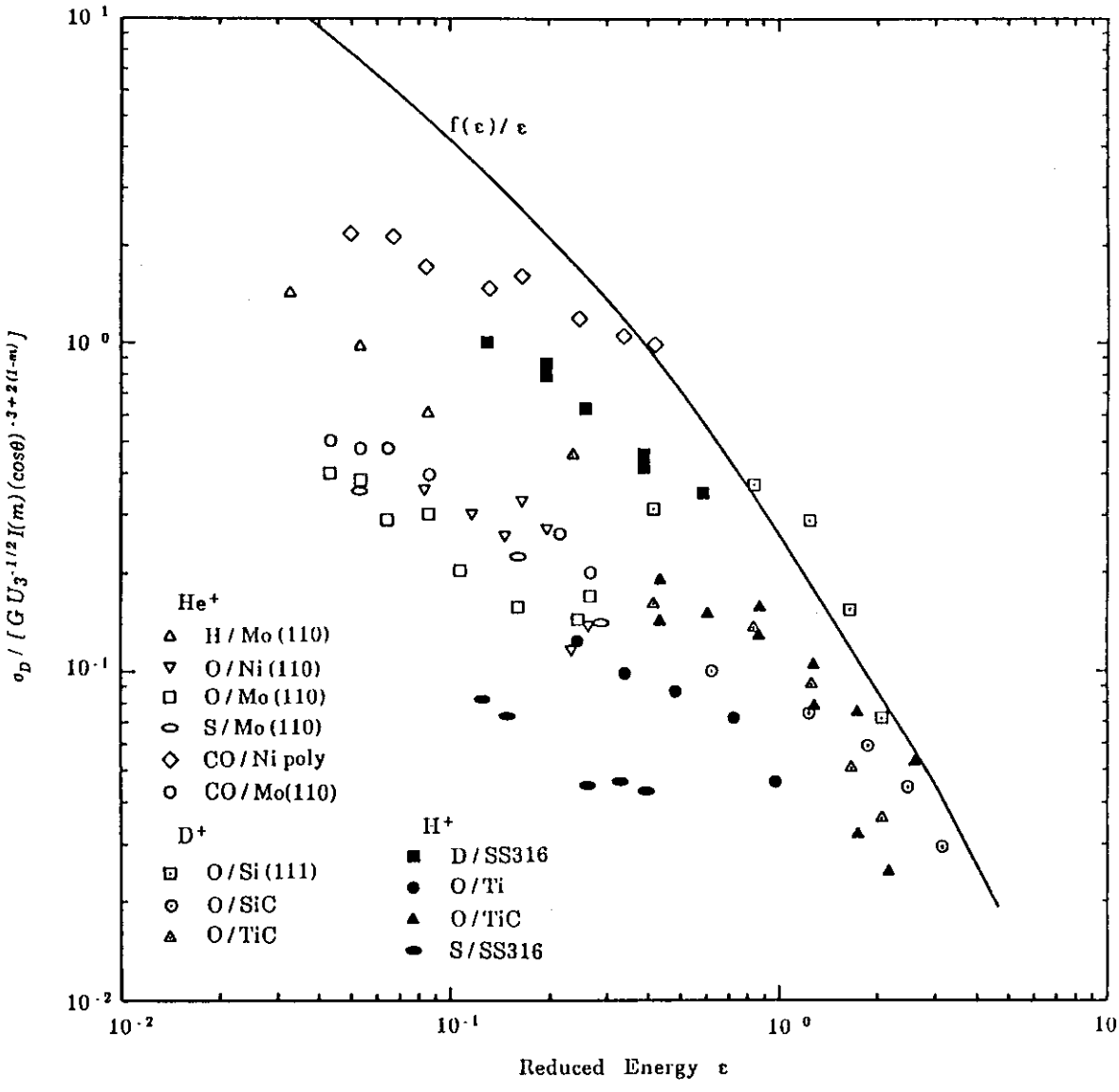

Fig. 55 Normalized desorption cross section as a function of reduced energy ε

4.4 Contributions of the sputtered atoms to desorption process

The sputtering yield for heavy ions is given by

$$S(E,\cos\theta) = (3.559/U_2)a^*[M_1/(M_1+M_2)][Z_1Z_2/(Z_1^{2/3}+Z_2^{2/3})^{1/2}] \times (-d\varepsilon/d\rho)(\cos\theta)^{-1} , \quad (4.26)$$

where U_2 is expressed in eV unit, $(-d\varepsilon/d\rho)$ is the nuclear stopping cross section expressed by dimensionless unit and given by (2.37) in section 2-5 and the values of a^* are shown in Table 11. The desorption cross section due to the sputtered atoms has already been given by eq.(2.23). Inserting eq.(4.26) into (2.23), we can get the desorption cross section

$$\sigma_D = G(Z_1,Z_2,M_1,M_2)(r_{23}U_2/U_3)F\{r_{12}r_{23}E/U_3, r_{23}U_2/U_3\} \times (1-U_2/r_{12}E)^{-2}\, s_n(\varepsilon) , \quad (4.27)$$

with

$$G(Z_1,Z_2,M_1,M_2) = 7.23[3.559\, a^*/(U_2\cos\theta)][M_1/(M_1+M_2)] \times [Z_1Z_2/(Z_1^{2/3}+Z_2^{2/3})^{1/2}] . \quad (4.28)$$

where σ_D is expressed in $(\text{angstrom})^2$ unit. As can be seen in eq.(4.27), the desorption cross section depends on the energy E through $F\{r_{12}r_{23}E/U_3, r_{23}U_2/U_3\}$, $(1-U_2/r_{12}E)^{-2}$ and $s_n(\varepsilon)$. However, the energy dependence of $F\{r_{12}r_{23}E/U_3,r_{23}U_2/U_3\}\times(1-U_2/r_{12}E)^{-2}$ is very weak over the energy range except at low ε, as shown in Fig. 56. It can, therefore, be that $F\{r_{12}r_{23}E/U_3,r_{23}U_2/U_3\}\times(1-U_2/r_{12}E)^{-2}$ has no dependence on projectile energy. The energy dependences of experimental desorption cross sections for Ne^+, Ar^+ and Xe^+ ions are shown in Figs. 57 and 58 as a function of reduced energy. The normalized desorption cross sections which are obtained from the experimental data divided by $G(Z_1,Z_2,M_1,M_2)(r_{23}U_2/U_3)$, and $s_n(\varepsilon)$ are shown in Fig. 59. Although the energy dependence of the normalized desorption cross sections is similar to $s_n(\varepsilon)$ for heavy ions, a significant deviation from $s_n(\varepsilon)$ can be found in some cases for Ne^+ and Ar^+ ions. This may arise from the contribution of the reflected ions to desorption process, which is not taken into account here.

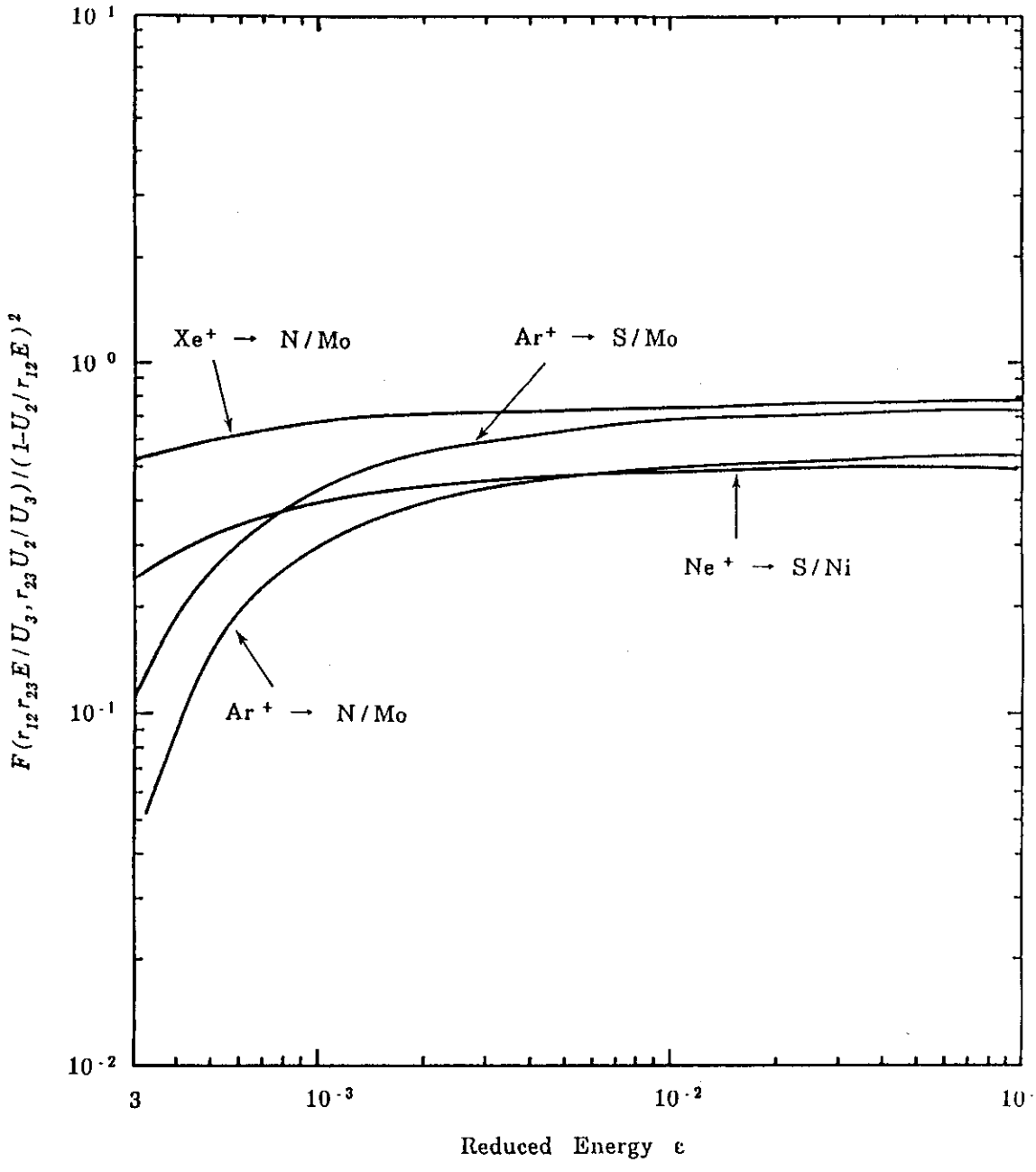

Fig. 56 Energy dependence of $F(r_{12}\ r_{23}\ E/U_3,\ r_{23}\ U_2/U_3)/(1-U_2/r_{12}\ E)^2$

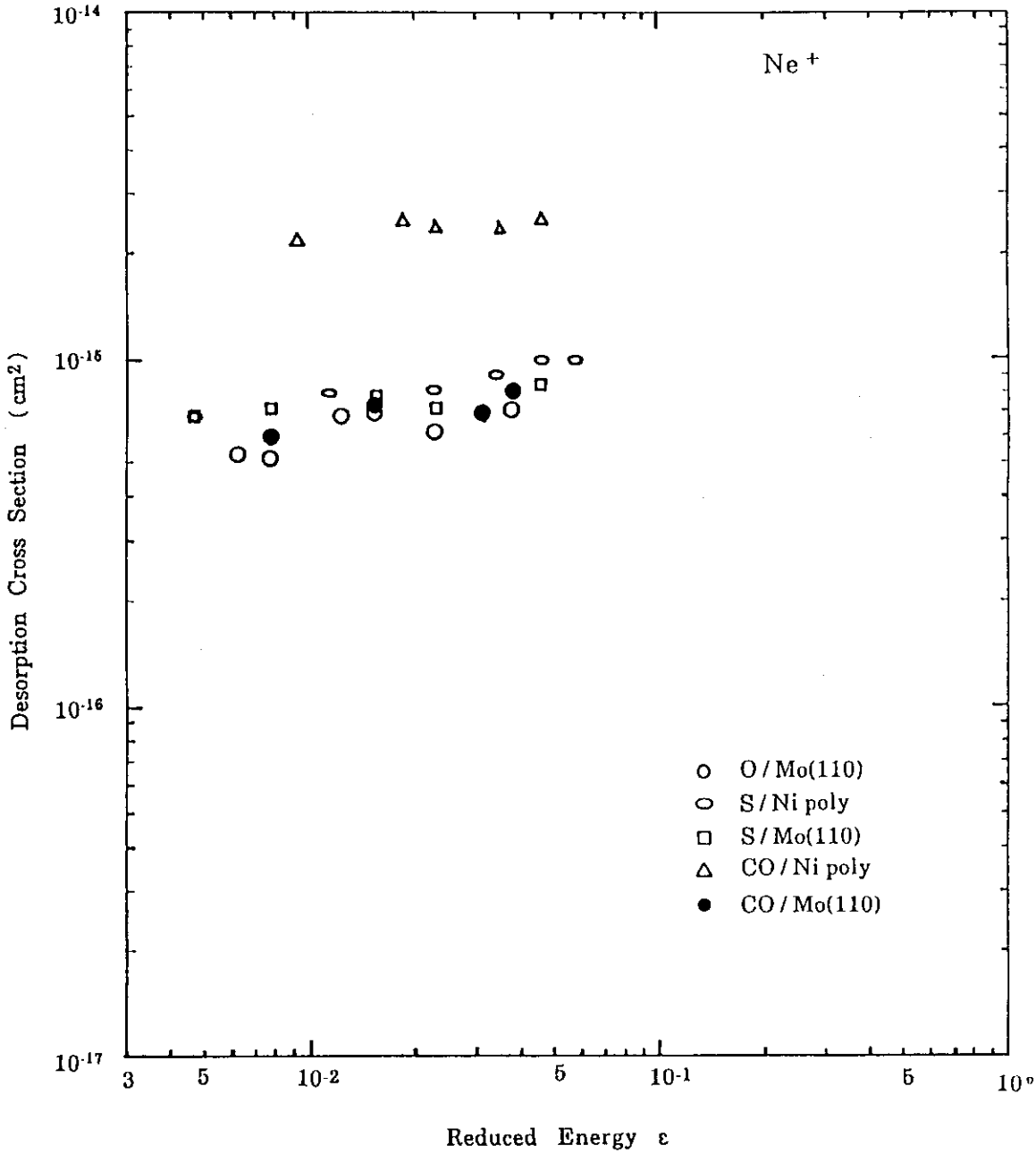

Fig. 57 Desorption cross section as a function of reduced energy ε

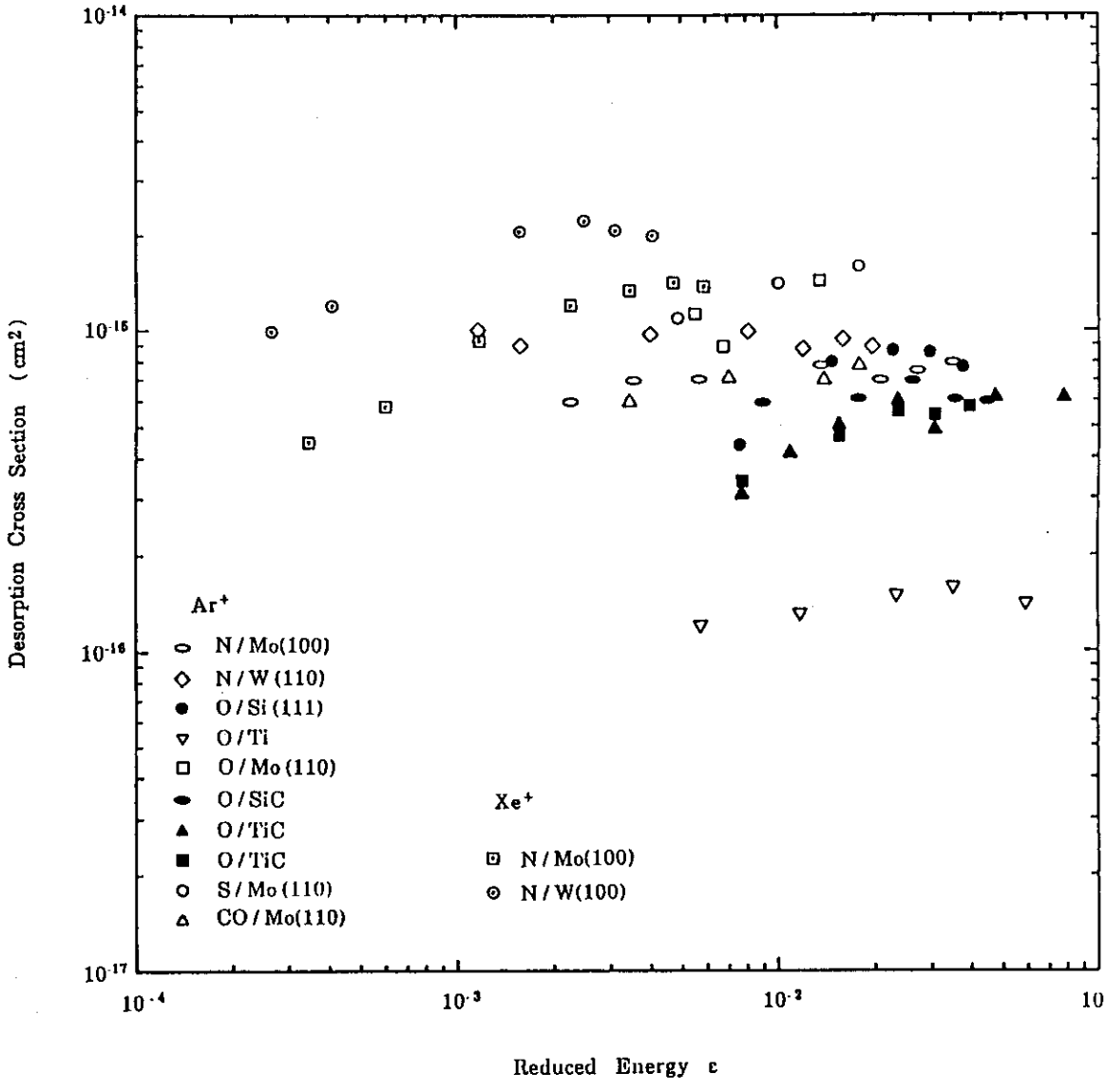

Fig. 58 Desorption cross section as a function of reduced energy ε

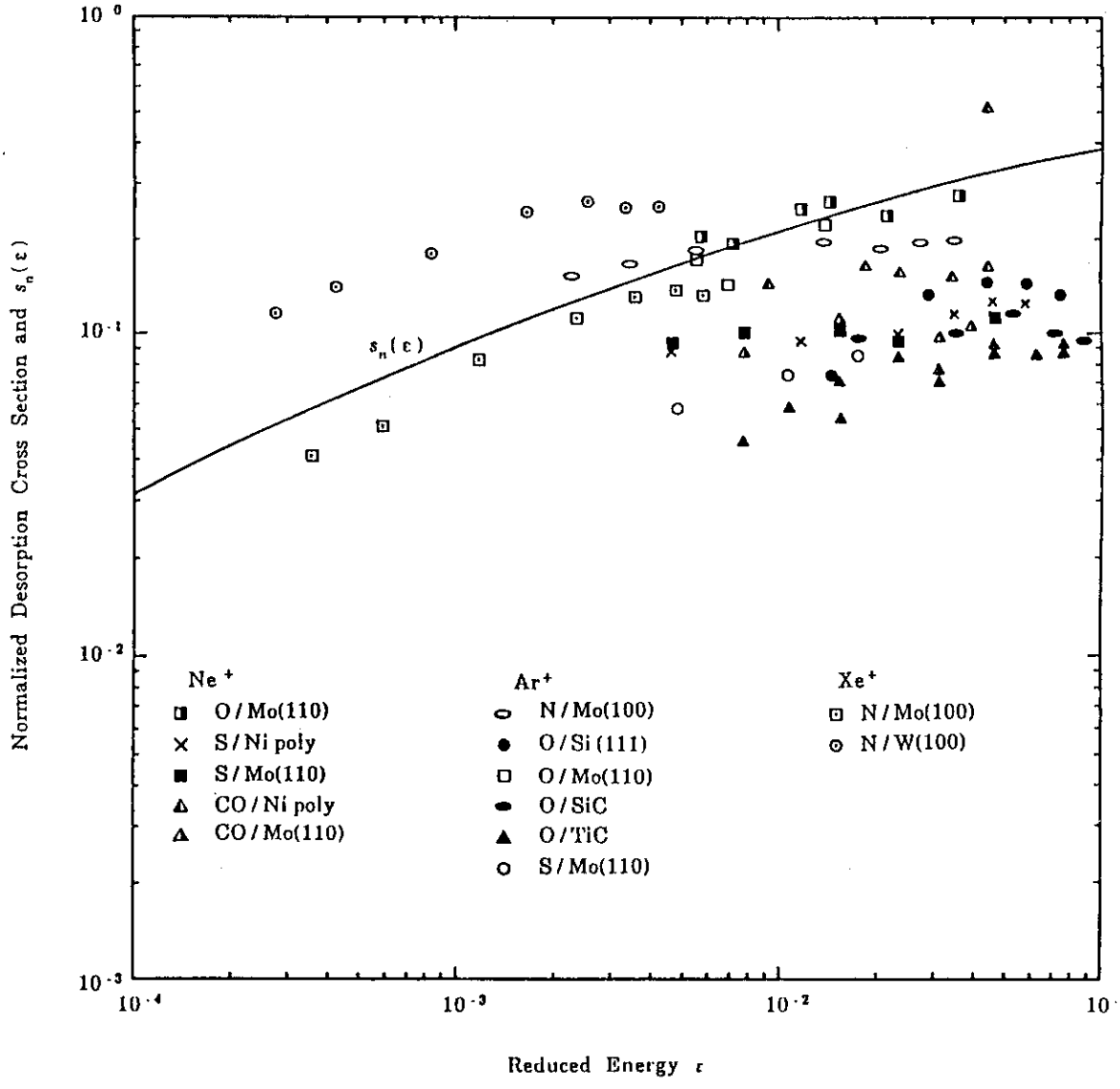

Fig. 59 Normalized desorption cross section as a function of reduced energy ε

4.5 Other energy dependences of desorption cross section

As has been discussed in section 3, some of the experimental desorption cross sections cannot be explained not only quantitatively but also qualitatively by Winters and Sigmund's model. These data increase with the increase of incident energy, irrespective of ion species. Some of them rapidly increase according to E^a where a is larger than 1. The parameters a and Q obtained when the experimental data are assumed to be given by QE^a, have already been given in Table 17. The desorption cross sections for chemisorbed S atoms on Ni surface are shown in Fig. 60 as functions of projectile energy and projectile-ion species. The desorption cross sections for heavier ions are larger than those for light ions as expected, but their energy dependence cannot be explained by the model discussed in the previous section. Figure 61 shows the energy dependence of the desorption cross sections with an energy parameter $E/(U_3 r_{13}^{-1})$. In this case, the desorption cross section shows a linear dependence on the energy parameter in a log-log scale. It is roughly proportional to $[E/(U_3 r_{13})]^2$ regardeless of projectile ions. Figure 62 shows the normalized desorption cross sections for Ne^+ ions as a function of reduced energy ε, where the normalized desorption cross sections are calculated from the same procedures discussed in section 4-4. It is also found that the desorption cross section shows a linear dependence on ε regardless of adsorbate-target combinations. It is roughly proportional to $\varepsilon^{2.5}$. Figure 63 shows the normalized desorption cross sections for Ar^+ and He^+ ions which increase linearly with reduced energy ε.

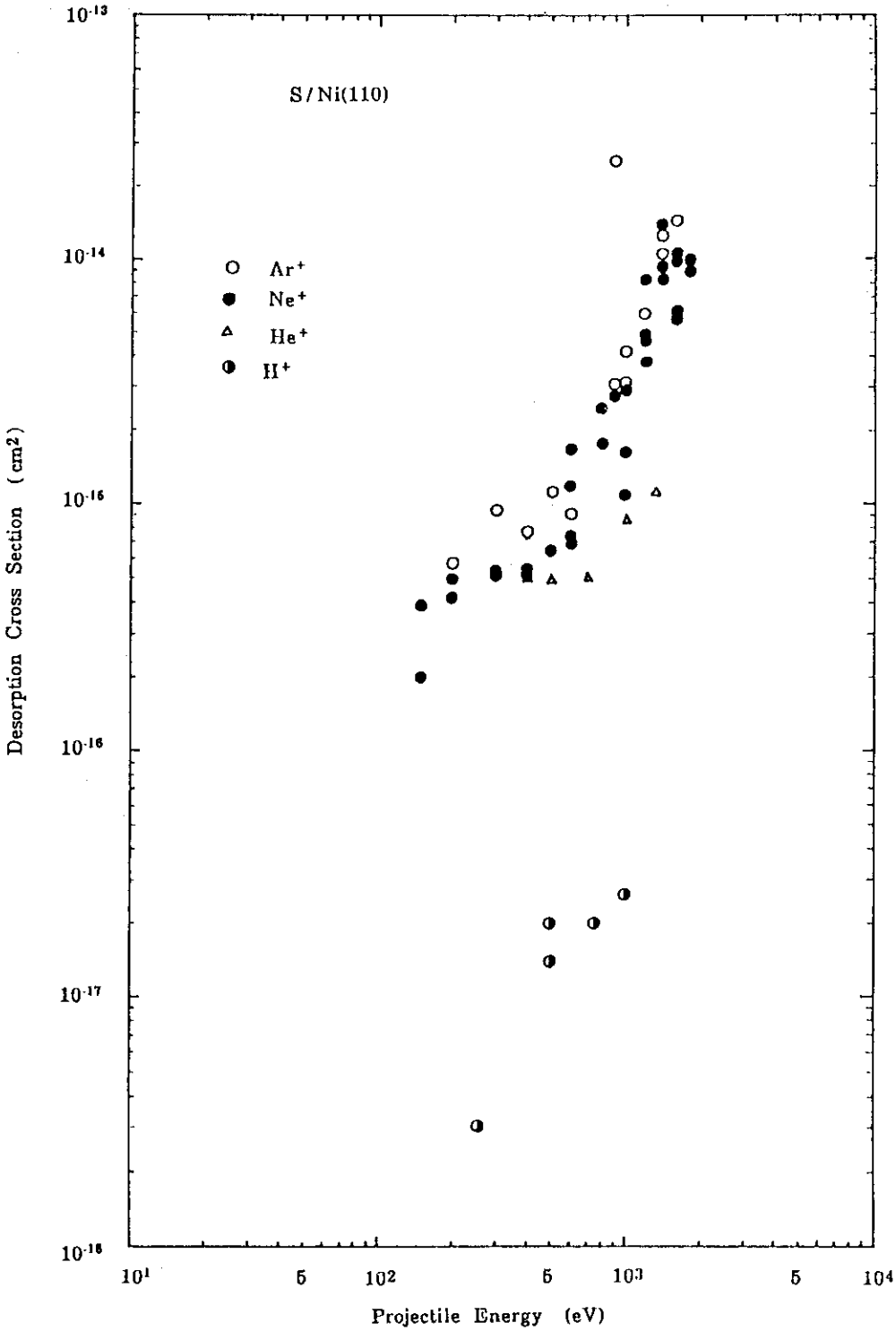

Fig. 60 Desorption cross section as a function of projectile energy

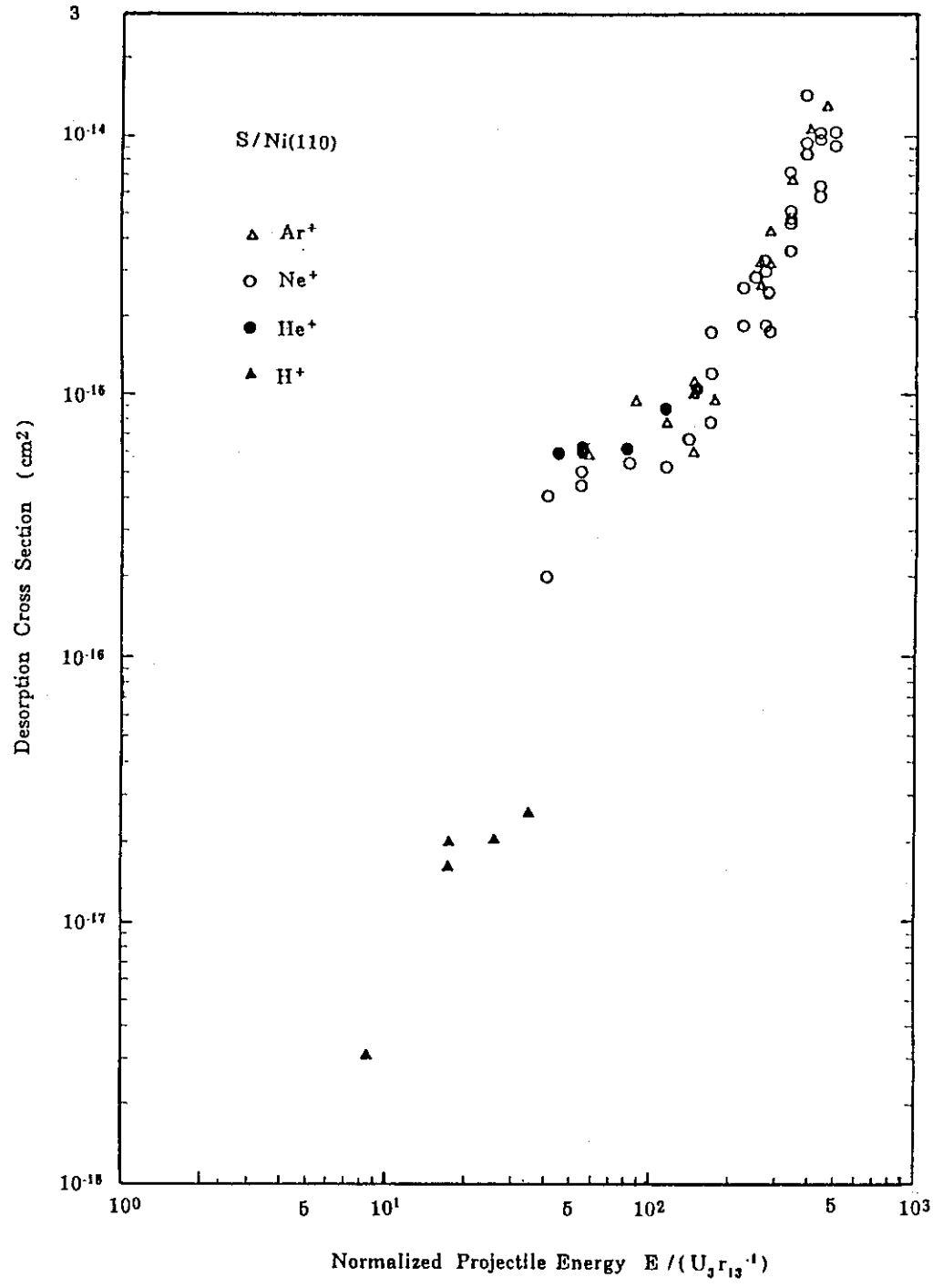

Fig. 61 Desorption cross section as a function of normalized projectile energy

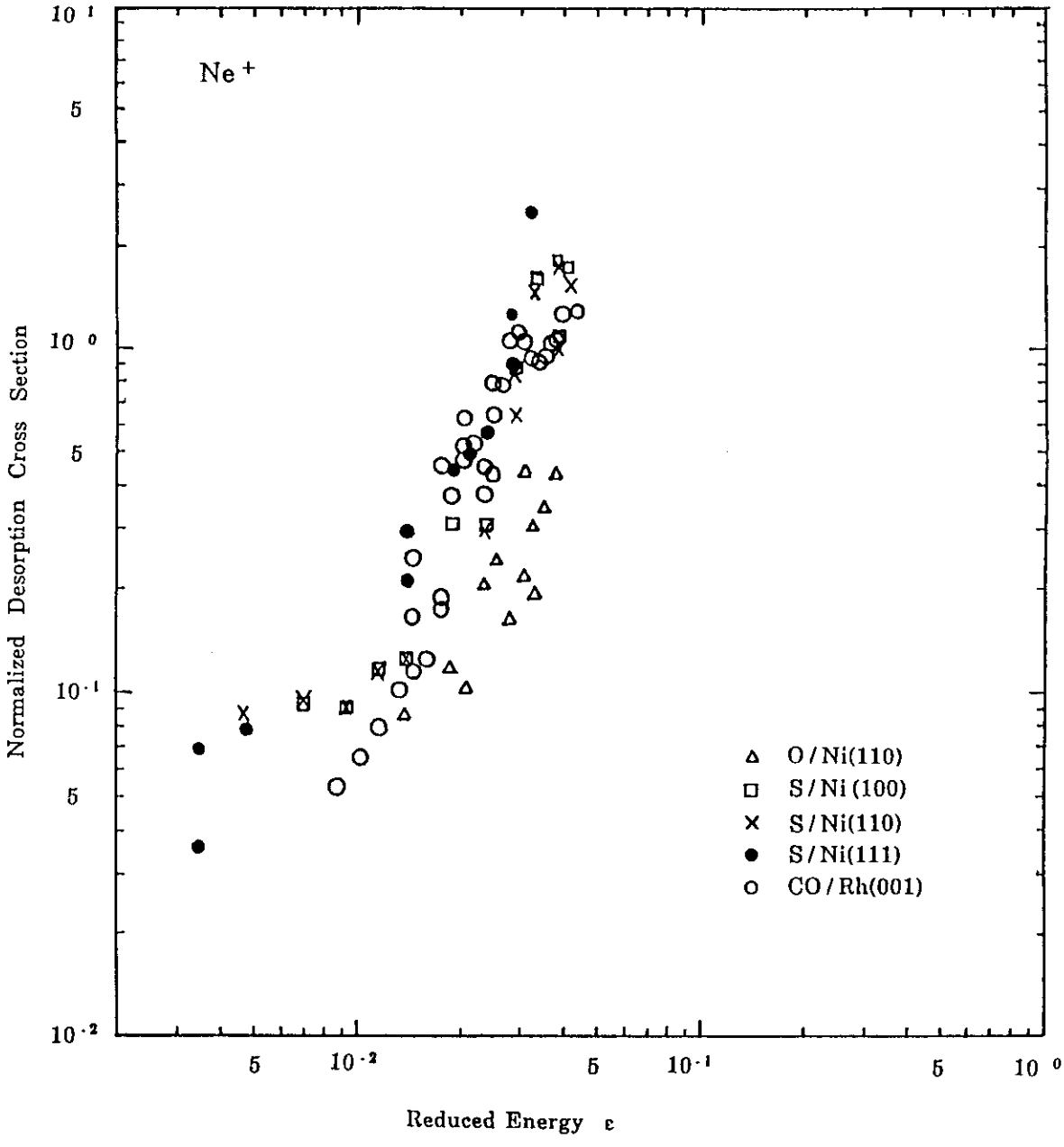

Fig. 62 Normalized desorption cross section as a function of reduced energy ε

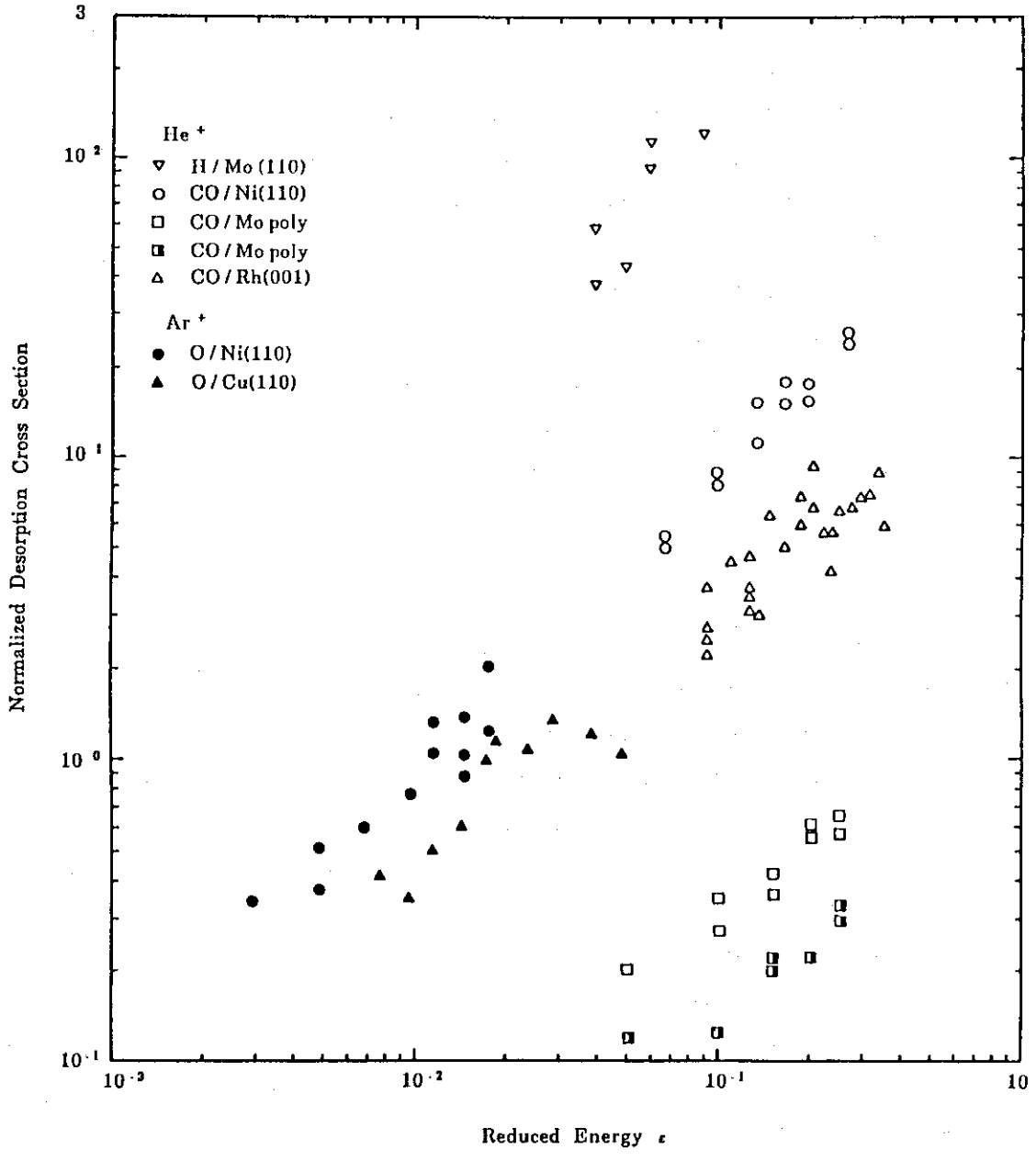

Fig. 63 Normalized desorption cross section as a function of reduced energy ε

5. Conclusions

Comparisons of the experimental and calculated ion-impact desorption cross sections have been carried out. It has been found that the model proposed by Winters and Sigmund is not sufficient to describe the desorption processes and further studies of desorption processes are needed to explain, for example, the energy dependence of the desorption cross section. For light ions such as H^+ and D^+ ions, the collision of the reflected ion with adsorbate atom is found to be important. In addition, the collision of primary recoil atoms created by the reflected ions with adsorbate atoms should be taken into account especially for He^+ ions. The fact that the reflected projectile is the principal source for desorption is the same to the situation of light-ion sputtering. For heavy ions such as Ar^+ and Xe^+ ions, the desorption processes can be explained fairly well on the basis of the linear collision cascade theory proposed by Sigmund with a modification from collision between sputtered and substrate atoms to collision between sputtered and adsorbed atoms on the surface. In the Sigmund theory, the collision of reflected ion with the substrate atom and the subsequent collisional cascade are not taken into account explicitly. This process is found to become dominant for the desorption processes for Ne^+ ions. The key to evaluate this effect is analytical description of the energy- and angular-distribution of the reflected ions in the energy range $0.5\ keV \ll E \ll 5\ keV$.

Since theoretical description of the energy dependence of the desorption cross section is insufficient, derivation of a simple empirical analytical curve from the compiled data is favourable. Figures 54, 57 and 58 show that all the desorption cross sections have similar shape against incident energy. This means that all curves fall in a curve by displacing appropriately in horizontal and vertical directions in a log-log scale. Namely, the desorption cross section may be expressed by a universal energy function.

Ion-impact desorption experiments have so far been carried out on single crystal surfaces covered with less than monolayer, but the crystallographic orientations of the substrate relative to the incident beam directions have not been cleary defined. On the other hand, the desorption processes discussed above are based on the reflection and sputtering for polycrystalline material. If anisotropic effects on the desorption processes can be taken into account, we may find a way to explain the energy-dependence discussed in section 4.5, where the desorption

cross sections increase with incident energy more rapidly than those expected from the theory. It has been reported that the sputtering yield of single crystal materials depends on the planes[48]. In the case of Ar^+ ions on (111) plane of Cu, the sputtering yields are larger than those of polycrystalline material. The yield curves show relatively sharp maximum at an energy. This energy depends on the crystallographic orientation of the surface plane and is much smaller than the corresponding energy for the polycrystalline materials. Consequently, the yields for a particular surface plane are more than two or three times larger than those for the polycrystalline materials.

References

1) K.L. Wilson; J. Nucl. Mater. 103/104 (1981) 453.
2) H.F. Winters and P. Sigmund; J. Appl. Phys. 45 (1974) 4760.
3) W. Eckstein and H. Verbeek; Nucl. Fusion, Special Issue, "Data Compendium for Plasma-Surface Interactions" edited by R.A. Langley et al. (IAEA, Vienna, 1984) p 12.
4) J. Bohdansky; Nucl. Instrum. & Methods Phys. Res. B2 (1984) 587.
5) E. Miyazaki and I. Yasumori; Surf. Sci. 55 (1976) 747.
6) T. Oshiyama, S. Nagai, K. Ozawa and F. Takeutchi; JAERI-M, 85-100 (1985).
7) O.B. Firsov; Sov. Phys. JETP 7 (1958) 308.
8) P. Gombas; Rev. Mod. Phys. 35 (1963) 512.
9) S. Kobayashi, T. Matsukuma, S. Nagai and K. Omeda; J. Phys. Soc. Jpn. 10 (1955) 759.
10) C. Lehmann; in the Interaction of Radiation with Solids and Elementary Defect Production edited by S. Amelinckx et al. (North Holland, New York, 1977) p 78.
11) J. Lindhard, V. Nielsen and M. Scharff; Mat. Fys. Medd. Dan. Vid. Selsk. 36 no.10 (1968).
12) P. Sigmund; Phys. Rev. 184 (1969) 383.
13) W. Eckstein and H. Verbeek; Max-Planck-Institute für Plasmaphysik Report IPP-9/32 (1979).
14) J. Bohdansky; Nucl. Fusion, Special Issue, "Data Compendium for Plasma-Surface Interactions" edited by R.A. Langley et al. (IAEA, Vienna, 1984) p 61.
15) L. Pauling; in the Nature of the Chemical Bond (Cornell University, Ithaca, 1960).
16) D.D. Eley; Disc. Faraday Soc. 8 (1950) 34.
17) D. Brennan and F.H. Hayes; Phil. Trans. Roy. Soc. London A 258 (1965) 347.
18) D.D. Eley and P.R. Norton; Proc. Roy Soc. London A 314 (1970) 301.
19) H.O. Pritchard and H.A. Skinner; Chem. Rev. 55 (1955) 745.
20) S. Trasatti; J. Chem. Soc. Faraday Trans. I 68 (1972) 229.
21) E.S. Mashkov; Radiat. Eff. 54 (1981) 1.
22) E.S. Mashkova and V.A. Molchanov; in the Medium Energy Ion Scattering from Surfaces of Solid (Atomizat, Moscow, 1980).
23) N.N. Koborov, V.A. Kurnaev, V.G. Telkovsky and G.I. Zhabrev; Radiat. Eff. 69 (1983) 135.

24) M.W. Thompson; Phys. Reports 4 (1981) 335.
25) H.H. Andersen and H.L. Bay; in the Sputtering by Particle Bombardment I, edited by R. Behrisch (Springer, Berlin, 1981) p 145.
26) P. Sigmund; in the Sputtering by Particle Bombardment I, edited by R. Behrisch (Springer, Berlin, 1981) p 9.
27) P. Sigmund; Rev. Roum. Phys. 17 (1972) 1079.
28) P. Sigmund; In the Inelastic Ion-Surface Collisions edited by N.H. Tolk et al. (Academic Press, New York, 1977) p 121.
29) D.L. Smith; J. Nucl. Matter. 75 (1978) 20.
30) N. Matsunami, Y. Yamamura, Y. Itikawa, N. Itoh, Y. Kazumata, S. Miyagawa, K. Morita and R. Shimizul Radiat. Eff. Lett. 57 (1980) 15.
31) R. Weissman and P. Sigmund; Radiat. Eff. 19 (1973) 7.
32) R. Weissman and R. Behrisch; Radiat. Eff. 19 (1973) 69.
33) J. Bohdansky; J. Nucl. Mater. 93/94 (1980) 44.
34) J. Bohdansky, J. Roth and H.L. Bay; J. Appl. Phys. 51 (1980) 2861.
35) H.L. Bay, J. Roth and J. Bohdansky; J. Appl. Phys. 48 (1977) 4722.
36) Y. Yamamura, Y. Itikawa and N. Itoh; Nagoya University Institute of Plasma Physics Report IPPJ-AM-26 (1983).
37) W. Eckstein and J.P. Biersack; Nucl. Instrum. & Methods Phys. Res. B 2 (1984) 550.
38) J.P. Biersack and W. Eckstein; Appl. Phys. A 34 (1984) 73.
39) G.M. McCracken and N.J. Freeman; J. Phys. B 2 (1969) 661.
40) J. Lindhard and M. Scharff; Phys. Rev. 124 (1961) 128.
41) J. Vukanic and P. Sigmund; Appl. Phys. 11 (1976) 265.
42) E. Kawatoh, R. Shimizu and J. Fujita; Jpn. J. App. Phys. 24 (1985) 1150.
43) L.C. Feldman and J.W. Mayer; in the Fundamentals of Surface and Thin Film Analysis (North-Holland, New York, 1986) p 33.
44) J. Vukanic. R.K. Janev and D. Heifetz; Nucl. Instrum. & Methods Phys. Res. B 18 (1987) 131.
45) U. Littmark and S. Fedder; Nucl. Instrum. & Methods 194 (1982) 607.
46) Y. Yamamura, N. Matsunami and N. Itoh; Radiat. Eff. 71 (1983) 65.
47) G. Falcone and A. Oliva; Nuovo. Cimento 5 (1985) 464.
48) H.E. Roosendaal; in the Sputtering by Particle Bombardment I, edited by R. Behrisch (Springer, Berlin, 1981) p 219.

Appendix

Table A1 Experimental data on heat of O_2 adsorption

Element	Q (kcal/mole)			
Al	211 [1]			
Ti	236 [1]	233 [2]		
Cr	174 [1]			
Mn	150 [1]	157 [2]		
Fe	136 [1]	135 [2]		
Co	100 [1]	101 [2]	98 [3]	
Ni	107 [1]	119 [2]	107 [3]	
Nb	208 [1]	207 [2]		
Mo	172 [1]	178 [2]	192 [3]	110 [4]
Ru	80 ~ 90 [5]			
Rh	76 [1]	123 [2]		
Pd	67 [1]	70 [2]		
Ta	212 [1]	213 [2]		
W	194 [1]	200 [2]	183 [3]	118 ~ 119 [9]
	127 [10]	92 [11]	137 [12]	132 [13]
	110 [14]			
Ir	65 [6]	70 [7]		
Pt	67 [1]	72 [2]	69 [8]	40 [15]

1) D. Brennan, D.O. Hayward and B.M.W. Trapnell, Proc, Roy. Soc. London A256, 81-105 (1960).
"The Calorimetric Determination of the Heats of Adsorption of Oxygen on Evaporated Metal Films"

2) J.J. Burton, Surf. Sci. 66, 647-651 (1977).
"A General Rule for the Adsorption of Gases on Metals"

3) D. Brennan and M.J. Graham, Disc. Faraday Soc. 41, 95-101 (1966).
"Heat of Adsorption of Oxygen on Evaporated Films of Molybdenum, Tungsten, Cobalt and Nickel at 77, 90 and 273 °K, and Nature of Adsorbed Layers"

4) P.A. Redhead, Can. J. Phys. 42, 886-905 (1964).
"Interaction of Slow Electrons with Chemisorbed Oxygen"

5) T.E. Madey, H.A. Engelhardt and D. Menzel, Surf. Sci. 48, 304-328 (1975).
"Adsorption of Oxygen and Oxidation of CO on the Ruthenium (001) Surface"

6) V.P. Ivanov, G.K. Boreskov and V.I. Savchenko, Surf. Sci. 61, 207-220 (1976).
"The Chemisorption of Oxygen on the Iridium (111) Surface"

7) J. Küppers and A. Plagge, J. Vac. Sci. Technol. 13, 259-263 (1975).
"Interaction of CO and O_2 with Ir (111) Surfaces"

8) G. Kneringer and F.P. Netzer, Surf. Sci. 49, 125-142 (1975).
"Adsorption Studies of Oxygen and Carbon Monoxide on a Pt (100) Surface"

9) D.A. King, T.E. Madey and J.T. Yates, Jr., J. Chem. Phys. 55, 3236-3246 (1971).
"Interaction of Oxygen with Polycrystalline Tungsten I. Sticking Probabilities and Desorption Spectra"

10) C.G. Goymour and D. King, J. Chem. Soc. Faraday I 68, 280-289 (1972).
"Field Emission Study of the Formation and Desorption of Oxide Layers on Tungsten Surfaces"

11) C. Kohrt and R. Gomer, J. Chem. Phys. 52, 3283-3294 (1970).
"Adsorption of Oxygen on the (110) Plane of Tungsten"

12) Yu. G. Ptushinskii and B.A. Chuikov, Surf. Sci. 6, 42-56 (1967).
"Mass Spectrometric Invesitgation of the Interaction of Oxygen with a Tungsten Surface"

13) W. Engelmaier and R.E. Stickney, Surf. Sci. 11, 370-394 (1968).
"Adsorption Studies Based on Thermonic Emission Measurement 2. Oxygen on Single Crystal Tungsten"

14) T.E. Madey, Surf. Sci. 33, 355-376 (1972).
"Adsorption of Oxygen on W(100): Adsorption Kinetics and Electron Stimulated Desorption"

15) D.M. Collins, J.B. Lee and W.E. Spicer, Surf. Sci. 55, 389-402 (1976).
"A Photoemission and Thermal Desorption Study of Carbon Monoxide and Oxygen Adsorbed on Platinum"

Table A2 Experimental data on heat of N_2 adsorption

Element	Q (kcal/mole)
Cr	105 [1]
Fe	70 [11] 40 [2] 50 ~ 60 [3]
Zr	150 [2]
Mo	63 [12] 65 [2]
Rh	58 [4]
Ta	138 [1] 139 [2] 140 [5] 102 [6]
W	95 [1] 119 [2] 79 [7],[8] 75 [10] 74 [13],[14]
Ir	58 [4]
Pt	62 [9]

1) O. Beeck, W.A. Cole and A. Wheeler, Disc. Faraday Soc. 8, 314-321 (1950).
"Determination of Heats of Adsorption Using Metal Films"

2) J.J. Burton, Surf. Sci. 66, 647-651 (1977).
"A General Rule for the Adsorption of Gases on Metals"

3) G. Erü, M. Grunze and M. Weiss, J. Vac. Sci. Technol. 13, 314-317 (1876).
"Chemisorption of N_2 on an Fe (100) Surface"

4) V.J. Mimeault and R.S. Hansen, J. Phys. Chem. 70, 3001-3003 (1966).
"Nitrogen Adsorption on Iridium and Rhodium"

5) R.P.H. Gasser, C.P. Lawrence and D.G. Newman, Trans. Faraday Soc. 62, 2916-2921 (1966).
"Interaction of Nitrogen wist Tantalum"

6) R. Griffiths and J.A. Pryde, Trans. Faraday Soc. 63, 2599-2604 (1977).
"Solubility of Nitrogen in Tantalum"

7) P.W. Tamm and L.D. Schmidt, Surf. Sci. 26, 286-296 (1971).
"Crystallographic Anisotropies in Condensation: N_2 on (110) W"

8) P.J. Estrup and J. Anderson, J. Chem. Phys. 46, 567-570 (1967).
"LEED Studies of the Adsorption Systems W (100) + N_2 and W (100) + N_2 + CO"

9) M. Wilf and P.T. Dawson, Surf. Sci. 60, 561-581 (1976).
"Adsorption of Nitrogen on Platinum"

10) T.A. Delchar and G. Ehrlich, J. Chem. Phys. 42, 2686-2702 (1965).
"Chemisorption on Single-Crystal Planes: Nitrogen on Tungsten"

11) J. Bagg and F.C. Tompkins, Trans. Faraday Soc. 51, 1071-1080 (1955).
"Calorimetric Heat of Sorption of Gases on Evaporated Iron Films"

12) T. Oguri, J. Phys. Soc. Jpn. 19, 77-83 (1964).
"Chemisorption of Nitrogen on Molybdenum"

13) L.R. Clavenna and L.D. Schmidt, Surf. Sci. 22, 365-391 (1970).
"Interaction of N_2 with (100) W"

14) D.L. Adams and L.H. Germer, Surf. Sci. 27, 21-44 (1971).
"Adsorption on Single-Crystal Planes of Tungsten I. Nitrogen"

Table A3 Experimental data on heat of H_2 adsorption

Elements	Q (kcal/mole)
Ti	39 [1]
Cr	45 [1),2)]
Fe	33 [2)] 27 [3)] 28 ~ 36 [1)]
Co	24 ± 4 [2)] 34 [3)]
Ni	30 [2)] 24 [2)] 37 [5)] 35 [5)] 23 [6)]
Cu	28 ± 4 [2)] 28 [1)]
Nb	27 ± 3 [4)]
Mo	40 [1),2),3)]
Ru	26 ± 2 [2)]
Rh	26 [2)] 27 [3)]
Pd	26 [2),3)] 28 [1)]
Ta	45 [1),2)]
W	46 [2)] 43 [3)] 32 [8),9)] 45 [1)] 38 [14)]
Re	30 [10)]
Ir	26 ± 2 [2)] 24 [8)]
Pt	27 ± 1 [2)] 37 [3)] 31 [11)] 32 [12),13)] 26 [1)]

1) S. Trasatti, J. Chem. Soc. Faraday Trans. I 68, 229-235 (1972). "Electronegativity, Work Function, and Heat of Adsorption of Hydrogen on Metals"

2) D.P. Stevenson, J. Chem. Phys. 23, 203 (1955). "Heat of Chemisorption of Hydrogen in Metals"

3) J.J. Burton, Surf. Sci. 66, 647-651 (1977). "A General Rule for the Adsorption of Gases on Metals"

4) D.I. Hagen and E.E. Dowaldson, Surf. Sci. 45, 61-76 (1974). "Interaction of Hydrogen with a (100) Niobium Surface"

5) D. Lichtmann, F.N. Simon and T.R. Kirst, Surf. Sci. 9, 325-346 (1968). "Electron Probe Surface Mass Spectrometry Study of the Hydrogen - 100 Nickel System"

6) J. Lapujoulade and K.S. Neil, J. Chem. Phys. 57, 3535-3545 (1972). "Chemisorption of Hydrogen on the (111) Plane of Nickel"

7) B.J. Mimeault, R.H. Hansen, J. Chem. Phys. 45, 2240-2250 (1966).
"Flash Desorption and Isotopic Mixing of Hydrogen and Deuterium Adsorbed on Tungsten, Iridium and Rhodium"

8) P.W. Tamm and L.D. Schmidt, J. Chem. Phys. 51, 5352-5363 (1969).
"Interaction H_2 with W(100) I. Binding States"

9) P.W. Tamm and L.D. Schmidt, J. Chem. Phys. 54, 4775-4787 (1971).
"Binding States of Hydrogen on Tungsten"

10) K.F. Poulter and J.A. Pryde. J. Phys. D 1, 169-172 (1968).
"Chemisorption of Hydrogen on Rhenium"

11) V.A. Lampton, Thesis, Chemical Engineering Department, University of California, Berkeley 1971.

12) H. Chon, R.A. Fisher and J.G. Aston, J. Am. Chem. Soc. 82, 1055-1057 (1960).
"On the Preparation of Platinum Black with Clean Surface. Preliminary Heats of Adsorption of Hydrogen"

13) W.H. Weinberg, D.R. Monroe, V. Lampton and R.P. Merrill, J. Vac. Sci. Technol. 14, 444 (1977).
"Interaction of H_2 and O_2 on platinum (111)"

14) D.D. Eley and P.R, Norton, Proc. Roy. Soc. Lond. A 314, 301-318 (1970).
"Heats of Adsorption on Metal Wires. I Hydrogen on Polycrystalline Tungsten"

Table A4 Experimental data on heat of CO adsorption

Element	Q (kcal/mole)				
Mg	76 [1]				
Ti	156 [2]				
Cr	150 [1]				
Mn	80 [2]				
Fe	46 [2]				
Co	46 [1]	48 [2]			
Ni	40 [1]	42 [2]	30 [3]		
Zr	148 [1]	146 [2]			
Nb	116 [1]	133 [2]			
Mo	60 [1]	75 [2]	99 [4]	77 [5]	50 [4]
Ru	28 [6]	23 [13]			
Rh	44 [1]	49 [2]	30 [7]		
Pd	40 [1]	43 [2]	34 ~ 40 [8]	38 [9]	
	29 [14]				
Ta	128 [1]	136 [2]			
W	80 [1]	100 [2]	* see references 15 ~ 21		
Ir	32 ~ 34 [12]				
Pt	44 [1]	51 [2]	40 [10]	31 [11]	

1) D. Brennan and F.H. Hayes, Phil. Trans. Roy. Soc. London A258 347-373 (1965).
"The Adsorption of Carbon Monoxide on Evaporated Metal Films"

2) J.J. Burton, Surf. Sci. 66, 647-651 (1977).
"A General Rule for the Adsorption of Gases on Metals"

3) J.C. Tracy, J. Chem. Phys. 56, 2736-2747 (1972).
"Structure Influences on Adsorption Energy II. CO on Ni (100)"

4) E. Gillet, J.C. Chiarena and M. Gillet, Surf. Sci. 66, 596-612 (1977).
"Chemsorption du Monoxyde de Carbone Sur La Face (110) du Molybdene I. Etude Experimentale de l'Adsorption-Desorption de CO/Mo (110)"

5) C. Guillot, R. Rinan and J. Lecante, Surf. Sci. 59, 581-592 (1976).
"Dissociation of CO on Mo (100)"

6) P.D. Reed, C.M. Comrie and R.M. Lambert, Surf. Sci. 59, 33-45 (1976).
"Chemisorption, Surface Structural Chemistry, and Electron Impact Properties of CO on Ru (101)"

7) R.A. Marbow and R.M. Lambert, Surf. Sci. 67, 489-500 (1977).
"Chemisorption, Surface Structural Chemistry, and Electron Impact Properties of Carbon Monoxide on Rhodium (110)"

8) H. Conrad, G. Ertl, J. Koch and E.E. Latta, Surf. Sci. 43, 462-480 (1974).
"Adsorption of CO on Pd Single Crystal Surfaces"

9) J.C. Tracy and P.W. Palmberg, J. Chem. Phys. 51, 4852-4862 (1969).
"Structural Influences on Adsorbate Binding Energy I, Carbon Monoxide on (100) Palladium"

10) W.L. Winterbottom, Surf. Sci. 37, 195-204 (1973).
"Application of Thermal Desorption Methods in Studies of Catalysis, I. Chemisorption of Carbon Monoxide on Platinum"

11) R.M. Lambert and C.M. Comrie, Surf. Sci. 46, 61-80 (1974).
"The Oxidation of CO by NO on Pt (111) and Pt (110)"

12) J. Küppers and A. Plagge, J. Vac. Sci. Technol. 13, 259-263 (1975).
"Interaction of CO and O_2 with Ir (111) Surfaces"

13) T.E. Madey, H.A. Engelhardt and D. Menzel, Surf. Sci. 48, 304-328 (1975).
"Adsorption of Oxygen and Oxidation of CO on the Ruthenium (001) Surface"

14) T.E. Madey, J.T. Yates, Jr., A.M. Bradshaw and F.M. Hoffmann, Surf. Sci. 89, 370-380 (1979).
"Evidence for "Inclined" CO on Pd (210)"

15) P.A. Redhead, Trans. Faraday Soc. 57, 641-656 (1960).
"Chemosorption on Polycrystalline Tungsten, Part I Carbon Monoxide"

16) C. Kohrt, R. Gomer, Surf. Sci. 24, 77-103 (1971).
"The Adsorption of CO on the (110) Plane of Tungsten"

17) M.R. Leggett and R.A. Armstrong, Surf. Sci. 24, 404-416 (1971).
"A Study of Hydrogen Adsorption on a (100) Tungsten Surface Using a Simple HEED System"

18) L.R. Clavenna and L.D. Schmidt, Surf. Sci. 33, 11-26 (1972).
"Decomposition of CO_2 on (100) W"

19) D.A. King, C.G. Goymour and J.T. Yates, Jr., Proc. Roy. Soc. London A331, 361-376 (1972).
"Chemisorption of Carbon Monoxide on Tungsten"

20) C. Kohrt and R. Gomer, Surf. Sci. 40, 71-84 (1973).
"The Adsorption of CO on Tungsten, the Sticking Coefficient and Absolute Surface Coverages"

21) J.T. Yates, Jr., T.E. Madey and N.E. Erickson, Surf. Sci. 43, 257-274 (1974).
"ESCA Study of Carbon Monoxide and Oxygen Adsorption on Tungsten"

Table A5 Experimental data on heat of S_2 adsorption

Element	Q (kcal/mol)		
C_r	66.1		
Fe	45.3		
Ni	55.1		
Cu	42.6	38	
Mo	51.8		
Ag	29	24.2	22.0
Pt	37.1	44.9	

* J. Benard, Surf. Sci. 88 L35 - L41 (1987).
"The Thermodynamics of Some Metallic 2D Suphides"

Table A6 List of Compilations on Atomic and Molecular Data

1. "Production processes of multiply charged ions by electron impact": N. Oda, JAERI-M 8675 (1980) (in Japanese).
2. "Review of theories of charge transfer processes involving highly stripped heavy ions": M. Matsuzawa, JAERI-M 8676 (1980) (in Japanese).
3. "Data on collisions of helium atoms and ions with atoms and molecules I. (Cross sections for charge transfer of He, He^{+}, and He^{++} with H, H_2, and He": Y. Nakai, M. Sataka, and T. Shirai, JAERI-M 8849 (1980) (in Japanese).
4. "Cross section for charge transfer collision involving hydrogen atoms": Y. Kaneko, T. Arikawa, Y. Itikawa, T. Iwai, T. Kato, M. Matsuzawa, Y. Nakai, K. Okuno, H. Ryufuku, H. Tawara, and T. Watanabe, IPPJ-AM-15 (1980).
5. "Ionization cross sections for ion-atom and ion-molecule collisions I (Ionization cross sections for H^{+}, H_2^{+}, H_3^{+}, He^{+} and He^{++} incident on H, H_2 and He)": M. Sataka, T. Shirai, A Kikuchi and Y. Nakai, JAERI-M 9310 (1981).
6. "Report of workshop on particle material interactions for fusion research", A & M data research committee, JAERI-M 9775 (1981) (in Japanese).
7. "Electron capture and loss cross sections for collisions between heavy ions and hydrogen molecules.": Y. Kaneko, Y. Itikawa, T. Iwai, T. Kato, Y. Nakai, K. Okuno, and H. Tawara, IPPJ-AM-20 (1981).
8. "Negative ion formation and neutralization process (I) - Related to plasma heating by "Negative ion based neutral beam injection" -": T. Sugiura, JAERI-M 9902 (1982) (in Japanese).
9. "Negative ion formation and neutralization process (II) - Related to plasma heating by "Negative ion based neutral beam injection" -": T. Sugiura, JAERI-M 82-116 (1982) (in Japanese).
10. "Data on trapping and re-emission of energetic hydrogen isotopes and helium in materials": S. Yamaguchi, K. Ozawa, Y. Nakai, and Y. Sugizaki, JAERI-M 82-118 (1982).
11. "Data on collisions of hydrogen atoms and ions with atoms and molecules I (cross sections for charge transfer of H, H^{+} and H^{-} with H_2, N_2, O_2, H_2O, C and carbon containing molecules)": Y. Nakai, A. Kikuchi, T. Shirai, and M. Sataka, JAERI-M 83-013 (1983).

12. "Data on thick target bremsstrahlung produced by electrons": S. Tanaka, R. Tanaka, T. Tabata, R. Ito, Y. Nakai, and K. Ozawa, JAERI-M 83-019 (1983).
13. "Atomic structure calculation of energy levels and oscillator strength in Mo ion, I ($3p^6 3d^8$-$3p^5 3d^9$ $3d^8$-$3d^7 4p$ and $3d^8$-$3d^7 4f$ transitions in Mo XVII)": K. Ishii, JAERI-M 83-034 (1983).
14. "Data on collisions of hydrogen atoms and ions with atoms and molecules II (Cross sections for charge transfer of H, H^+ and H^- with He, Ne, Ar, Kr and Xe)": Y. Nakai, A. Kikuchi, T. Shirai, and M. Sataka, JAERI-M 83-143 (1983).
15. "Atomic structure calculation of energy levels and oscillator strength in Ti ion, I (3s-3p and 3p3d transitions in Ti IX)": K. Ishii, JAERI-M 83-155 (1983).
16. "Atomic structure calculation of energy levels and oscillator strength in Ti ion, II (3s-3p and 3p3d transitions in Ti X)": K. Ishii, JAERI-M 83-164 (1983).
17. "Atomic structure calculation of energy levels and oscillator strength in Ti ion, III (3s-3p and 3p3d transitions in Ti XI)": K. Ishii, JAERI-M 83-198 (1983).
18. "Stopping power for ions in solids": M. Kitagawa, JAERI-M 83-223 (1983) (in Japanese).
19. "Report of workshop on computer simulation of atomic collision processes in solids": A & M data research committee, JAERI-M 83-226 (1983) (in Japanese).
20. "Report of the 2nd workshop on particle material interactions for fusion research": A & M data research committee, JAERI-M 83-235 (1983) (in Japanese).
21. "Atomic structure calculation of energy levels and oscillator strength in Fe ion, I (3s-3p and 3p3d transitions in Fe XV)" K. Ishii, H. Kubo, and K. Ozawa, JAERI-M 83-240 (1983).
22. "Data on ionization, excitation, dissociation, and dissociative ionization of targets by helium ion bombardments (I) (Target ionization, excitation, dissociation, and dissociative ionization induced by several keV to 3.5MeV helium ions incident on a thin gas targets)": N. Oda and J. Urakawa, JAERI-M 84-049 (1984).

23. "Data on collisions of helium atoms and ions with atoms and molecules II (Cross sections for charge transfer of He^{2+}, He^{+}, He and He^{-} with He, Ne, Ar, Kr and Xe)":. Y. Nakai, A. Kikuchi, T. Shirai, and M. Sataka, JAERI-M 84-069 (1984).
24. "Data compilation of radiation effects on hydrogen recycle in fusion materials": K. Ozawa, K. Fukushima, and K. Ebisawa, JAERI-M 84-089 (1984).
25. "Data compilation for depth distribution of ion-induced damage and ion-implanted atom": M. Terasawa, S. Nakahigashi, and K. Ozawa, JAERI-M 84-092 (1984).
26. "Data on trapping and re-emission of energetic hydrogen isotopes and helium in materials, supplement 1": S. Yamaguchi, K. Ozawa, Y. Nakai, and Y. Sugizaki, JAERI-M 84-093 (1984).
27. "Data compilation for particle impact desorption": T. Oshiyama, S. Nagai, K. Ozawa, and F. Takeuchi, JAERI-M 84-094 (1984).
28. "Data on collisions of hydrogen atoms and ions with atoms and molecules III (Cross sections for charge transfer of H, H^{+} and H^{-} with metal vapors)": Y. Nakai, T. Shirai, M. Sataka, and T. Sugiura, JAERI-M 84-169 (1984).
29. "Cross sections for electron capture and loss by positive ions in collisions with atomic and molecular hydrogen": H. Tawara, T. Kato, and Y. Nakai, Atom. Data Nucl. Data Tables 32, 235 (1985).
30. "Hydrogen re-emission data analysis in austenitic stainless steel": K. Fukushima, K. Ozawa, K. Ebisawa, and M. Terasawa, JAERI-M 85-099 (1985).
31. "Data compilation for particle impact desorption II": T. Oshiyama, S. Nagai, K. Ozawa, and F. Takeuchi, JAERI-M 85-100 (1985).
32. "Review on the calculations of atomic collisions in solids": M. Fuse and T. Iwata, JAERI-M 85-118 (1985) (in Japanese).
33. "Data compilation for radiation effects on ceramic insulators": K. Fukaya, K. Ozawa, M. Terasawa, and S. Nakahigashi, JEARI-M 86-127 (1986).
34. "Spectral data and Grotrian diagrams for highly ionized titanium, Ti V - Ti XXII": K. Mori, W.L. Wiese, T. Shirai, Y. Nakai, K. Ozawa, and T. Kato, Atom. Data Nucl. Data Tables 34, 79 (1986).
35. "Computer simulations of knock-on processes in BCC Ta crystal": M. Fuse, T. Taji, and T. Iwata, JAERI-M 87-026 (1987) (in Japanese).

36. "Grotrian diagrams for the hydrogen I isoelectronic sequence H I through Kr XXXVI": Y. Funatake, T. Shirai, and Y. Nakai, JAERI-M 87-053 (1987).
37. "Data compilation for radiation damage on ceramic insulators (Revised with updated data and review)": K. Fukuya, M. Terasawa, and K. Ozawa, JAERI-M 87-217 (1987).
38. "Cross sections for charge transfer of hydrogen atoms and ions colliding with gaseous atoms and molecules": Y. Nakai, T. Shirai, T. Tabata, and R. Ito, Atom. Data Nucl. Data Tables, 37, 69 (1987).
39. "Spectral data and Grotrian diagrams for highly ionized nickel, Ni IX - Ni XXVIII": T. Shirai, K. Mori, J. Sugar, W.L. Wiese, Y. Nakai, and K. Ozawa, Atom. Data Nucl. Data Tables 37, 235 (1987).
40. "Spectral data for molybdenum ions, Mo VI - Mo XLII": T. Shirai, Y. Nakai, K. Ozawa K. Ishii, J. Sugar, and K. Mori, J. Phys. Chem. Ref. Data 16, 327 (1987).
41. "Investigation on particle-solid interactions - Basic process relating to the plasma particle deposition profiles in solids -": S. Yano, JAERI-M 88-007 (1988) (in Japanese).
42. "Ion-impact desorption": T. Oshiyama, S. Nagai, and K. Ozawa, JAERI-M 88-146 (1988).

Available upon request to Nuclear Data Center, Department of Physics, Japan Atomic Energy Research Institute, Tokai-mura 319-11, Japan